NAS8-2696-SR-00001

SUMMARY REPORT
FOR PERIOD JANUARY 1, 1964
TO AUGUST 31, 1964

RESEARCH & DEVEOPMENT OF AN OPEN CYCLE FUEL CELL SYSTEM

Contract No. NAS8-2696

Prepared for:

National Aeronautics and Space Administration
George C. Marshall Space Flight Center
Huntsville, Alabama 35812

ALLIS-CHALMERS
RESEARCH DIVISION
MILWAUKEE, WISCONSIN 53201

SEPTEMBER 30, 1964

NAS 8-2696-SR-001

RESEARCH AND DEVELOPMENT OF AN OPEN-CYCLE FUEL CELL SYSTEM

SUMMARY REPORT

PREPARED FOR

National Aeronautics and Space Administration
George C. Marshall Space Flight Center
Huntsville, Alabama

Research Division, Department 3341
Allis-Chalmers Manufacturing Company
Milwaukee, Wisconsin

Approved J. L. Platner

J. L. Platner
Program Manager

FOREWORD

This report was prepared by the Aerospace Power Systems Section, Research Division, Allis-Chalmers Manufacturing Company, Milwaukee, Wisconsin under Modification Number Three of Contract Number NAS 8-2696. The work was administered under the direction of the Electrical Components and Power Supplies Section, Astrionics Division, NASA, Huntsville, Alabama. Mr. Richard Boehme was the technical supervisor for NASA.

This Summary Report covers the work completed from 1 January 1964 to 31 August 1964.

Management direction at Allis-Chalmers included Mr. Will Mitchell, Jr., Director of Research; Dr. P. A. Joyner, Messrs. D. T. Scag, W. W. Edens, and R. G. Matters, Assistant Directors of Research. The Project management included J. L. Platner, Section Manager, D. P. Ghere, Section Supervisor, and P. D. Hess, Chief Engineer. Dr. J. R. Hurley was a technical consultant.

The report was written by Messrs. J. Ward, J. Euclide, R. Desai and D. Ghere.

ABSTRACT

13222

Verification tests were conducted on the Static Moisture Removal System and various operating parameters were determined. Operation with moisture removal from both the oxygen and hydrogen side of the fuel cell was accomplished.

A mathematical model of the Static Moisture Removal System was made and experimental verification obtained by using a gas chromatograph to measure the actual water vapor pressures within the various cell cavities.

Performance tests were accomplished to determine the effects of thin electrolyte vehicles. Life tests were conducted to evaluate various plate and electrode configurations and materials to improve performance ratings.

Multi-cell assemblies were built and tested to extend the performance data gathered from the single-cell units. In these tests series-parallel constructed fuel cell assemblies were tested and their performance compared with units assembled with electrical-series connection.

Thermal design studies were effected on the fuel cell system and subsystem to achieve optimum performance with minimum weight.

A thermal mockup of the 1.5 KW fuel cell system was constructed and tested for initial design verification of the heat removal subassembly.

A 1.5 KW fuel cell system was constructed in breadboard fashion and successfully tested.

author

SUMMARY

The theory of operation of the Allis-Chalmers hydrogen-oxygen capillary membrane fuel cell is presented. By-product water removal by means of Static Moisture Removal is discussed, and its advantages are presented.

Test results gathered from single and multi-cell assemblies operating with the Static Moisture Removal System are given. Cells performed satisfactorily for test durations up to 2,300 hours, and operating current densities in excess of 300 ma/cm^2.

Additional evaluation tests were conducted to determine the advantages of fuel cells constructed with a combination series-parallel electrical connection over a fuel cell module connected electrically in series. These tests definitely show a basic reliability advantage for the series-parallel construction.

A mathematical model of the fuel cell operating with the Static Moisture Removal System was made to allow a paper study and theoretical analysis of the system. Experimental verification of the model was obtained on operating fuel cells with the aid of a gas chromatograph. These studies have determined some of the various parameters in the mathematical model, such as diffusion coefficients, effective transfer areas, and length of vapor and liquid diffusion paths for a given fuel cell construction.

The purging requirements of a fuel cell operating with the Static Moisture Removal system were evaluated for both single-cell units and a 1.5 KW fuel cell system. It was shown that using commercial grade reactant gases that the voltage drop at a constant current density due to inert build-up for a single cell unit averaged 0.24% per ampere hour and 0.35% per ampere hour for the 1.5 KW breadboard system.

Two design approaches for water vapor pressure regulator were selected and these units fabricated and tested. The feasibility of both designs was verified.

Thermal design studies are presented which consider overall Fuel Cell Assembly weights as a function of fuel cell plate design. In addition these studies were extended to consider various heat sinks to which waste heat from the fuel cell assembly can be rejected. Among the various sinks evaluated were space radiators, evaporative coolers, sublimers. The use of boil-off from cryogenic propellant supply tanks was also considered.

Design verification testing of the heat-removal subsystem for the 1.5 KW fuel cell system was accomplished on a thermal mockup prior to fabrication of the fuel cell system.

Design, fabrication and 162 hours of testing on the 1.5 KW fuel cell breadboard system was accomplished. Operating characteristics of the various subsystems were determined and a total system evaluation conducted. Reactant purge requirements for the system were investigated with commercial reactants. Electrical outputs of up to 2,580 watts were demonstrated.

TABLE OF CONTENTS

PART II TASKS

1.0 INTRODUCTION

This is the Summary Report submitted under Modification Number Three of Contract NAS 8-2696. The purpose of this contract was to perform research and development on a fuel cell system employing the Static Moisture Removal System and to demonstrate its performance, life, controllability and reliability.

To accomplish these goals, the following general areas of investigation, separated into Part I and Part II Tasks, were conducted.

Part I Tasks

(a) Experimental and theoretical investigations were performed on a hydrogen-oxygen capillary fuel cell employing Static Moisture Control for the by-product water removal. The performance and life characteristics of this system were investigated.

(b) Thermal design investigations were accomplished to achieve optimum system performance with minimum weight. Various types of system cooling and integrated system-vehicle tradeoffs were also considered.

Part II Tasks

A 28 volt, 1500 watt fuel cell system was constructed in breadboard fashion. The design performance goal is 950 watt-hours per pound at rated power for 720 hours. The overall system efficiency goal is 55% to 65%.

2.0 STATIC MOISTURE REMOVAL SYSTEM

2.1 Static Moisture Removal Concept

A fuel cell is an electrochemical device that converts the chemical energy of fuels directly into electrical energy, reactant products and heat. In the case of the hydrogen-oxygen fuel cell the reaction product is water. Efficient and sustained operation of the hydrogen-oxygen fuel cell requires that the product water and excess heat produced be removed from the fuel cell system in a controlled manner.

Static Moisture Removal is a method whereby the product water formed in a capillary fuel cell is removed from the fuel cell stack entirely by diffusion mechanisms and is therefore static in nature. The water is removed from the cell stack in the vapor state and may be ejected directly to space, thereby significantly reducing the heat burden imposed upon a fuel cell cooling system. As an alternative, the water vapor may be condensed, and in this case, the advantages of the static system are applicable, but the overall system thermal advantage is not gained.

The following discussion describes the details of the Static Moisture Removal Concept.

2.1.1 Capillary Membrane Fuel Cell

The basic cell consists of two porous nickel electrodes separated by the capillary membrane which holds the electrolyte. The most distinctive feature of this cell is the capillary membrane. The capillary potential of the membrane, defined as the differential pressure required to force liquid from its largest pore, is approximately 100 psi. This property enables the membrane

to hold the electrolyte in its proper position between the electrodes, effectively separates the reactant gases, and allows communication of water and hydroxyl ions between the electrodes.

When a cell is assembled, the asbestos membrane is filled with electrolyte and swells to a larger volume than when dry. During assembly, the associated electrodes are compressed against the asbestos membrane and some of the electrolyte is squeezed from the membrane into the electrodes, forming the necessary catalyst-electrolyte interfaces. The asbestos membrane remains filled with electrolyte.

In an operating hydrogen-oxygen fuel cell, water is formed within the hydrogen electrode at the interface of catalyst, electrolyte and hydrogen. If not removed, the water dilutes the electrolyte until it fills the entire pore volume of the electrodes (overwetting). If the water is removed from the cell faster than it is formed, the electrolyte volume decreases to the point where the wetting front begins to recede from the electrodes into the asbestos (overdrying). Both overwetting and overdrying are accompanied by a decline in cell performance.

The capillary membrane fuel cell is capable of satisfactory performance over a range of electrolyte concentrations and volumes. The range of controllable electrolyte concentrations is a function of thickness and porosity of the fuel cell electrodes and the amount and concentration of the electrolyte added to the capillary membrane at the time of construction. Experiments have shown that the average electrolyte concentration should be maintained between 27% and 45% for adequate performance, with a concentration of 35% being near optimum. The typical performance of an individual cell as a function of average electrolyte concentration is shown in Figure 1. If the temperature is held constant, then the water vapor pressure of the electrolyte increases rapidly as the electrolyte becomes more dilute, as shown in Figure 2. This characteristic forms the basis for Static Moisture Removal.

2.1.2 Principle of Operation of Static Moisture Removal

Static Moisture Removal utilizes the principles of gas and liquid diffusion, the changing vapor pressure characteristics of the fuel cell under load, and the capillary nature of the KOH impregnated membrane.

In this system, a second asbestos capillary membrane (the water transport membrane) containing concentrated KOH solution is placed adjacent to, but slightly separated from, the hydrogen electrode as illustrated in Figure 3. Hydrogen and oxygen reactants are dead-ended into the cell. The cavity located behind the water transport membrane is evacuated to a pressure corresponding to the vapor pressure of the desired maximum concentration of KOH solution to be maintained in the cell. A differential pressure of about 30 psi exists across the water transport membrane, but this presents no problem since pressure differentials approaching 100 psi are required to expel the KOH solution from the water transport membrane. Hydrogen will not flow through the water transport membrane because the pores of the membrane are completely filled with KOH solution. Water vapor is transported from the cell electrode to the water transport membrane by diffusion through the reactant gas due to the difference in vapor pressure between the cell electrolyte and the KOH contained in the water transport membrane. The water vapor condenses and tends to dilute the KOH in the water transport membrane. This causes the pressure in the evacuated cavity adjacent to the water transport membrane to increase. As the water vapor pressure rises, water vapor is removed from the cavity (and, hence, from the cell) to an external condenser where it may be condensed to potable water. If there is no need for the water, it may be vented directly to space and by so doing reject approximately 35% of the heat formed within the cell.

The controlled removal of water from the cell may be accomplished simply by maintaining the proper pressure upon the water transport membrane corresponding to the vapor pressure of the maximum concentration of the electrolyte desired in the operating cell. The maintenance of this pressure

prevents excess water removal. When the cell operates under load and produces water, the subsequent dilution of the cell electrolyte and rapid rise in electrolyte vapor pressure provides the driving force for water removal.

2.1.3 Thermal Considerations

A thermal advantage may be gained with the Static Vapor Pressure Control system as previously stated. The following discussion defines the thermal advantage that may be gained and predicts the allowable temperature variation in an operating cell.

Characteristic of fuel cell operation, some waste heat is produced during the fuel cell reaction. The amount of waste heat produced depends on the thermal efficiency and the power output as shown in the following analysis.

The thermal efficiency, assuming 100% current efficiency, is defined as:

$$\eta t = \frac{\triangle F}{\triangle H^\circ} \times 100 \qquad (2\text{-}1)$$

$\triangle H^\circ$ = Enthalpy of reaction per mole of product at the standard state*

$\triangle F$ = Observed free energy change per mole of product (observed electrical work)

* Standard state

Hydrogen at 1 atm, 25° C
Oxygen at 1 atm, 25° C
H_2O liquid at 1 atm, 25° C

Explicit definition of $\triangle H$ and $\triangle F$ requires an explicit definition of reactions taking place in the fuel cell. Operating temperature must also be defined since the thermodynamic properties ($\triangle F$ and $\triangle H$) are temperature dependent properties. Therefore, for the following discussions the efficiencies are based on the following defined reactions:

$$H_2\ (g) + 1/2\ O_2\ (g) \xrightarrow{25^\circ C} H_2O\ (liq.)$$

Since $$\triangle F = - n \mathcal{F} E \qquad (2\text{-}2)$$

n = electrons transferred per mole of product

$\mathcal{F}$ = Faraday's constant (96, 500 coulombs per equivalent)

E = observed voltage

$\triangle F$ is proportional to E and $\triangle F^\circ$ is proportional to E° (1.23 volts). Thus, with reactants and products at 25° C and one atmosphere, the thermal efficiency may be determined from the relationship:

$$\eta t = \frac{E}{E^\circ} \times \frac{\triangle F^\circ}{\triangle H^\circ} \qquad (2\text{-}3)$$

$$\eta t = 0.67\ E \qquad (2\text{-}4)$$

$\triangle F^\circ$ = Free energy change per mole of product at standard state, -56.693 K cal/g. mole

$\triangle H^\circ$ = Enthalpy change per mole of product at standard state, -68.372 K cal/g. mole

E° = Theoretical open circuit voltage, 1.23

E/1.23 is the ratio of the actual cell voltage to the theoretical cell voltage. The last term, $\frac{\Delta F^\circ}{\Delta H^\circ}$, is the maximum possible thermal efficiency at standard state. The total rate of heat production is dependent on the load and efficiency, as previously stated, and can be easily determined from the relationship:

$$Q = P \left(\frac{1}{\eta t} - 1 \right) \qquad (2\text{-}5)$$

from Equation (2-4) and (2-5)

$$Q = P \left(\frac{1}{0.67\ E} - 1 \right) \qquad (2\text{-}6)$$

where P = power in watts

Q = total rate of heat production in watts

In a space application, heat energy will be ejected from the system with the water vapor, (if the vapor is vented to space) thereby significantly reducing the heat burden to be dissipated by a vehicle cooling system. The amount of heat energy exhausted in this manner is in direct relationship to the amount of water produced in the cell and to the cell temperature.

The relationship for determining the amount of water produced in an operating cell is:

$$M = C \times A \times N \qquad (2\text{-}7)$$

where C = constant = 0.336 grams per ampere hour

A = ampere-hours

N = number of cells

M = mass of water, gms

The total heat energy of water vapor at 93.3°C and 33 mm Hg pressure with respect to liquid water at 1 atm and 25° C is 0.712 watt-hours per gram. Thus:

$$Q' = 0.240\ A\ N \qquad (2\text{-}8)$$

where Q' = heat rejected in the product water vapor in watt-hours

The heat rejected in this manner usually amounts of about 35% of the total heat burden.

If the water vapor is condensed and collected, the heat of condensation must be rejected from the vehicle cooling system and the overall thermal advantage is no longer gained.

The maximum permissible temperature variation assuming a fixed cavity control pressure may be predicted by referring to Figure 2. Assuming an acceptable operating range of KOH concentration from 32% to 40%, the temperature can vary from 87.5° C to 95° C, about an optimum operating point of 90° C (35% KOH).

This temperature range limitation is eliminated however, by providing temperature compensation to the water vapor cavity controller. In this case the cavity control pressure is adjusted through temperature sensing to correspond to the required cell operating characteristics. Thus, wide fluctuation in cell operating temperature will not adversely affect moisture control.

3.0 STATIC MOISTURE REMOVAL STUDIES

An analytical study of the Static Moisture Removal System was accomplished to develop a better understanding of the total system and to determine the limiting characteristics of this fuel cell control method.

3.1 Mathematical Model

A simplified mathematical model of the system was developed from an analytical study of the Static Moisture Removal Mechanism. This model assumes that each segment of the electrode operates at a common current density, the cell temperature is uniform and the flow rate of reactants is independent of the direction normal to the reactant flow. Variation of the total pressure within a cell is neglected.

Under the above conditions, the fuel cell may be represented as shown in Figure 4, where conditions are constant in the direction perpendicular to the paper and the dimension of the cell in that direction is unity. Two variations of reactant flow are considered:

(a) Parallel flow, where both hydrogen and oxygen enter at the same end of the fuel cell,

(b) Counter flow, where hydrogen and oxygen enter at opposite ends of the cell.

For brevity, only the case of parallel flow will be discussed here. All that is involved in changing to counter flow is a change in the indexing of the variables.

The length of the cell may be divided into n equal elements; each element being numbered sequentially starting with one at the hydrogen inlet. Consider a general element i shown in Figure 4. A water balance on the hydrogen side of this element gives:

$$W_{c_i} = \frac{D\mathcal{M}A}{n\delta W}(C_{H_i} - C) - \frac{R_H m_H I}{R\mathcal{F} n}\left[\left(\frac{P_{VH_i - 1}}{P - P_{VH_i - 1}}\right)(n - i + 1)\right. \tag{3-1}$$

$$\left. - \left(\frac{P_{VH_i}\,\mathcal{N}}{P - P_{VH_i}}\right)(n - i)\right] - \frac{R_H m_H I}{R\mathcal{F} n} + \frac{D_H A_H n}{L R T}\left(P_{VH_{i+1}} - P_{VH_i - 1}\right)$$

The first term on the right of Equation (3-1) represents the water transported through the water removal membrane. The second term is the net transport of water into the element with the flowing hydrogen stream. The third term is the amount of water generated in the element due to the consumption of reactants. The fourth term is the net transport of water into the element by diffusion of water vapor from adjacent elements through the hydrogen stream.

Solution for the actual electrolyte concentration in the cell begins by making an initial guess at the concentration on the hydrogen side. Since the specification of concentration at a given temperature uniquely determines the vapor pressure of the electrolyte, Equation (3-1) may be solved for W_{c_i}, $i = 1, 2, 3, \cdots n$.

Then the distribution of electrolyte concentration on the oxygen side may be calculated from

$$C_{O_i} = C_{H_i} + \frac{\sigma n}{D A} \left(W_{C_i} - \frac{R_H m_H I}{R \mathcal{F} n} \right) \qquad (3\text{-}2)$$

A water balance on the oxygen side gives

$$W'_{C_i} = \frac{R_O m_O I}{R \mathcal{F} n} \left[\left(\frac{P_{VO_{i-1}}}{P - P_{VO_{i-1}}} \right) (n - i + 1) \left(\frac{P_{VO_i}}{P - P_{VO_i}} \right) (n - i) \right]$$

$$- \frac{D_O A_O n}{R L T} \left(P_{VO_{i+1}} - P_{VO_{i-1}} \right) \qquad (3\text{-}3)$$

Initially, W_{C_i} and W'_{C_i} will differ by an amount which will depend on the accuracy of the initial guess of electrolyte concentration. The assumed concentration distribution can be made more nearly equal to the actual concentration distribution by solving for vapor pressure (and hence electrolyte concentration) in the equation following where $\varkappa$ is a number between 0 and 1. If $\varkappa = 1/2$, the right-hand side of Equation (3-4) is the arithmetic average of W_{C_i} and W'_{C_i}.

$$\frac{D\,\mu\,A}{n\,\delta\,W}\,(C_{H_i} - C) - \frac{R_H\,m_H\,I}{R\,\mathcal{F}\,n}\left[\left(\frac{P_{VH_{i-1}}}{P - P_{VH_{i-1}}}\right)(n - i + 1)\right.$$

$$\left. - \left(\frac{P_{VH_i}}{P - P_{VH_i}}\right)(n - i)\right] - \frac{R_H\,m_H\,I}{R\,\mathcal{F}\,n} + \frac{D_H\,A_H\,n}{L\,T\,R}$$

$$\left(P_{VH_{i+1}} - P_{VH_{i-1}}\right) = (1 - \psi)\,W_{C_i} + \psi\,W'_{C_i} \qquad (3\text{-}4)$$

The values obtained from Equation (3-4) can be used to calculate improved values for the concentrations on the oxygen side of the cell, and so the iteration will proceed until

$$\left| W_{C_i} - W'_{C_i} \right| \leq \epsilon \qquad i = 1, 2, 3, \cdots n$$

where ϵ is the desired accuracy.

NOMENCLATURE

A	active cell area (cm^2)
A_H	cross section of hydrogen flow channel (cm^2)
A_O	cross section of oxygen flow channel (cm^2)
C	water concentration in electrolyte in water removal cavity (gm of water/cc of electrolyte)
C_H	water concentration in electrolyte on hydrogen side of cell (gm of water/cc of electrolyte)
C_O	water concentration in electrolyte on oxygen side of cell (gm of water/cc of electrolyte)
D	diffusion coefficient of water in the electrolyte solution as held in the asbestos matrix (cm^2/second)
D_H	diffusion coefficient of water in hydrogen at cell temperature and pressure (cm^2/second)
D_O	diffusion coefficient of water in oxygen at cell temperature and pressure (cm^2/second)
$\mathcal{F}$	Faraday constant (96,500 coulombs per gram equivalent)
I	cell current (amp)
L	dimension of cell in direction of reactant flow (cm)
m_H	chemical equivalent weight of hydrogen (gm)

m_O	chemical equivalent weight of oxygen (gm)
P	total pressure in cell (dynes/cm^2)
P_{VH}	vapor pressure on hydrogen side of cell (dynes/cm^2)
P_{VO}	vapor pressure on oxygen side of cell (dynes/cm^2)
R	gas constant for water vapor (erg/gm ° K)
R_H	gas constant for hydrogen (erg/gm ° K)
R_O	gas constant for oxygen (erg/gm ° K)
T	absolute temperature of cell (° K)
W_C	net exchange of water between the hydrogen and oxygen streams, as calculated from a water balance on the hydrogen side (gm/sec)
W'_C	net exchange of water between the hydrogen and oxygen streams, as calculated from a water balance on the oxygen side (gm/sec)
δ	distance between the electrolyte interfaces on the hydrogen and oxygen electrodes (cm)
δ_W	distance between surface of water removal membrane and interface of electrolyte in the membrane support plaque (cm)
ϵ	allowable error for convergence in the iterative solution (gm/sec)
μ	ratio of effective area for diffusion through the water removal membrane to the cell active area (unitless)
α	acceleration factor for use in the iteration procedure (dimensionless)

The equations just derived represent the basic form of the mathematical model of the moisture removal system. Several of the constants in those equations could not be obtained by simple direct measurement or from tabulated physical constants. The values of those constants, the diffusion coefficient (D), diffusion path lengths, (δ and δ_W), and diffusion area ($\frac{1}{4}$ A), were determined by using the model in conjunction with the experimental chromatography data.

3.2 Experimental Investigation and Correlation with the Mathematical Model

In order to determine the unknown constants in the mathematical model for the Static Moisture Removal Method and to determine the accuracy and range of applicability of the model, tests were performed on an operating fuel cell with the aid of a gas chromatograph. The chromatograph was used to determine the water vapor partial pressure which existed at various positions within the hydrogen and oxygen cavities.

The test apparatus is shown schematically in Figure 5. The apparatus consists of four general sections:

(a) The fuel cell with necessary controls and instrumentation.

(b) A temperature-controlled sampling system.

(c) The gas chromatograph with controls and carrier gas conditioner.

(d) A calibration bath.

Gas samples are taken from both the hydrogen and oxygen cavities of the fuel cell with sampling positions located as shown below.

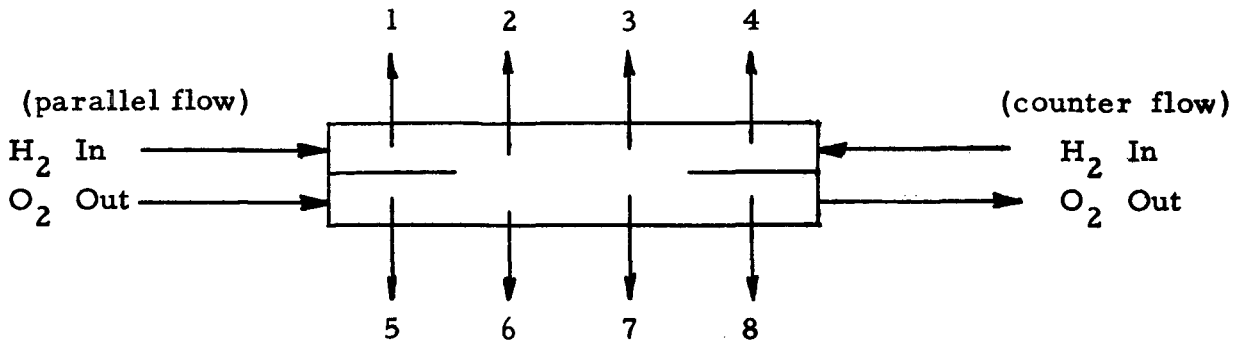

The samples of reactant gas and water vapor were analyzed with the gas chromatograph. The water removal cavity pressure was monitored by a pressure transducer. Operation of the cell was thus monitored while load, cavity pressure, and cell temperature were varied in turn.

The data obtained by chromatograph was compared with predictions given by the model for various ranges of the unknown constants. The values of the constants providing the best fit of model with experimental data were then assumed to be the true values and incorporated into the model. The values used were

$$D = 2.5 \times 10^{-5} \text{ cm}^2/\text{second}$$

$$\delta = 0.061 \text{ cm}$$

$$\delta_W = 0.061 \text{ cm}$$

$$\mu = 0.7$$

Figures 6 and 7 show the agreement between experimental data and model values for the water vapor pressure distribution in the hydrogen and oxygen cavities. The operating conditions were 175 ma/cm^2, 88° C, 2.0 atmospheres reactant pressure, 240 mm Hg water cavity pressure, and a cell length of 15.9 cm. Figure 6 depicts the situation where the reactant gases flow concurrently. Figure 7 differs in that the reactant gases were fed at opposite ends of the cell. The greatest observed differences between model and experimental data occurred at the ends of the cell. These discrepancies are attributed to non-uniform current density and temperature along the cell as well as the fact that the model assumes a smooth fully developed flow profile in the reactant cavities whereas in the actual cell the reactants are introduced through relatively small orifices causing considerable non-uniformity in flow.

4.0 FUEL CELL PERFORMANCE TESTS

From the discussion in the preceding section, it is apparent that the concept of Static Moisture Removal offers considerable advantages as a space vehicle auxiliary power system.

Initial performance testing of the Static Moisture Removal system was conducted to accomplish the following:

(a) Verify the diffusion transport of the product water from the cell.

(b) Determine if the rate of water removal by static means is sufficient for practical current densities.

(c) Evaluate and compare water removal from the hydrogen and from the oxygen electrode.

(d) Evaluate the feasibility of controlling multi-cell units.

The tests were conducted in three phases. The first phase utilized single-cell units. Although in some cases cell construction differed between tests, the same basic control system, Figure 8, was used for all tests. In the second phase, four-cell modules were assembled and operated. Phase three utilized an eight-cell breadboard system to extrapolate the results obtained from phases one and two to a larger system.

4.1 Single and Four-cell Fuel Cell Tests

Test Number 1 - A single cell was constructed as shown in Figure 9. This cell operated for a total of 68 hours at a current density of 93.5 ma/cm^2 with an average total of 0.82 volt. Water was removed from the hydrogen side of the cell for 41 hours and the oxygen side for 27 hours.

Test Number 2 - This single cell, with the same construction as in Test Number 1, operated for a total of 77 hours at a current density of 88 ma/cm^2 with an average voltage of 0.80 volt. Water was removed from both sides of the cell for the first 34.5 hours and from the oxygen side for the remainder of the test.

Test Number 3 - A third cell, constructed in the same manner as the previous two cells, was operated for 135 hours at a current density of 88 ma/cm^2 with an average potential of 0.81 volt, with water removal effected on the oxygen side (except for short periods at the beginning and end of the test).

Test Number 4 - This four-cell module was operated for 220 hours with a cyclic load profile. Manifolding was altered to permit individual regulation of hydrogen and oxygen cavity pressures. Figure 10 illustrates the overall module performance with the cavity vapor pressure expressed in terms of equivalent KOH concentration. A summary of total module operating time at various loads is shown in the following table.

TABLE I

PERFORMANCE SUMMARY OF TEST NUMBER 4

Load Current (amperes)	Current Density (ma/cm^2)	Potential (volts)	Power (watts)	Time (hours)
20	47.3	3.51	70.3	77.0
30	70.9	3.38	101.4	74.5
40	94.5	3.28	131.0	68.5
		TOTAL TIME		220.0 Hours

Test Number 5 - This four-cell module was assembled using improved electrodes and a new plate design specifically for the Static Vapor Pressure Control system. The new design provided improved heat removal, water removal and sealing. The module was operated for over 100 hours at various loads ranging from 10 amperes (24 ma/cm^2) to 90.5 amperes (214 ma/cm^2). Potential at 10 amperes was 3.70 volts, at 90.5 amperes it averaged 3.00 volts, varying between 2.97 volts and 3.08 volts. The performance of this module was definitely superior to previous modules.

The completion of the above five tests indicated that sufficient water could be removed from one side of the cell even at high current densities (i.e., above 200 ma/cm^2). The previous tests had also indicated that slightly improved operation and control characteristics were obtained by removing the by-product water from the back side of the anode. This of course is logical since the water is formed at the anode and by removing the moisture from the anode side of the cell shortens the overall path that the water must diffuse through before exiting from the cell.

Following the above tests, improvements were made in electrode performance and cell design which allowed continuous operation of a cell at 214 ma/cm^2 at potentials exceeding 0.8 volt. Cell operation at 300 ma/cm^2 was accomplished with no adverse effects for durations over two hours.

4.2 Eight-Cell Breadboard System Testing

Upon completion of the single and four-cell tests which verified basic operating principles, and established certain parametric relationships, an eight-cell system constructed in breadboard fashion was tested to extrapolate the preceding test results to larger fuel cell systems.

A control panel was constructed which formed a complete breadboard system when coupled with a fuel cell module operating with Static Moisture Removal. This breadboard, pictured in Figure 11, contains all the components necessary for semi-automatic operation and requires only hydrogen, oxygen and vacuum inputs. However, for laboratory use, heaters and timers are supplied from standard 110 volt a.c., instead of being powered by the module. Many instruments are also included for laboratory purposes.

A breadboard system comprised of this control panel and an eight-cell module capable of output of 400 watts was operated continuously under load except for weekend shutdowns for a total of 405 hours.

The cells which comprised this module contained the same active area (420 cm^2) as the four-cell feasibility tests modules. However, the eight cell module was designed for moisture removal from the hydrogen electrodes only, hence no water removal cavity existed behind the oxygen plates. The member which contains the oxygen electrode of one cell, also contained the water removal cavity for the adjacent cell. Photographs of the test plates are shown in Figures 12 and 13.

This was the first multi-cell module to be operated with moisture removal from the hydrogen electrode only. It was therefore necessary to show that sufficient moisture could be removed in this manner at all load levels.

In the first part of the test (162.5 hours) the module was operated on a load program in which the load was increased in 10 ampere increments from 20 to 70 amperes, each load being maintained for approximately 24 hours. During the run at each load, the cavity pressure was varied in an effort to seek optimum cell performance.

During the next 122.5 hours of operation, an attempt was made to duplicate the performance of the first hours while using a constant cavity pressure equivalent to an average electrolyte concentration of 43% KOH at the cell operating temperature of 91° C, the value which appeared to be optimum for 70 ampere operation. The module was again operated for 24-hour periods at 20, 30, 40, 50, and 60 amperes.

During the final 120 hours of the test, the module was operated continuously at 40 amperes (95.5 ma/cm^2). The combined time of all the tests plus miscellaneous operations, totalled 405 hours under load. Module performance in terms of voltage, current and cavity vapor pressure (% KOH) is shown in Figure 14, for the first 162.5 hours of operation. This period of operation is typical for the 405 hours.

The above test was significant for two reasons:

(a) This represented the longest period of operation of fuel cell modules controlled by the Static Vapor Pressure Method.

(b) The feasibility of operating a multi-cell unit with moisture removal from the hydrogen electrode only was demonstrated with a single cavity pressure setting for a wide range of loads.

4.3 Cell Improvement Tests

Tests were conducted to study and improve the performance, life and reliability of fuel cells using the Static Moisture Removal method. These investigations provided evaluation of electrodes, electrolyte vehicles, and various configurations of electrode holders.

4.3.1 Electrolyte Vehicle Tests

To improve the fuel cell performance, electrolyte vehicles thinner than the standard 30 mil capillary membranes were investigated. The improved performance is believed to be a result of lower internal electrical resistance and a reduction in the difference in electrolyte concentration across the cell membrane.

Performance tests have been completed on electrolyte vehicles of 10, 15, and 20 mil in thickness.

The increase in current density at a constant voltage as the thickness decreases is particularly striking. The following table of data taken from the curves illustrates this for a case where the cell voltage is taken at 0.8 volt.

Electrolyte Vehicle Thickness (mils)	Current Density (ma/cm^2)	Current Density % of Standard 30 mil Thickness
Type A cell - 0.8 volt		
10	500	222
15	370	164
20	310	138
30 (standard)	225	100
Type B cell - 0.8 volt		
10	345	203
15	275	162
20	215	126
30 (standard)	170	100

These tests were run on cells of standard construction, except as noted, and with an active area of 172 cm^2.

Measurements of capillary potential were conducted with the various thicknesses of asbestos in question. The capillary potential, which represents the pressure differential across the membrane which will force liquid (KOH) from the largest pores of the membrane, is an important factor in choosing the electrolyte vehicle. Figure 15 shows the results of preliminary test data.

From the data obtained so far improvements in fuel cell performance can be obtained by reducing the thickness of the electrolyte vehicle, while still maintaining adequate tolerance to reactant pressure differentials.

4.3.2 Life Tests

As fuel cell current densities have increased, it was noted that the output of early cells gradually decreased with time even though all other operating conditions were held constant. In order to obtain uniform output for extended periods of operation at high current densities, several cells constructed with new combinations of electrodes were tested. One construction, Type "B", exhibited excellent life characteristics. The initial performance of this cell was lower than Type "A". However, the performance has remained extremely stable.

The first Type "B" cell was constructed with a 30 mil electrolyte vehicle and operated for approximately 2,300 hours under a constant load of 162 ma/cm^2 with a 5% decrease in cell voltage. The total test time span was in excess of 4,000 hours.

Duplicate cells have been tested for periods up to 1800 hours with similar life characteristics noted.

4.3.3 Series-Parallel Fuel Cell Operation

In an operating fuel cell module, it is not uncommon for some cells to be slightly stronger than others. If two or more single cells were connected in parallel, the stronger cells would, in effect, support the weaker ones by assuming a greater proportion of the shared load. A number of these parallel connected sub-modules could then be connected in series to produce the desired total voltage. In addition to the resultant improvement in system reliability, several advantages for fabrication and assembly can be realized by series-parallel construction.

A schematic of the four-cell parallel test module is shown in Figure 16. In order to investigate parallel operation, the setup shown in Figure 17 was used. This allowed individual cell voltages and currents to be monitored to determine cell load sharing. Figure 18 illustrates a typical load sharing determination.

Load sharing studies on a four-cell module electrically connected in parallel, indicated that the fuel cells in a parallel stack share the current demand in proportion to their ability to meet a common voltage. That is, for a given current demand, the cells adjust their individual current output until a common voltage is reached. No circulating currents between the cells were apparent. These studies were conducted over a range of loading with cell performance at various levels of depreciation. As an extreme, tests were conducted with the hydrogen gas flow completely blocked from one cell to determine if any current would pass through the cell due to the voltage produced by the other cells. The cell with the gas flow closed would not supply a current large enough to be detected by a milliammeter. When this cell was placed in parallel with the three other cells on open circuit of 1.05 volts, a circulating current of approximately 30 milliamperes was observed passing through the dead cell. This current decreased as the parallel stack was loaded since the common voltage decreased. At a current load of 120 amperes, the circulating current through the dead cell was approximately 20 milliamperes, or less than 0.02% of the current output.

In a continuation of this test, a power supply was connected in series with the module and adjusted to deliver six volts at 100 amperes. This would simulate several modules in series with the test module. As expected, no change in the current levels through the dead cell or change in the module voltage output was observed.

In order to force appreciable currents through a fuel cell with an external voltage source, electrolysis must occur. Electrolysis theoretically occurs if the applied voltage is greater than 1.23 volts. Experiments indicate that the voltage necessary for electrolysis is, in practice, near 1.5 volts. A single hydrogen-oxygen fuel cell has a theoretical maximum open circuit voltage of 1.23 volts and a normal actual open circuit voltage of about 1.1 volts. Thus a fuel cell could not electrolyze water in a cell connected in parallel with it and no appreciable current could pass through a dead cell in a stack of parallel connected cells.

4.3.4 Half-Cell Tests

An experimental setup was constructed so that individual voltage measurements could be made of the cathode, anode and IR losses in an operating fuel cell. It was planned to make these measurements as a function of KOH concentration, fuel cell temperature and reactant gas pressure.

The first test completed was a check of cell performance versus cell reactant pressure. This cell was assembled with a standard nickel anode and a Type "B" cathode. The electrolyte vehicle was the standard 0.030" asbestos. The cell was operated at a constant temperature of 88° C and a constant cavity pressure equivalent to 35% KOH. The electrode characteristics were measured at reactant pressures of 1.5, 2.0, 2.5, and 3.0 atmospheres. Figure 19 illustrates the relative effect on anode and cathode as well as the total effect. The internal resistance was not measurably affected by the varying pressure.

Following the completion of the first test series, this work was discontinued at the request of MSFC so that a corresponding effort could be added to the scheduled work planned for the other work tasks, which were felt to be of more immediate importance.

5.0 REACTANT PURGE REQUIREMENTS

5.1 General

As reactant gases are consumed in a fuel cell operating with the reactant gas flow "dead-ended" in the cell, any constituents which do not react in the cell will collect and must be periodically removed by purging. The magnitude of this buildup can be illustrated by the following simplified sample calculation (which assumes all impurities are nitrogen):

Assume

Gas Purity	=	0.995
Cell Volume	=	20 cc
Cell Pressure	=	2.5 atm.
Cell Temperature	=	90° C

If the cell could be operated until it is 100% full of nitrogen, or the partial pressure of nitrogen equalled the total pressure, the total weight W of nitrogen present would be:

$$W = \frac{p\ V}{R\ T} = \frac{(2.5)\ (0.020)}{(0.00293)\ (363)} = 0.0470 \text{ grams}$$

p	=	2.5 atm
V	=	20 cc or 0.020 liters
R	=	0.00293 liters - atm/gm ° K for nitrogen
T	=	363° K

Oxygen is being consumed at the rate of 0.299 gm/ampere-hour. Converting the gas analysis to gravimetric analysis provides the following:

Oxygen	=	99.562 %
Nitrogen	=	0.438 %

Therefore, nitrogen will collect at the rate of 0.00131 gm/ampere-hour.

Considering the maximum amount of nitrogen which the cell is capable of containing at cell operating conditions, a total of $\frac{0.0470}{0.00131}$ or 35.8 ampere-hours would be sufficient to completely fill the cell. Actually this figure could not be attained because some oxygen would be required to maintain a reaction. The electrolyte provides a partial pressure of water vapor which would further reduce the available space. However, as a limiting case for theconditions specified, the example illustrates the rate at which inert impurities can collect within a cell. If the reactant purity was 0.9995 instead of 0.995, the limit would be ten times as great, or 358 ampere-hours.

As the inert constituents build up within the cell, the partial pressure of oxygen or hydrogen is reduced. This, in turn, affects the cell performance. The magnitude of this effect may be dependent on a number of factors such as load, cell vapor pressure, cell design, etc. Testing was accomplished to define the quantity and frequency of purge required to maintain performance within given specifications.

To verify the actual purge requirements of a fuel cell system operating with the Static Moisture Removal Method, tests were initially run on a single-cell and finally on a 1.5 KW fuel cell system.

The reactant gas purities used in these tests were established with the aid of the mass spectrometer to be:

Hydrogen		Oxygen	
Hydrogen	- 99.94%	Oxygen	- 99.73%
Argon and Oxygen	- less than 0.01%	Argon	- 0.22%
Nitrogen	- less than 0.02%	Nitrogen	- 0.005%
CH_4	- less than 0.01%		
CO	- less than 0.01%		
CO_2	- less than 0.01%		

5.2 Single-Cell Purge Tests

The single-cell tests were designed so that a fixed volume of 3 cc was purged from each reactant cavity every 30 minutes while a constant load of 30 amperes was maintained on the cell. A plot of cell voltage versus time was obtained. Typically illustrated on Figure 20.

Analysis of these data showed that a 3 cc purge every 6 minutes (0.9% of the stoichiometric consumption) would maintain the cell voltage within 0.7% and a 3 cc purge every 10 minutes (0.5% of the stoichiometric consumption) would maintain the voltage within 1.0%.

5.3 1.5 KW Fuel Cell Breadboard System Purge Requirements

System voltage versus time was recorded on the 1.5 KW breadboard system with a purge cycle every 6 minutes for 6.5 seconds and a purge cycle every 10 minutes for 10 seconds. For both cases the average amount of reactant gas purged in pounds per hour was constant.

Analysis of the data from the 1.5 KW system showed than an average system voltage drop of 0.35% per ampere-hour was obtained compared to an average voltage drop of 0.24% per ampere-hour for the single-cell investigations.

This comparison reflects usage of reactants with the same purity, however, a 3.5% purge was used for the 1.5 KW system and approximately 1% purge for the single-cell test. The purge quantities are expressed as percent of stoichiometric reactant consumption.

These tests indicate that the single cell purge data is not realistic because there are no reactant manifolds which must be purged in addition to the cell cavities. Furthermore, it is not expected that all the cells in a large system would purge uniformly so that a proportionately larger volume of reactants is required for purge.

6.0 WATER VAPOR PRESSURE CONTROLLER

A critical item in the operation of a fuel cell using Static Moisture Removal Method is the water vapor pressure controller placed on the exhaust of the water removal cavity of the fuel cell. Two design approaches were investigated for this item. The first approach was an absolute pressure mechanical relief valve and the second and more desirable approach was an electronically controlled solenoid valve. The electronic controller will easily lend itself to temperature compensation.

6.1 Mechanical Relief Valve

To evaluate the mechanical relief valve approach, the valve shown in Figure 21 was fabricated and tested. The long spring used in this model gave high sensitivity over a full range of adjustment from 0.1 to 1.0 atmospheres pressure. Fluctuation of downstream vacuum did not seriously affect the control setting which was maintained within $\pm$ 1 mm Hg. This valve controlled the cavity pressure of an operating fuel cell satisfactorily indicating that it represents a feasible solution. However, considerably more effort would be required to develop a space oriented device.

6.2 Electronic Controller

The second approach, the electronic controller, Figure 22, was developed and tested. This controller utilizes a signal from the pressure transducer which monitors the cavity pressure, to operate a solenoid valve that opens to vacuum. The controller, designed to operate on 115 volts, a.c. for laboratory use, also provides a reference voltage of 3 volts for the transducer. The controller will

control at any setting from 13 to 3,000 millivolts. The control relay opens and closes with 1 millivolt or less change in signal. Two types of pressure transducers are presently in use in the laboratory: 0 - 15 psia and 0 - 50 psia. The controller could then control the cavity pressure within 0.25 mm Hg for the first type and 0.86 mm Hg for the second type, providing that the system, transducer, and valve time-constants were such that oscillations in pressure would not occur. Tests on operating cells proved the feasibility of the unit. This controller was used on the 1.5 KW fuel cell breadboard system described in Section 9.0 of this report.

7.0 THERMAL DESIGN STUDIES

7.1 General

As in any power supply which produces excess heat, the controlled removal of this heat must be accomplished for the system and its comprising subsystems.

The thermal design of a fuel cell system depends first of all on the thermal efficiency of the fuel cell, which determines the amount of heat which must be dissipated. Secondly, this heat must be conducted out of the cell through the electrode holder plates without causing a detrimental temperature differential across the surface of the cell. The cooling system must then pick up this heat from the cell and reject it from the fuel cell system.

7.2 Fuel Cell Thermal Efficiency

Characteristic of fuel cell operation, some waste heat is produced during the fuel cell reaction. The amount of waste heat produced depends on the thermal efficiency and the power output as was discussed in Section 2.1.3.

7.3 Thermal Optimization of Fuel Cell Plates

A fuel cell module with a given cell area can be built with numerous cell configurations. It is the object of this discussion to show how the minimum weight configuration may be determined subject to requirements of heat

removal from the cell. This is done by expressing weight as a function of cell configuration variables and determining the minimum point. Figure 23 shows the nomenclature on dimensions and general configuration of the cell plate used in the mathematical derivations.

Only the weights of the fuel cells and canister need be considered since weights of other components of the system are negligibly affected by cell configuration.

Rectangular cells externally cooled with fins on two edges are used due to ease of reactant manifolding and heat removal. The cell considered consists of two cell plates, whose weights depend upon cell configuration; electrodes, electrolyte and capillary membranes, all of whose weights are independent of cell configuration. The plate is considered as three separate regions (active cell region, seal region, and fins) to clarify calculations.

The weight of the active cell region of one cell plate, W_1, is:

$$W_1 = \rho_1 A \delta_a F_W$$

where:

ρ_1 = density of plate material

A = active cell area

δ_a = thickness of one cell plate in active cell region

F_W = fraction of metal remaining in active cell region after manifolding grooves for gas distribution are machined

If the two plates in one cell have different thicknesses, the average between the two values is used. Other parameters which are not the same for the two plates are handled in the same manner throughout this analysis.

Weight of seal region of one cell plate, W_2, is approximately:

$$W_2 = 2\rho_1 \ell_S (\ell_1 + \ell_2) \delta_S$$

where:

ℓ_S = width of seal region

ℓ_1 = length of uncooled side of active cell region

ℓ_2 = length of cooled side of active cell region

δ_S = thickness of plate in seal region

Weight of fins on one cell plate, W_3, is approximately:

$$W_3 = 2\rho_1 \ell_2 \ell_F \delta_F$$

where:

ℓ_F = width of fin

δ_F = thickness of fin

The cell plates are usually plated with a thin metal layer for protection from corrosion due to chemicals present in the fuel cell.

Weight of plating for corrosion protection, W_4, on one cell plate is approximately:

$$W_4 = 2\rho_P A_P \delta_P F_P + 4\rho_P \ell_S (\ell_1 + \ell_2) \delta_P + 4\rho_P \ell_F \ell_2 \delta_P$$

the terms referring respectively to plating on active region, seal region, and fins

with: ρ_P = density of plating material

δ_P = thickness of plating

F_P = surface area of active cell region with manifolding grooves compared to the surface area of a flat plate of equal size

Weights of electrodes, electrolyte, asbestos membranes, bolts, and end plates are essentially constant and are therefore omitted from this consideration of weight variation.

Canister weight, W_5, is small compared to fuel cell reactor weight and can be approximated by

$$W_5 = 2\rho_C \delta_C \ell_C (\ell_2 + \ell_1 + 2\ell_S)$$

where: ρ_C = density of canister material

δ_C = thickness of canister wall

ℓ_C = length of canister

For a fuel cell reactor composed of N cells (2 N cell plates), the combined reactor and canister weight affected by configuration is given by:

$$W = 2N (W_1 + W_2 + W_3 + W_4) + W_5$$

This problem is simplified by noting that values of many of these parameters are constants for a specific fuel cell application and can be determined from the following considerations.

N and A	are determined from output power and voltage requirements and cell performance characteristics
F_W , F_P	are determined from required manifolding
ρ_1	property of cell plate material which is selected for low density and high thermal conductivity
ℓ_S	determined by minimum seal width requirements
δ_S	determined by minimum thickness allowable for sealing and manifolding into cell
ℓ_F	determined from minimum area consistent with good heat transfer to coolant flowing over fins
δ_F	determined from minimum thickness consistent with machining and handling requirements
ρ_P	determined from the plating material selected for corrosion protection
δ_P	determined from minimum plating thickness required for corrosion protection
ρ_C	determined from material selected for the canister
δ_C	minimum canister thickness consistent with handling and fabrication requirements
ℓ_C	canister length fixed by seal thicknesses and number of plates in reactor

Then, Equation (7-1) expresses weight as a function of three variable plate dimensions (ℓ_1 , ℓ_2, and δ_a) with all other parameters constant for a specific application. In order to express weight as a function of a single configuration dimension, the following relations are used. From the constant

area condition we obtain

$$\ell_1 \ell_2 = A \tag{7-2}$$

For minimum weight δ_a should be a minimum. This minimum value of plate thickness is determined by the thickness required for conduction of waste heat from the inside of the cell to the cooling fins.

Assuming constant temperature along cooling fins and no heat loss through end plates, the problem becomes a one dimensional problem of heat conduction in a plate with constant heat flux into the plate surface. For a flat plate, the thickness, δ, and temperature drop, ΔT, in a length, γ, are related by

$$\delta = \frac{q_P \gamma^2}{2 K \Delta T}$$

where q_P = heat input per unit area per plate

K = thermal conductivity of the plate

In the fuel cell the thermal resistance between the plates is quite low so that the temperatures of both plates are very nearly equal. Therefore the plates remove heat depending upon their thicknesses and practically independent of which side of the cell the heat is generated.

Average values of the plate thicknesses can therefore be used. For the cell plate substituting $q_P = \frac{q}{2}$, $\delta = \frac{\delta_a}{F_\ell}$ and $\gamma = \frac{\ell_1}{2}$

then

$$\delta_a = \frac{q \ell_1^2 F_\ell}{16 K \Delta T_1} \tag{7-3}$$

where: ΔT_1 = permissible temperature difference between edge and center of cell (determined from operating characteristics)

F_ℓ = ratio of thermal resistance of plate with manifold grooves to the thermal resistance of an equal thickness plate of the same material without grooves

K = thermal conductivity of plate material

q = cell cooling load per unit cell area per unit time

The value of q is given as the heat produced per unit area per cell by the hydrogen-oxygen reaction minus the heat removed with the product water per unit area,

$$q = \frac{U - U'}{N A} \qquad (7\text{-}4)$$

where: $U = P\left(\frac{1}{.67\ E} - 1\right)$ watts

U' = (.240) I. N watts with the fuel cell operating at 93.3° C (see page 8)

P = power supplied by the fuel cell in watts

I = total current in amperes at rated load

E = voltage per cell at rated load

N = number of cells comprising the fuel cell reactor

Choosing to eliminate δ_a and ℓ_2 by combining Equations (7-1) through (7-4) yields weight as a function of ℓ_1 :

$$W = C_1 \ell_1^2 + C_2 \ell_1 + C_3 + \frac{C_4}{\ell_1} \qquad (7\text{-}5)$$

where the constants are:

$$C_1 = \frac{\rho_1 F_W F_\ell}{8 K \Delta T_1} \left(\sqcup - \sqcup' \right)$$

$$C_2 = 2N \left(2\rho_1 \delta_S \ell_S + 4\rho_P \delta_P \ell_S \right) + 2\rho_C \delta_C \ell_C$$

$$C_3 = 2N \left(2\rho_P A \delta_P F_P \right) + 4\rho_C \delta_C \ell_C \ell_S$$

$$C_4 = 2NA \left(2\rho_1 \left[\ell_S \delta_S + \ell_F \delta_F \right] + 4\rho_P \delta_P \left[\ell_S + \ell_F \right] \right)$$

$$+ 2A \rho_C \delta_C \ell_C$$

Since only weight variation is being considered, the term, C_3, that does not involve ℓ_1 may be omitted.

The derivative of Equation (7-5) can be set equal to zero and the resulting cubic equation solved to obtain the minimum weight configuration. However, more information is gained in a particular application by evaluating the constants in Equation (7-5) and plotting W versus ℓ_1. The optimum value of ℓ_1 is then selected from this graph and optimum values of ℓ_2 and δ_a are determined by substituting this value of ℓ_1 into Equations (7-2) and (7-3). The weight penalties for off-optimum dimensions are also shown by the curve.

This procedure determines cell dimensions for minimum system weight consistent with physical restraints and performance requirements. Weight penalties are also obtained from the resulting W, ℓ_1 curve for use when analyzing a system from standpoints other than minimum weight.

7.4 Thermal Design of the Fuel Cell Module

In the preceding section, the thermal design of fuel cell plates was discussed. Experimental measurements of temperature profiles within an operating cell have been performed to determine the validity of that analysis.

In the theoretical analysis, several simplifying assumptions were made. One of the assumptions was that heat loss along the axis of a module, or perpendicular to the individual plates, is negligible. In order to accomplish this in the fuel cell test module, end plates were fabricated of a heavy phenolic material. These end plates reduced the heat loss to about 0.25% of that for magnesium end plates. In addition, the test cell was the center cell of five cells, which further reduced heat flow in the axial direction and more nearly simulated the thermal conditions within a cell in a module comprised of a large number of cells. A total of 24 thermocouples were placed in the cell as illustrated in Figure 24. Additional thermocouples monitored the temperature at an outside

corner of each cell and the temperature of the center of the phenolic end plates. The measurements from these thermocouples confirmed that heat loss through these end plates was very small and could be considered negligible.

Another assumption made in the analysis was that there was a negligible temperature difference between the hydrogen and oxygen sides of a cell at any point. This test showed that this assumption can be considered true for design purposes. The temperature difference between a thermocouple on the oxygen side of the fuel cell and one directly opposing it on the hydrogen side was found to be less than 1° C at loads up to 175 ma/cm^2 (30 amperes). Loads above this level would have required a cooling system with greater heat transfer rates than the natural convection cooling used for the test.

Another assumption in the analysis was that heat flux from the two finned sides of the plates was uniform and no heat was transferred from the reactant manifold sides of the cell. This assumption was not closely approached in the experimental setup. The temperature profile measurements showed a substantial heat loss through the manifold ends of the cell. This was due to the method of cooling used in the experimental setup and does not invalidate the assumption for a system using a complete cooling system. The temperature profile of the portion of the cell midway between the manifold ends was least affected by these end losses. The temperature differences measured between positions in this portion of the cell were within 0.5° C of the predicted values.

The effect of Static Vapor Pressure Control System on heat removal was illustrated during these tests. With the moisture removal system operating normally, the temperatures would be very uniform and stable. If the shutoff valve for the water removal system was then closed, the temperatures throughout the cell would rise about 4 - 5° C within 30 seconds and then stabilize at this level or climb very gradually until the water removal system was placed back into operation.

In summary it can be concluded that two assumptions in the theoretical analysis were verified and can be considered correct for design purposes.

(1) Heat loss perpendicular to the individual plates, or through the end plates can be reduced to a negligible amount.

(2) Temperature differences between the hydrogen and oxygen sides of the cell are negligible for present operating current densities.

The assumptions that heat loss from the reactant manifold area was negligible and that heat flux from the finned area was uniform were not duplicated in the experimental setup due to the method of cooling used.

7.5 System Cooling Integration Studies

Waste heat energy may be rejected from a space vehicle in the form of radiation or in the form of internal energy of a disposable material. Selection of the heat sink for a particular mission will depend upon factors such as mission duration, heat load, vehicle configuration, and vehicle environment. General weight optimization studies can adequately considered only the first two of these factors.

For the analysis it was assumed that a suitable primary coolant (water-glycol, water-methanol, etc.) would be utilized in conjunction with a vehicle water evaporator or sublimer heat rejection system as the normal mode of operation. Then the weight trade-off existed between the water required to reject the heat burden plus the elimination of an internal secondary coolant loop in the FCA versus extra mechanical controls or equipment utilized to effect the use of the alternates.

The conceivable alternates considered were:

(1) Utilizing the main propellant rocket tank hydrogen boil-off (hydrogen-oxygen powered vehicle) as a source of direct coolant into the FCA if it were available in quantities required.

(2) Carrying excess hydrogen in the fuel cell hydrogen supply tankage to reject the FCA thermal burden.

(3) Using vehicle propellant boil-off as a coolant in a tube and shell heat exchanger design.

Of the alternate approaches considered, only the one utilizing the main hydrogen propellant rocket tank hydrogen boil-off as a source of direct coolant provided an overall system weight saving. The weight savings was estimated at 1.8 pounds per kilowatt hour.

Further studies have shown that for most mission applications, radiators will provide a much lighter vehicle heat sink that either an evaporator or sublimer.

REPRESENTATIVE FUEL CELL PERFORMANCE AT VARIOUS ELECTROLYTE CONCENTRATIONS

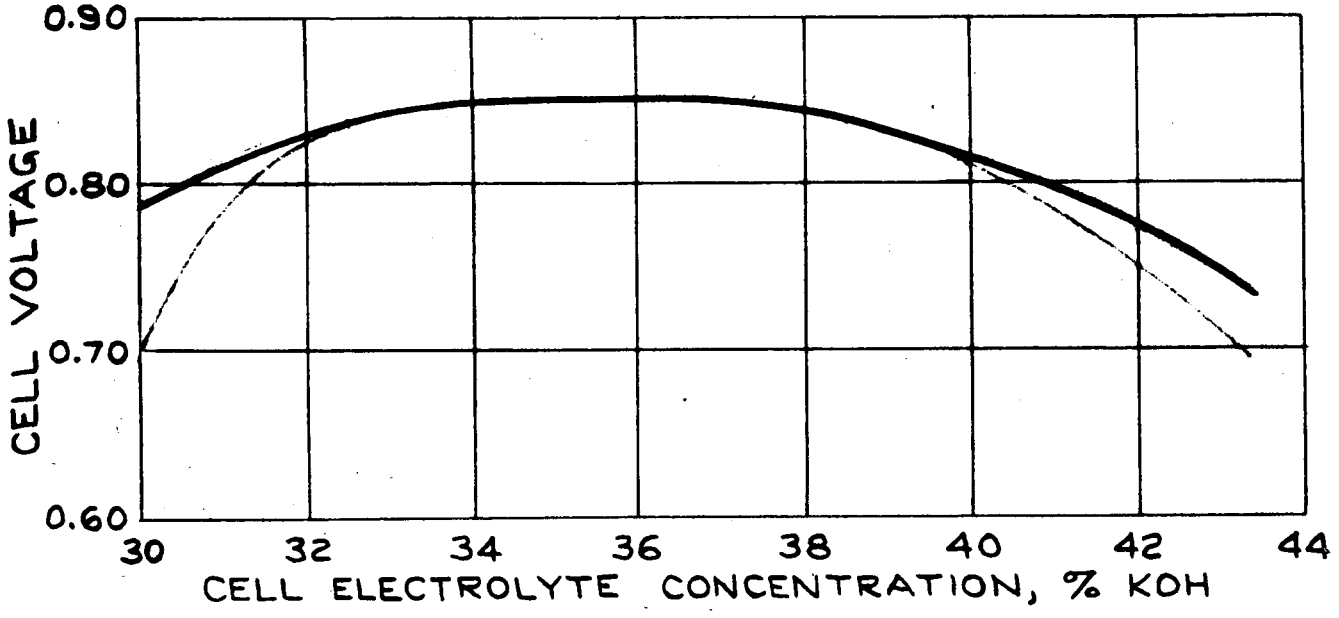

CELL PRESSURE = 30 PSIA
CELL TEMPERATURE = 200° F.

FIGURE 1

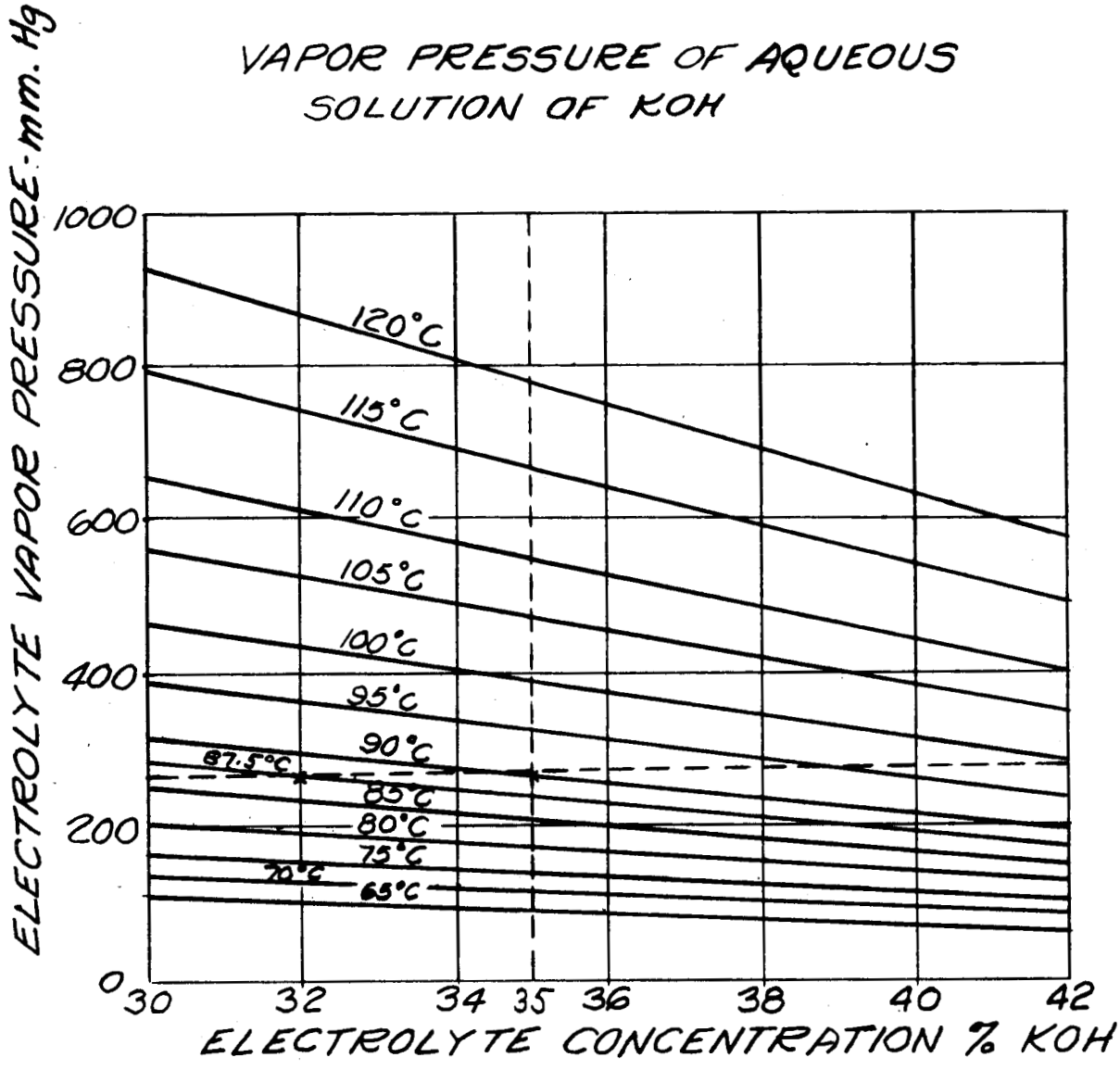
VAPOR PRESSURE OF AQUEOUS SOLUTION OF KOH
ELECTROLYTE VAPOR PRESSURE-mm. Hg
1000
800
600
400
200
0
120°C
115°C
110°C
105°C
100°C
95°C
90°C
87.5°C
85°C
80°C
75°C
70°C
65°C
30
32
34
35
36
38
40
42
ELECTROLYTE CONCENTRATION % KOH

FIGURE 2

FUEL CELL CONSTRUCTION USING STATIC MOISTURE REMOVAL SYSTEM

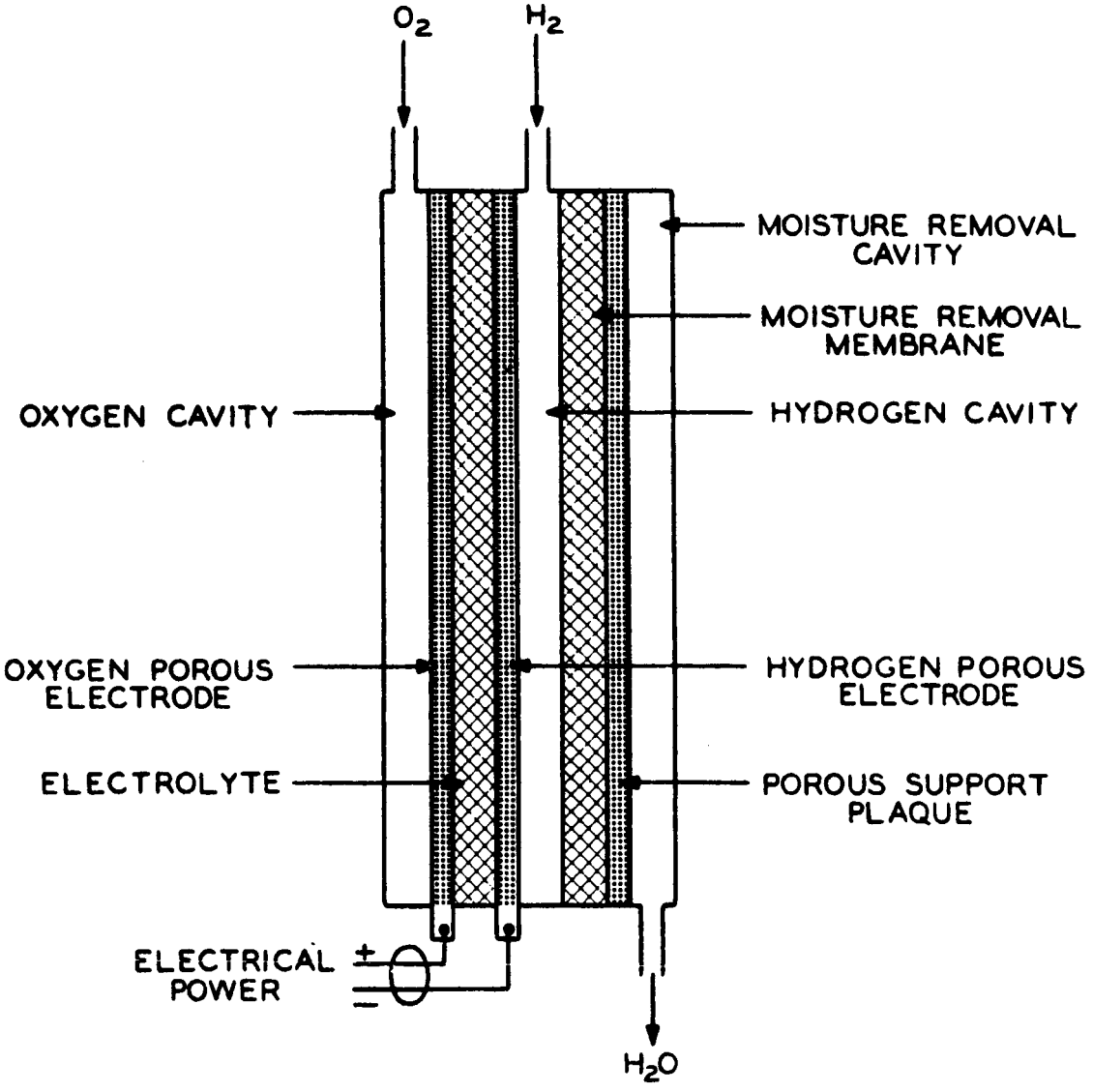

FIGURE 3

SIMPLIFIED REPRESENTATION OF A CELL OPERATING WITH STATIC MOISTURE REMOVAL

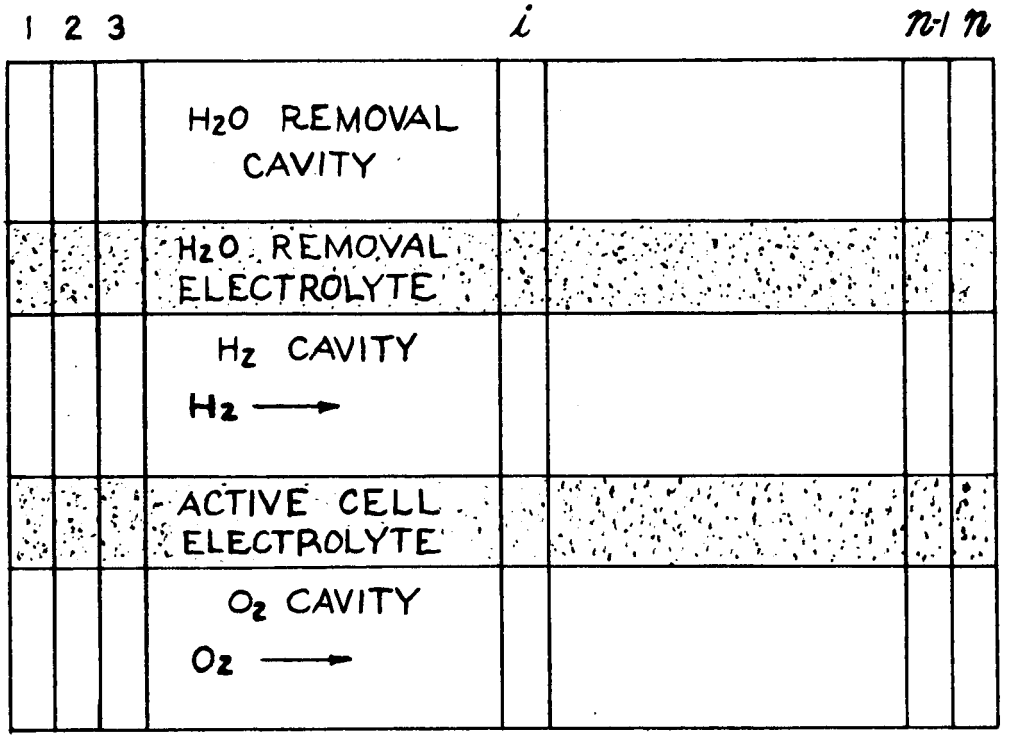

FIGURE 4

GAS CHROMATOGRAPH TEST SET-UP
STATIC VAPOR PRESSURE CONTROL SYSTEM

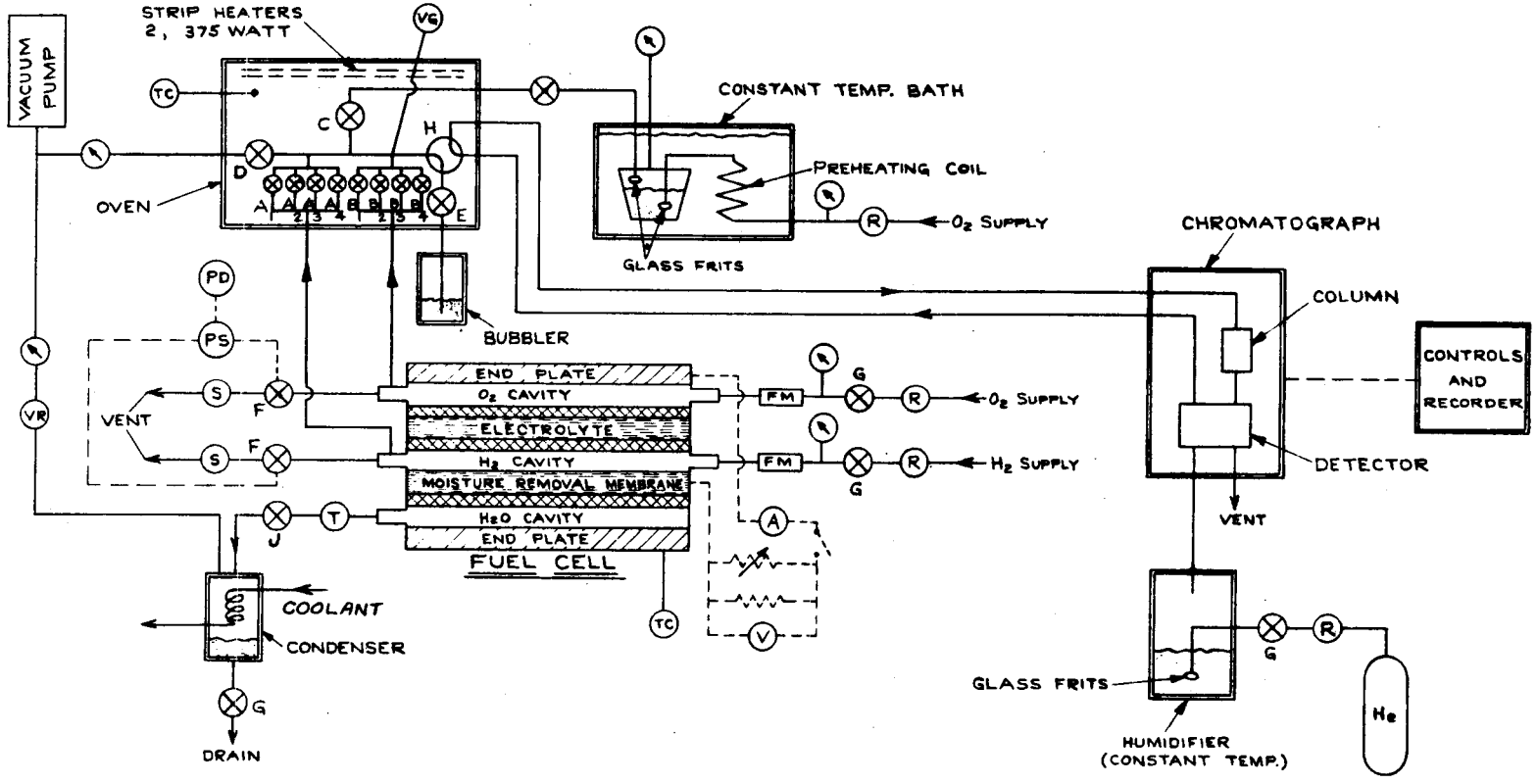

A - H_2 SAMPLING VALVE
B - O_2 SAMPLING VALVE
C - BATH SAMPLING VALVE
D - VACUUM VALVE
E - EXPANDER VALVE
F - PURGE RATE VALVES
G - SHUT OFF VALVES
H - SAMPLE VALVE
J - CAVITY PRESSURE REGULATOR

(PD) PURGE DURATION TIMER
(PS) PURGE SEQUENCE TIMER
(VR) VAPOR REGULATOR
(S) SOLENOID VALVE
(T) TRANSDUCER
(TC) TEMPERATURE CONTROLLER
(VG) VACUUM GAUGE
(R) REGULATOR

(FM) FLOW METER

(V) VOLTMETER
(A) AMMETER
(⊗) NEEDLE VALVE
(↖) GAUGE

FIGURE 5

W.P.B. 5-16-63

WATER VAPOR PRESSURE DISTRIBUTION IN A CELL USING STATIC MOISTURE REMOVAL WITH PARALLEL FLOW OF REACTANTS

TEMPERATURE: 88°C
PRESSURE: 2 ATM.
CURRENT DENSITY: 175 ma/cm²
H_2O CAVITY PRESSURE: 240 mm Hg
CELL LENGTH: 15.9 cm

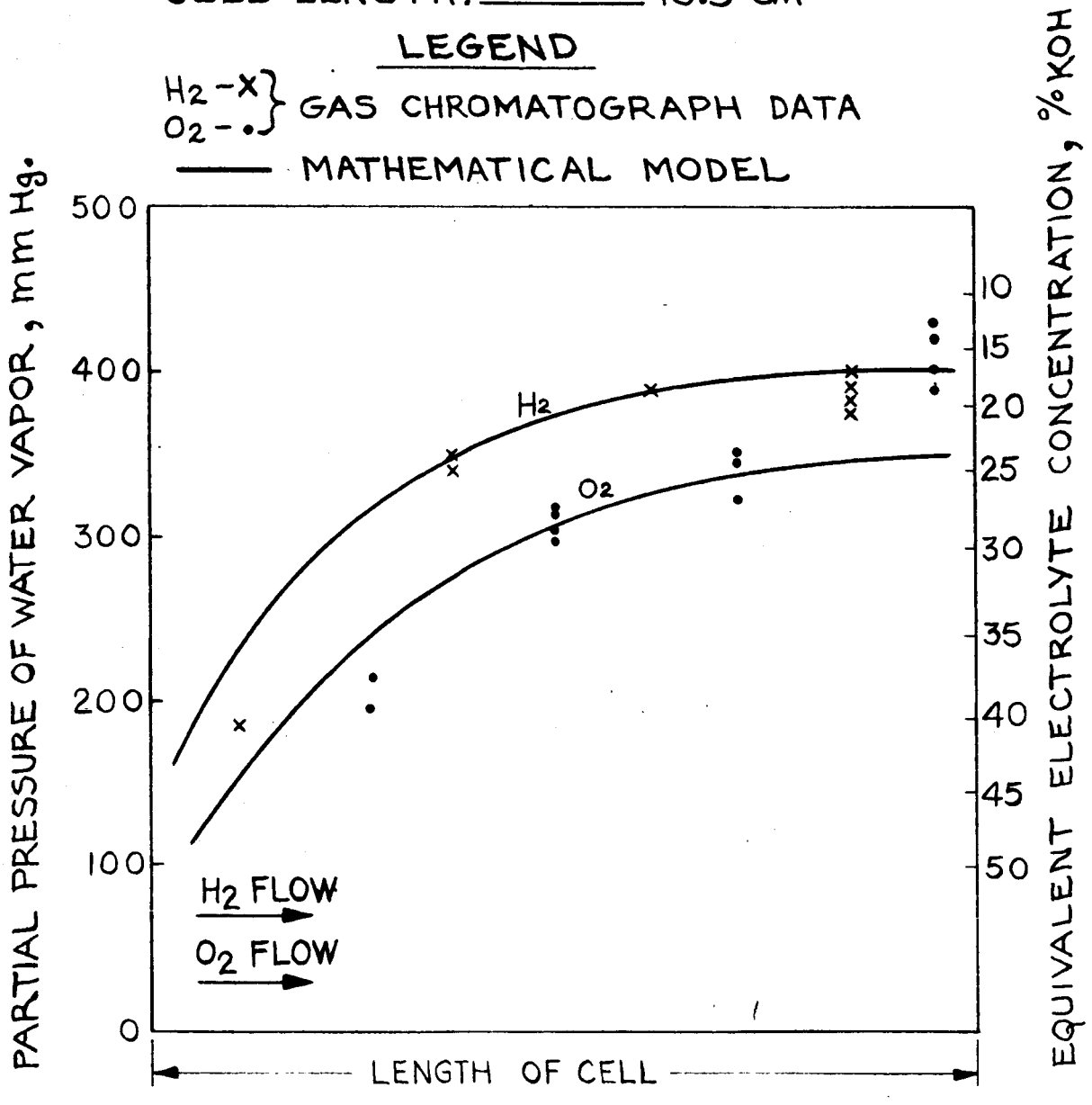

FIGURE 6

WATER VAPOR PRESSURE DISTRIBUTION IN A CELL USING STATIC MOISTURE REMOVAL WITH COUNTER FLOW OF REACTANTS

TEMPERATURE _____ 88°C
PRESSURE _____ 2 ATM.
CURRENT DENSITY ____ 175 mA/cm²
H_2O CAVITY PRESSURE ____ 240 mm Hg
CELL LENGTH _____ 15.9 cm

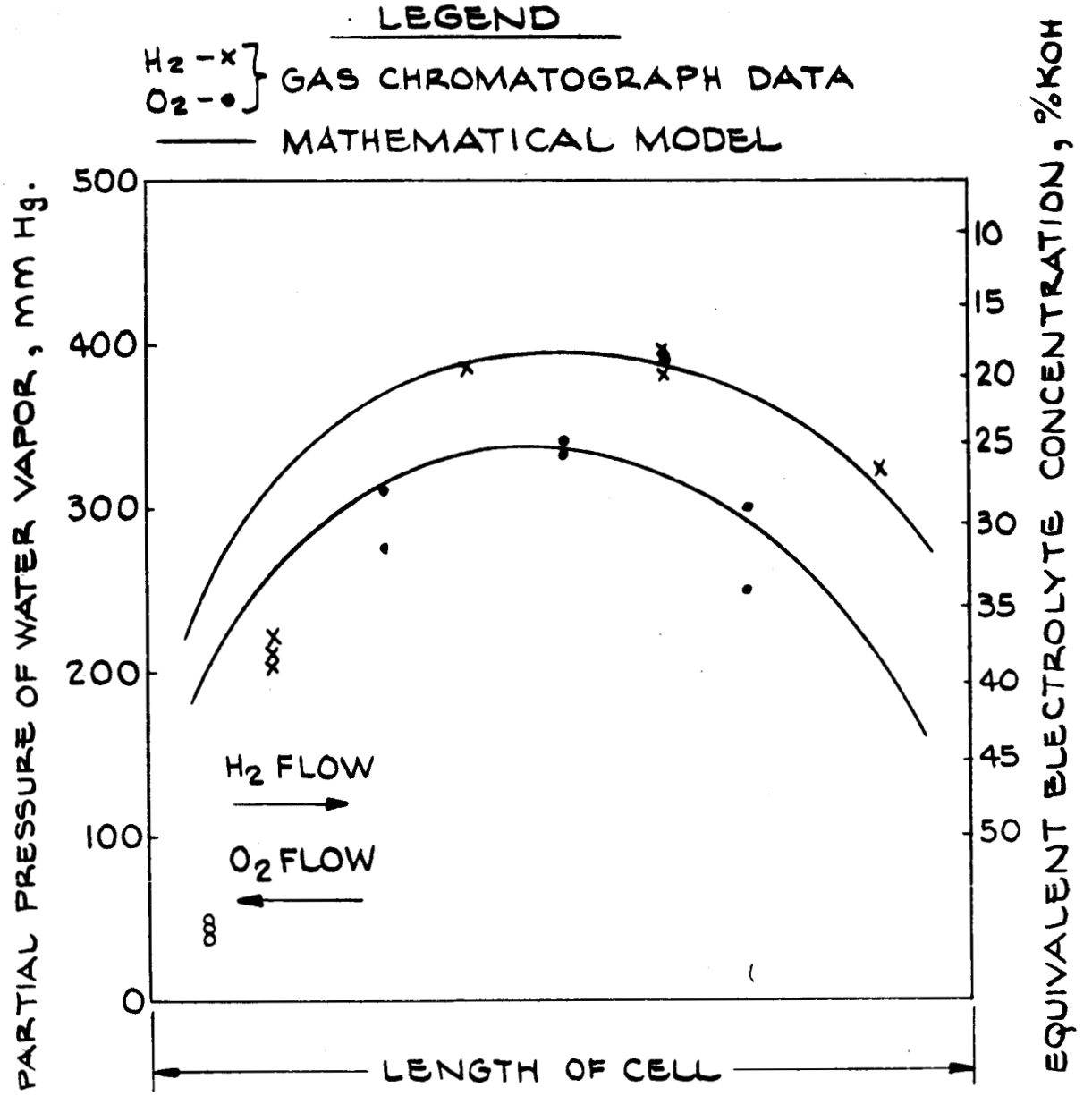

FIGURE 7

STATIC FOUR CELL MODULE SYSTEM SCHEMATIC

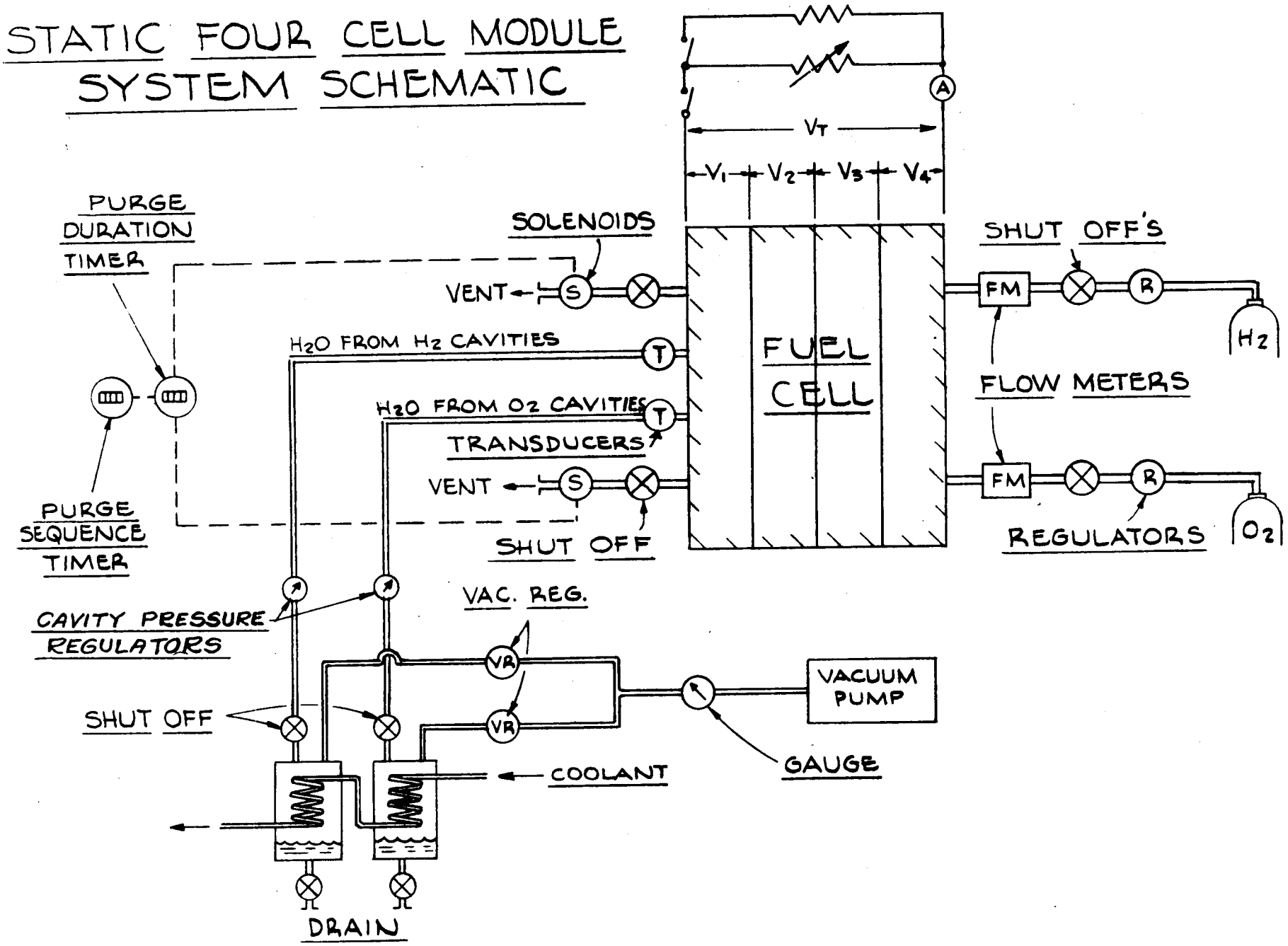

FIGURE 8

ISK63128-6
PLB 5-8-63

STATIC MOISTURE REMOVAL SYSTEM FOR THE H_2-O_2 FUEL CELL

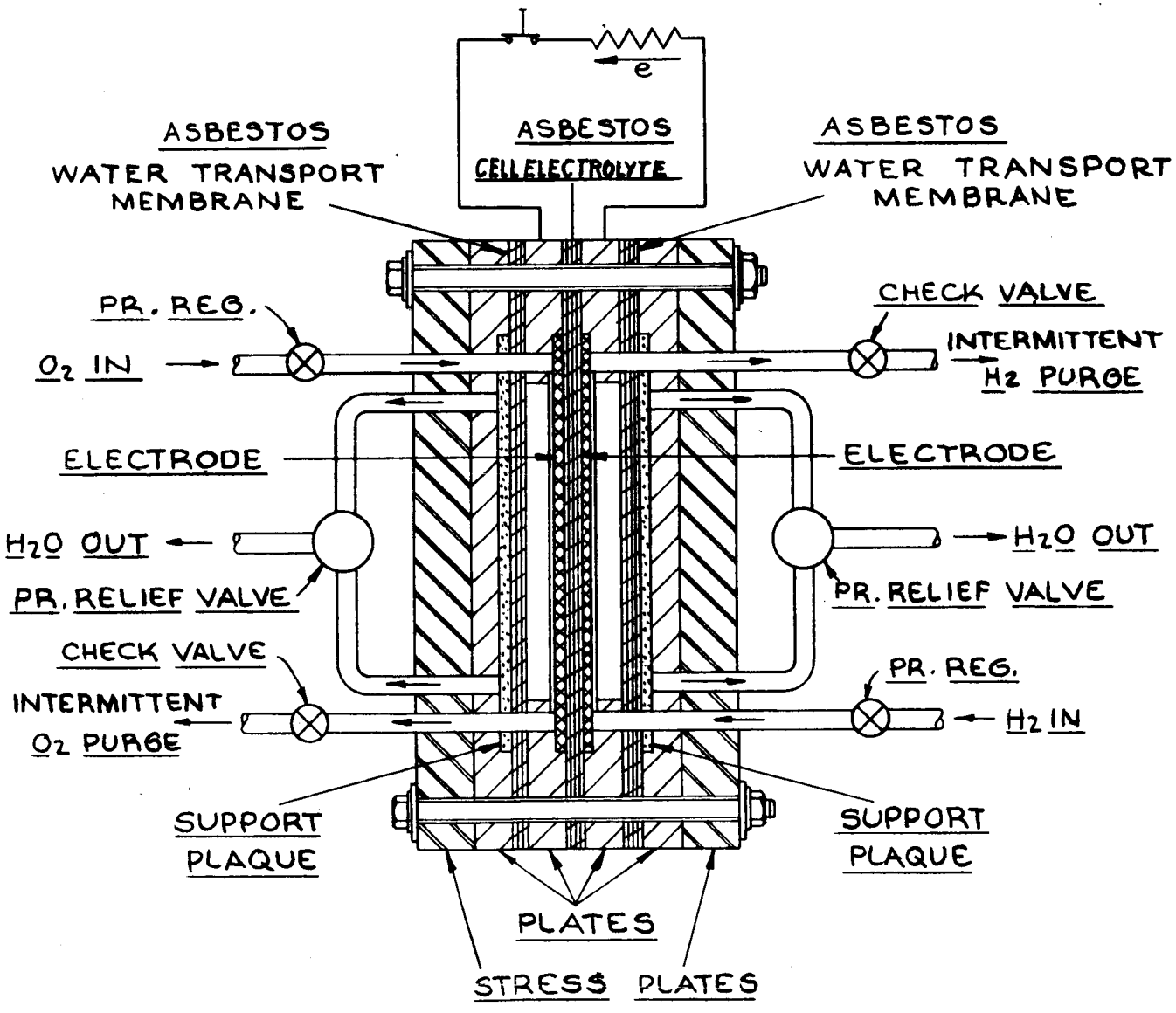

FIGURE 9

FOUR CELL MODULE TEST-Nº 4
STATIC VAPOR PRESSURE CONTROL

CELL PRESSURE = 2 ATMOS.
CELL TEMPERATURE = 79°C

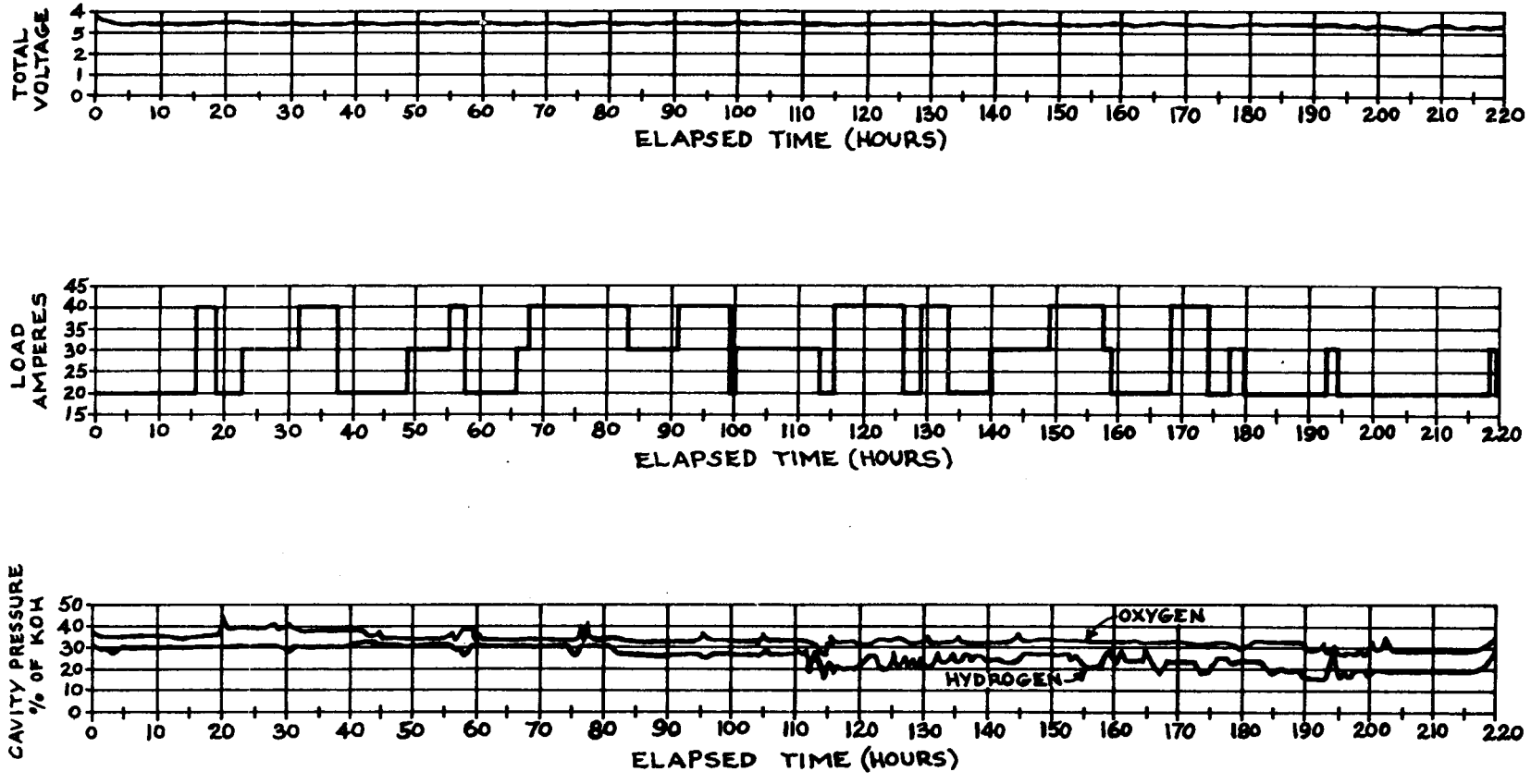

FIGURE 10

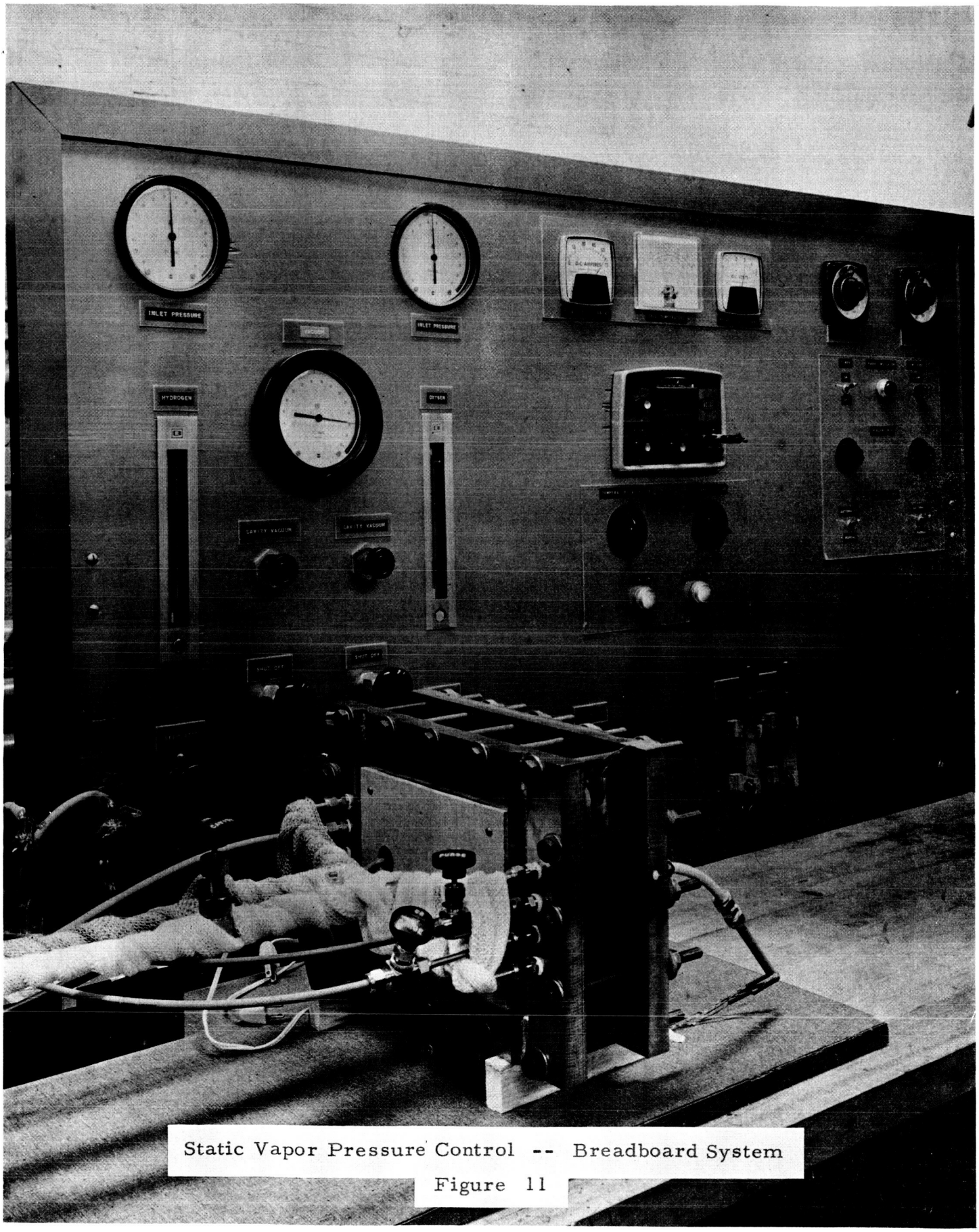

Static Vapor Pressure Control -- Breadboard System

Figure 11

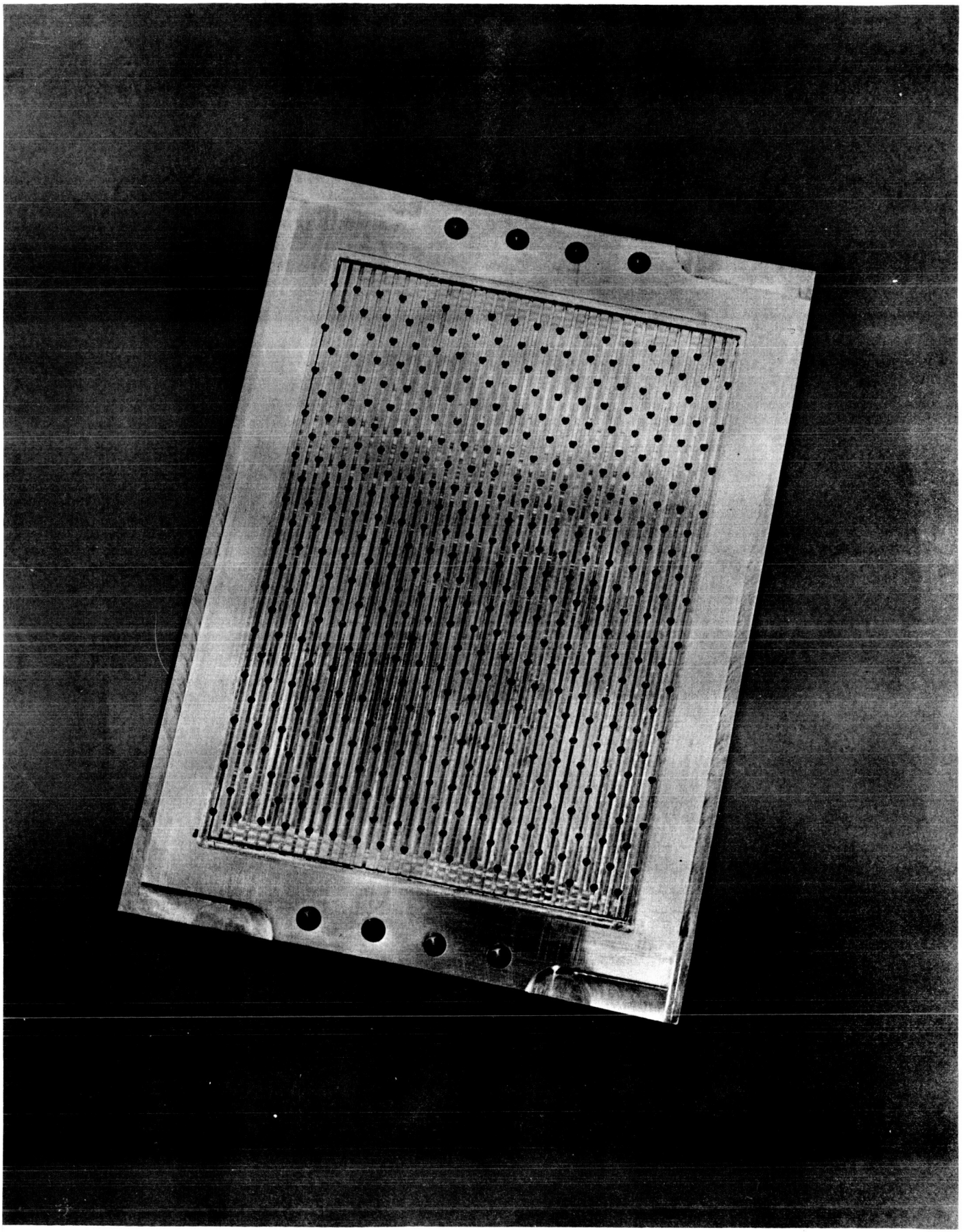

FIGURE 12

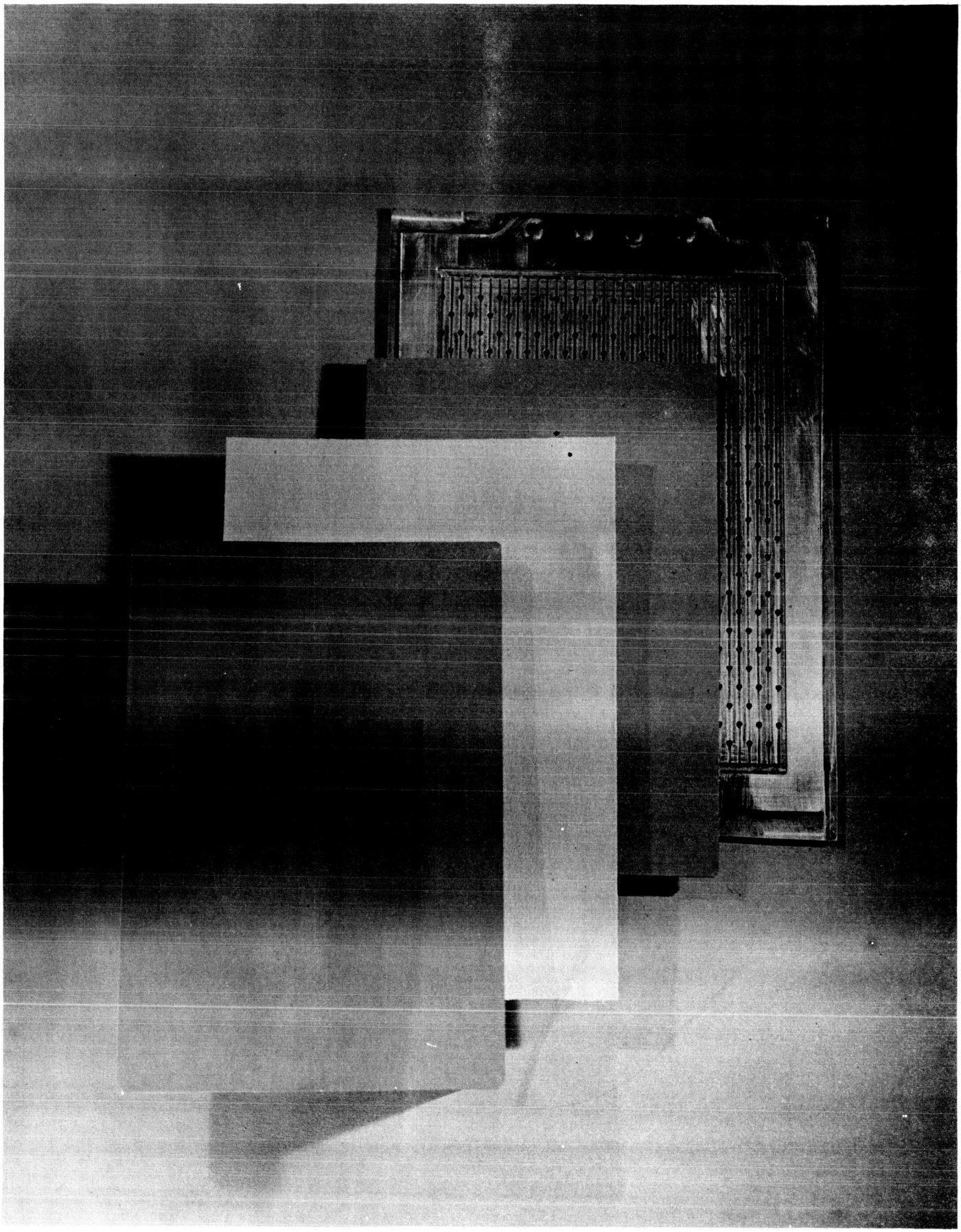

FIGURE 13

EIGHT CELL MODULE TEST, STATIC VAPOR PRESSURE CONTROL

CELL PRESSURE = 2.4 ATMOS. CELL TEMP. = 93° C

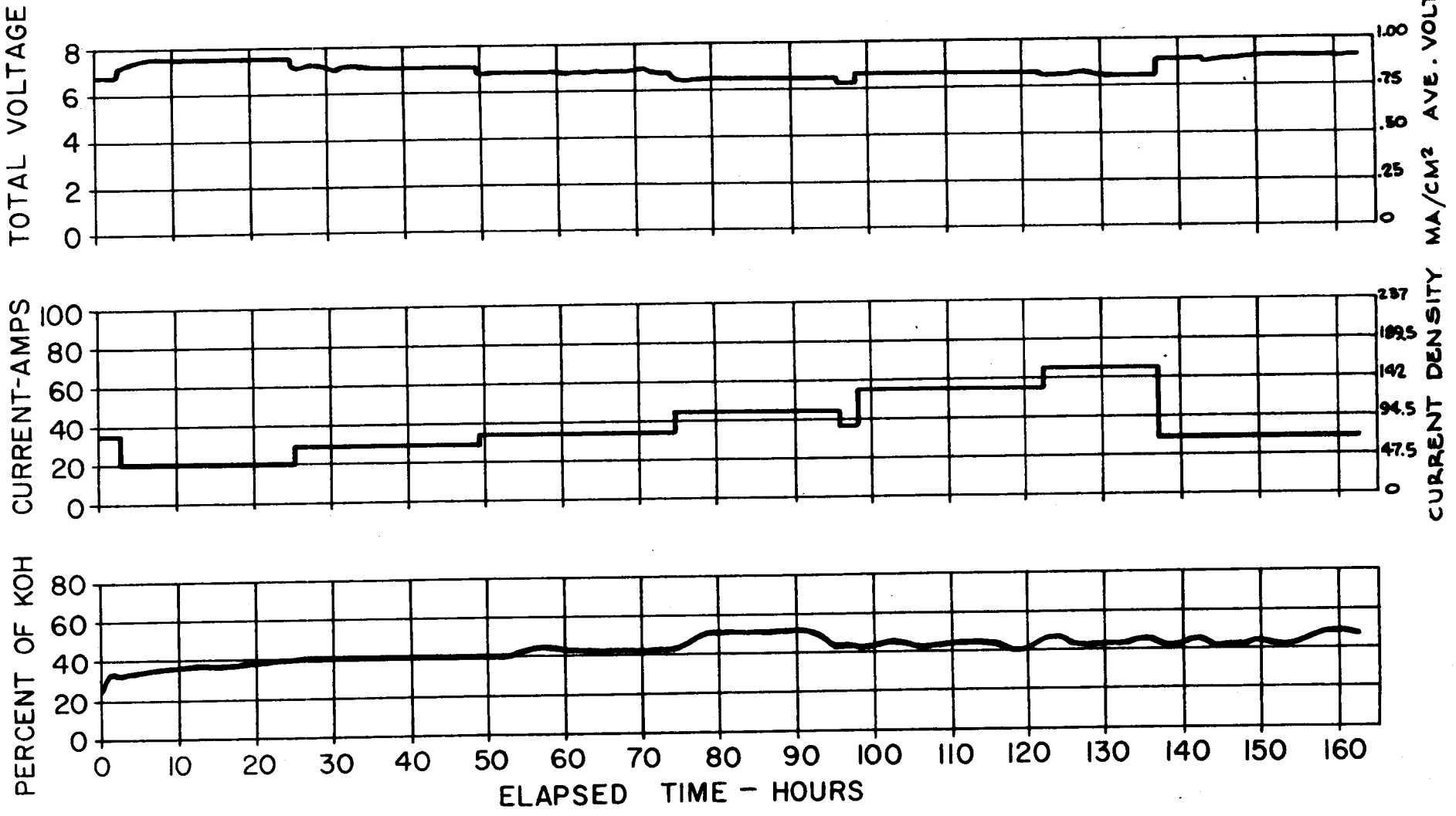

FIGURE 14

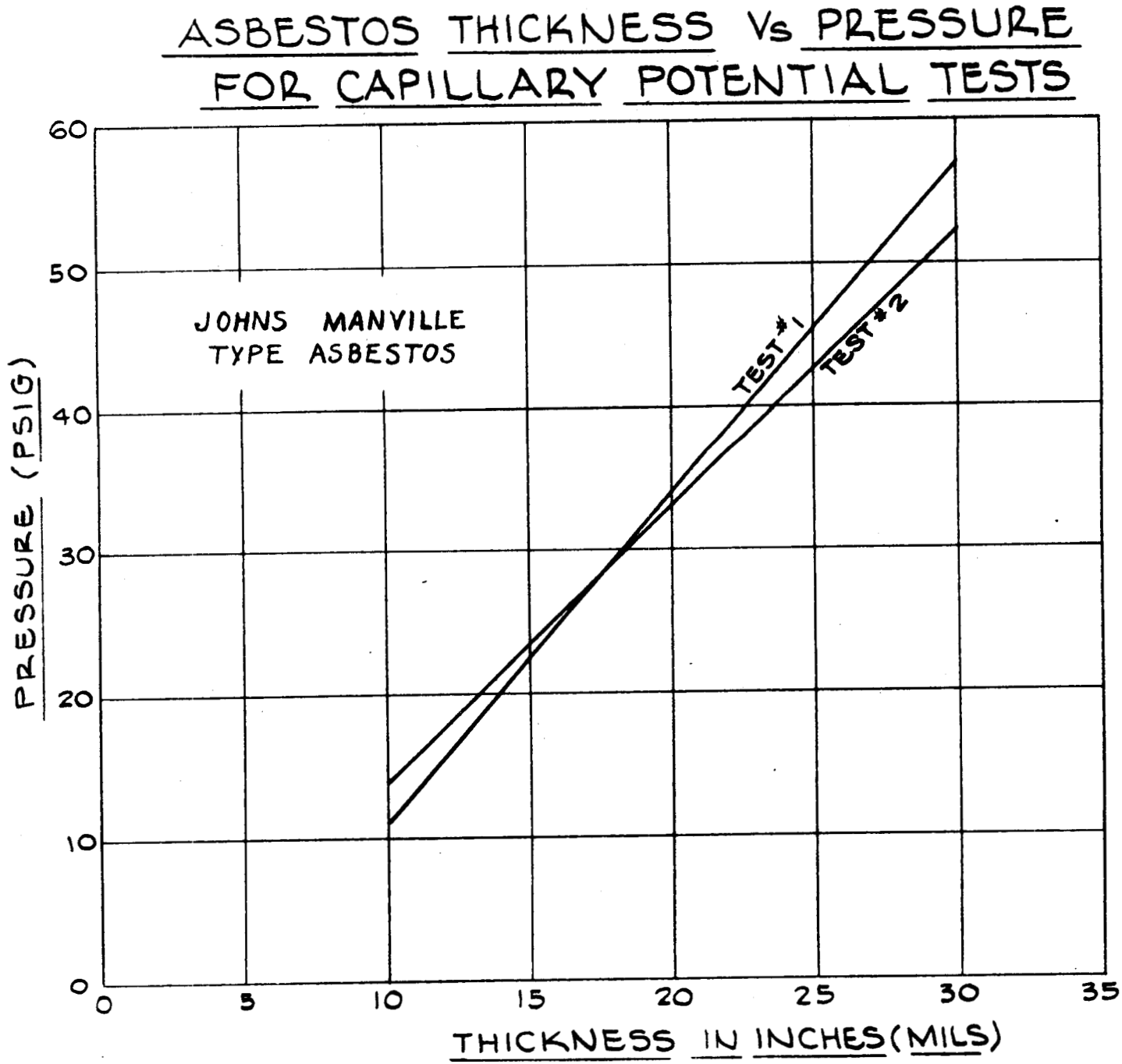
ASBESTOS THICKNESS Vs PRESSURE
FOR CAPILLARY POTENTIAL TESTS
JOHNS MANVILLE
TYPE ASBESTOS
TEST #1
TEST #2
PRESSURE (PSIG)
0
10
20
30
40
50
60
0
5
10
15
20
25
30
35
THICKNESS IN INCHES (MILS)

FIGURE 15

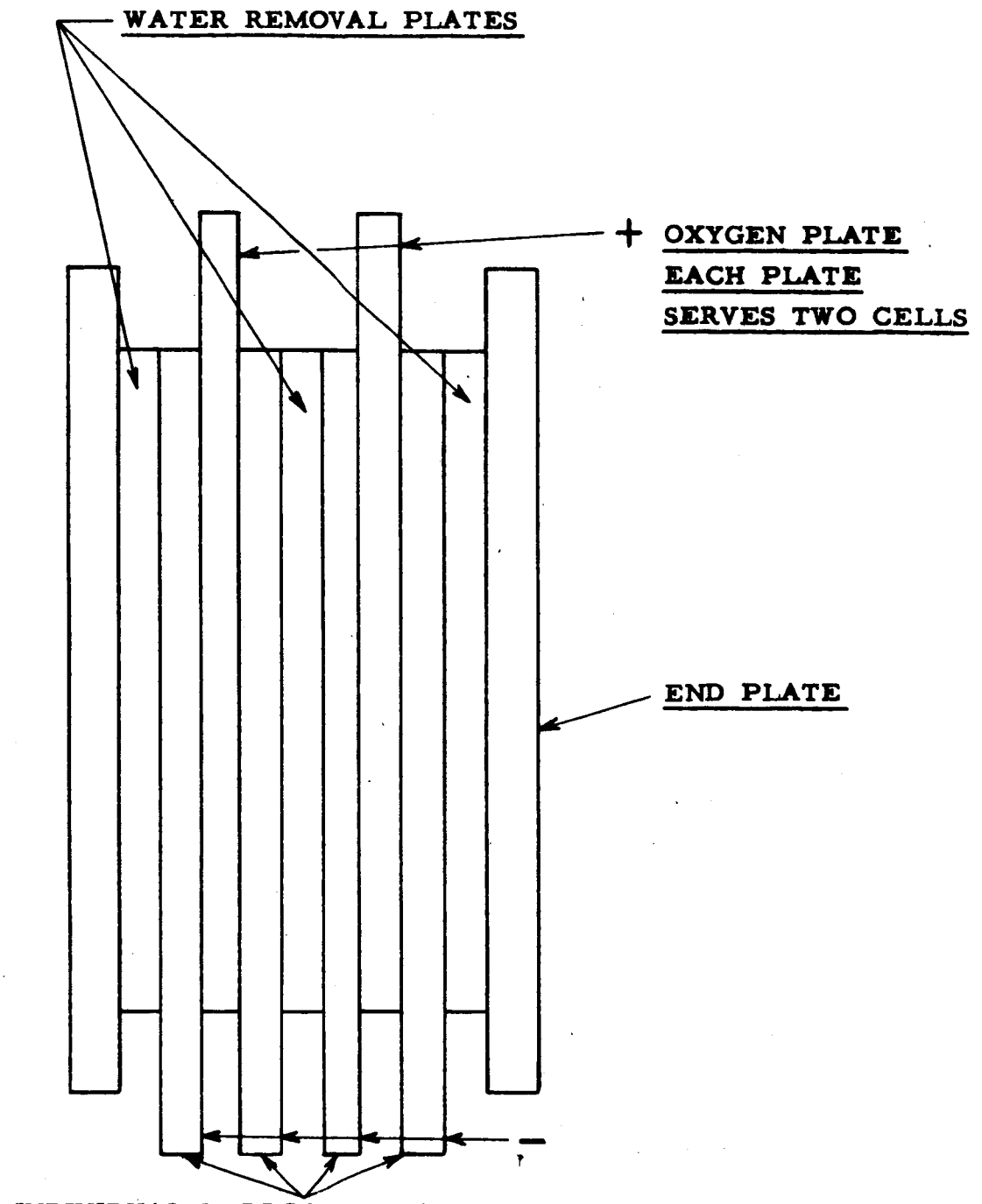

SCHEMATIC OF FOUR CELL PARALLEL TEST MODULE

FIGURE NO. 16

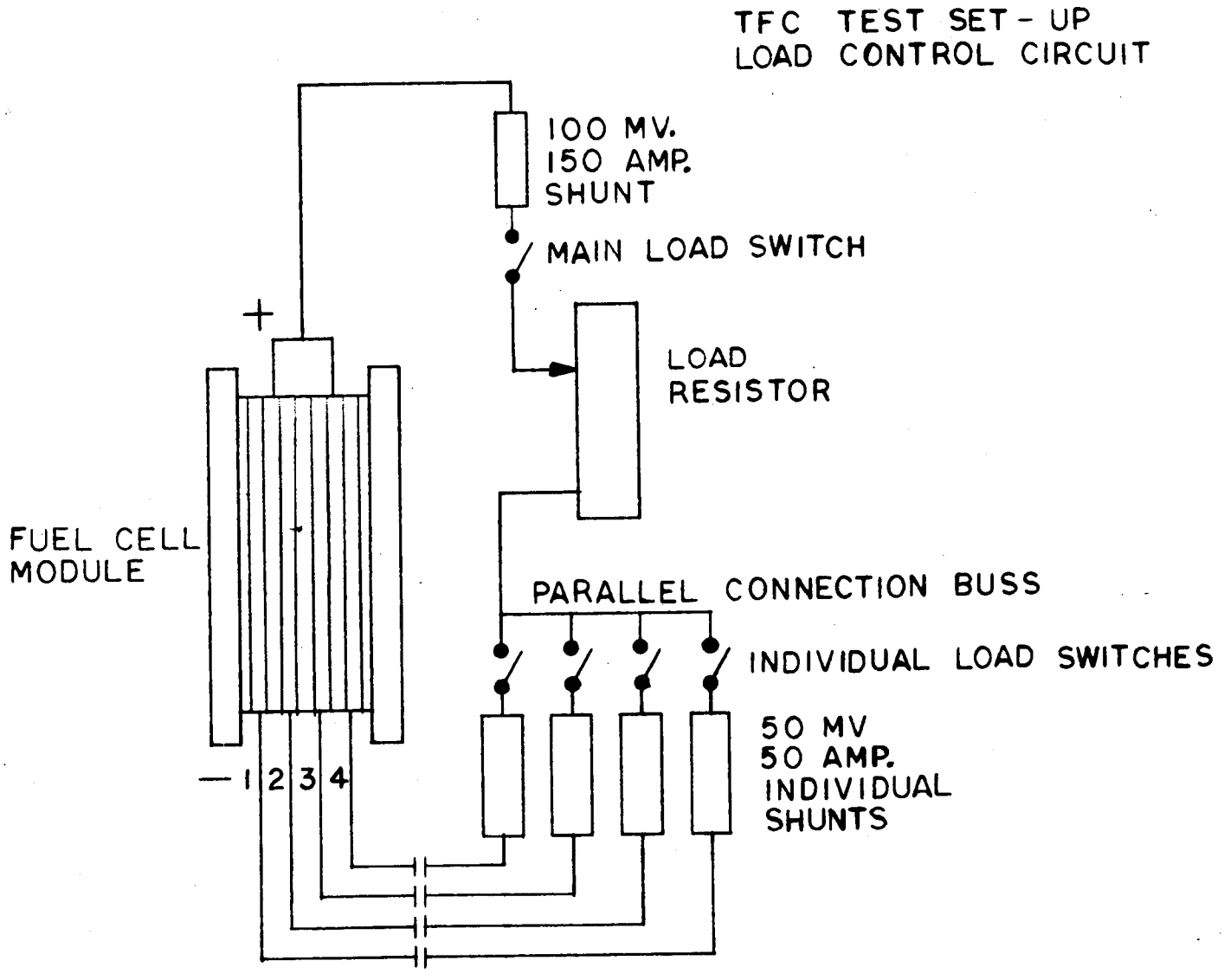
TFC TEST SET - UP
LOAD CONTROL CIRCUIT
100 MV.
150 AMP.
SHUNT
MAIN LOAD SWITCH
LOAD
RESISTOR
+
FUEL CELL
MODULE
PARALLEL CONNECTION BUSS
INDIVIDUAL LOAD SWITCHES
50 MV
50 AMP.
INDIVIDUAL
SHUNTS
— 1 2 3 4

FIG. 17

INDIVIDUAL CELL VOLTAGE-CURRENT CURVES
INCLUDING THE IR DROP TO COMMON POINT

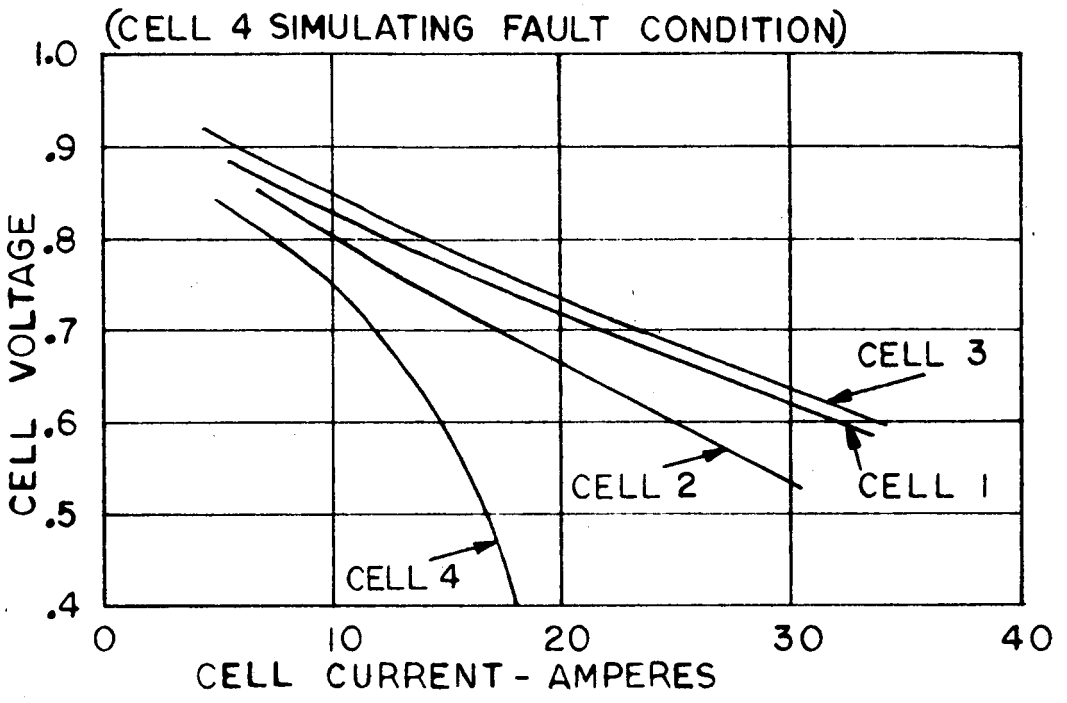

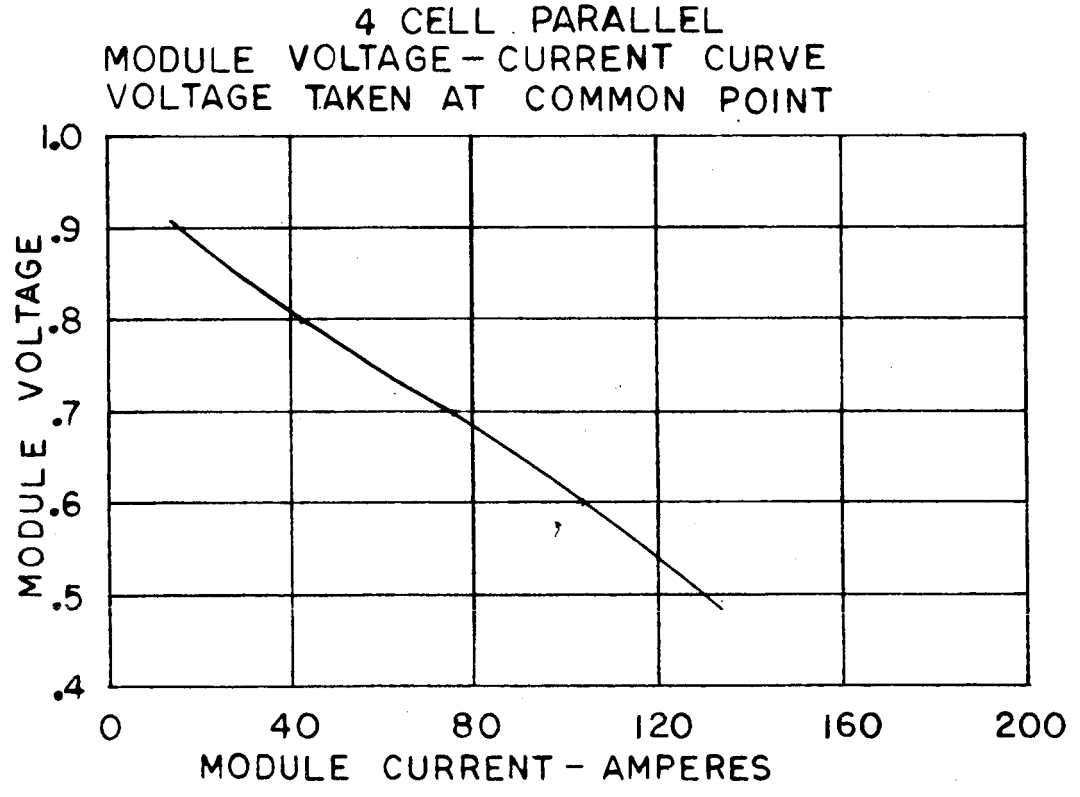

FIG. 18

ELECTRODE CHARACTERISTICS VS PRESSURE

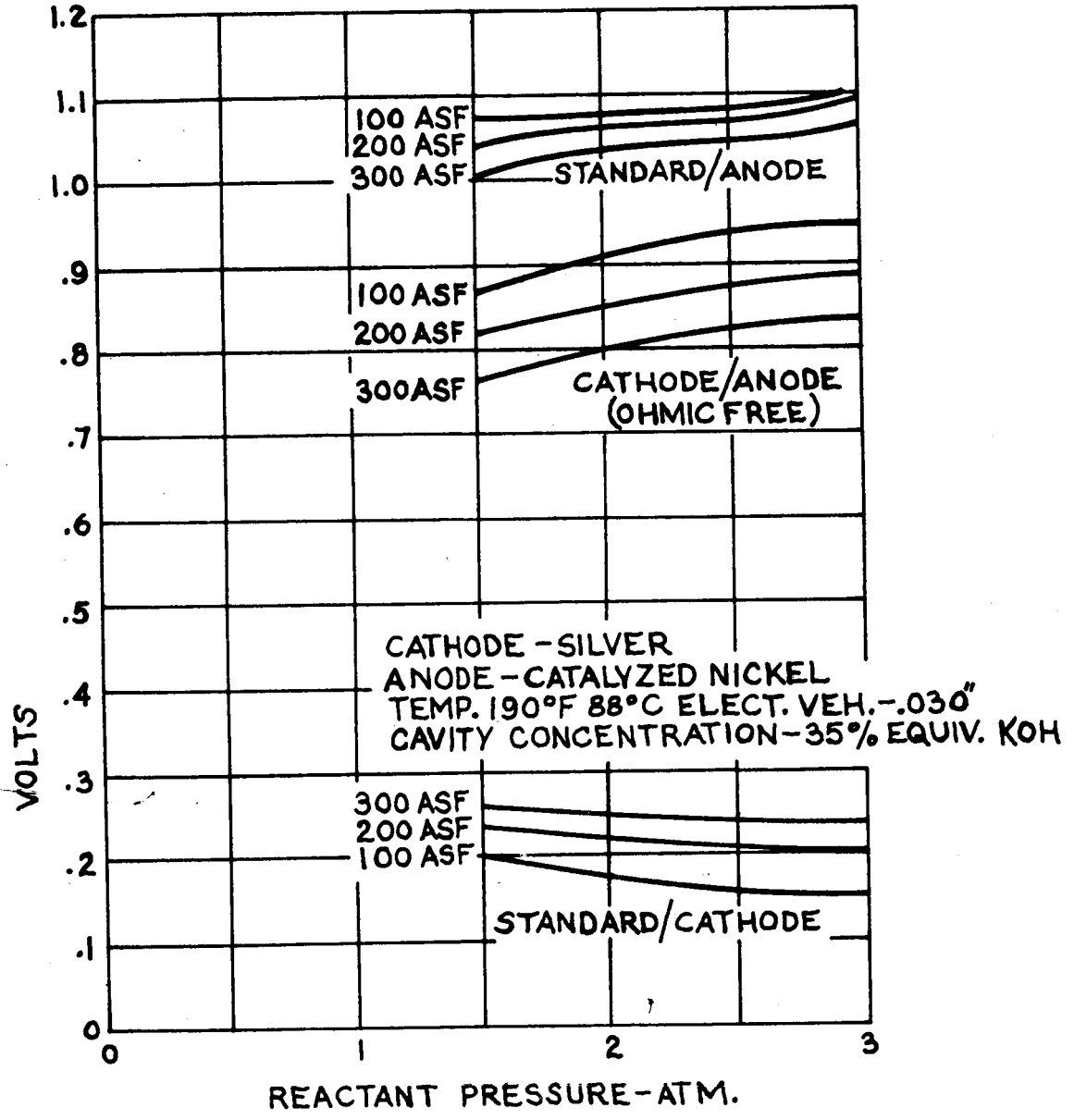

FIGURE 19

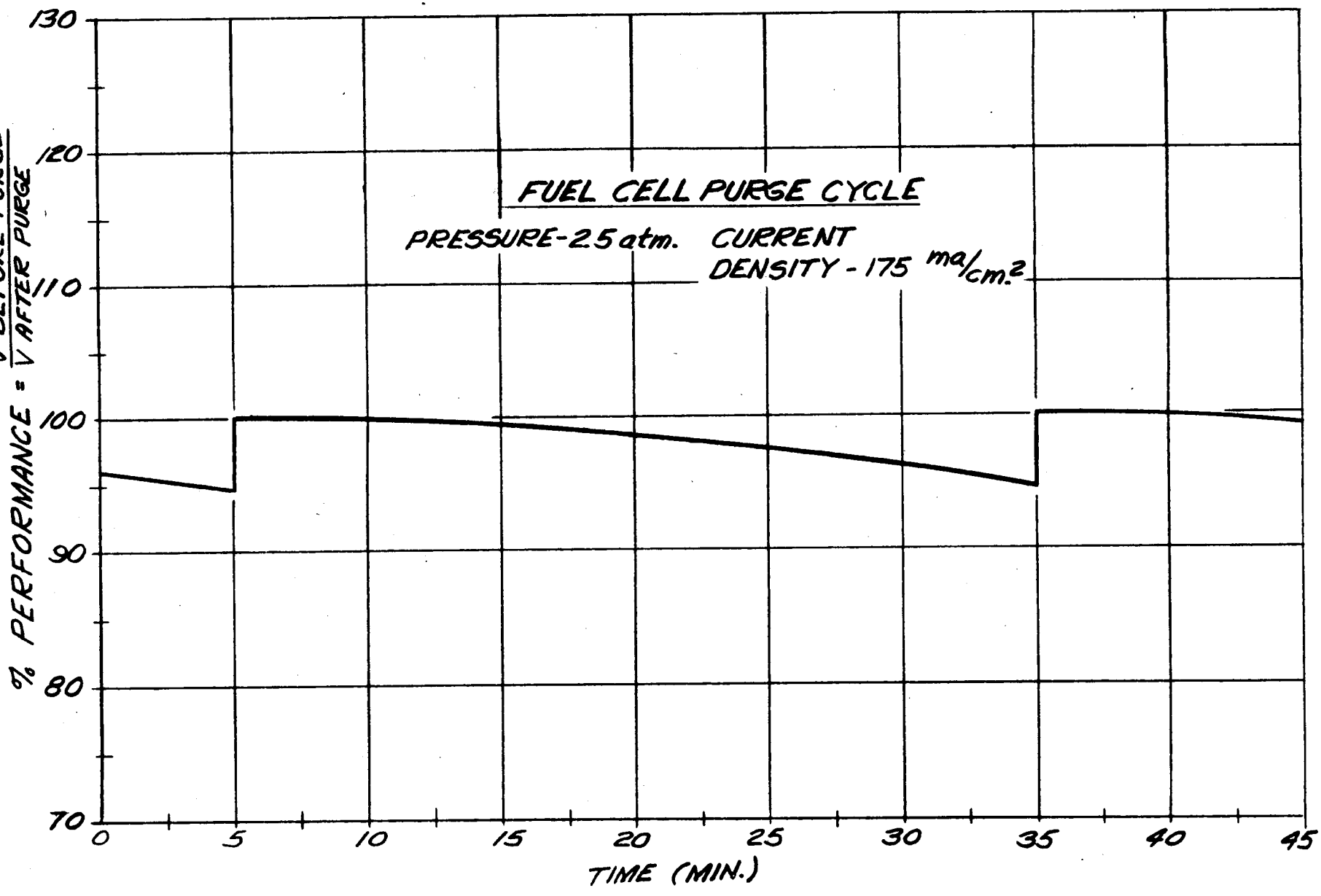
FUEL CELL PURGE CYCLE
PRESSURE-2.5 atm. CURRENT DENSITY - 175 ma/cm.²
% PERFORMANCE = V BEFORE PURGE / V AFTER PURGE
130
120
110
100
90
80
70
0
5
10
15
20
25
30
35
40
45
TIME (MIN.)

FIGURE 20

RELIEF VALVE VACUUM CONTROLLER

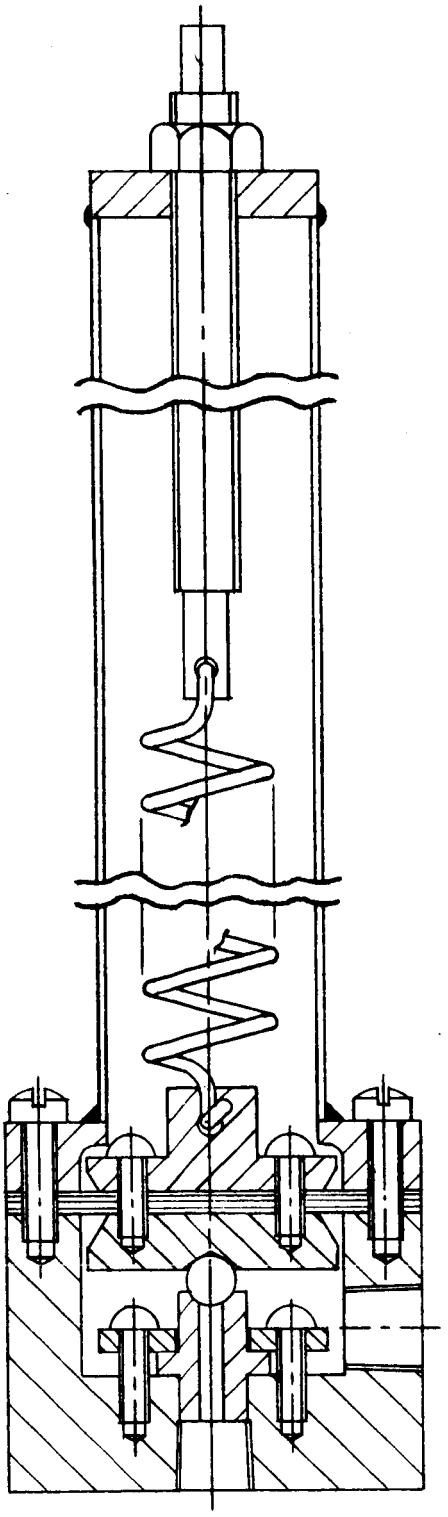

FIGURE 21

ELECTRONIC CAVITY PRESSURE CONTROL

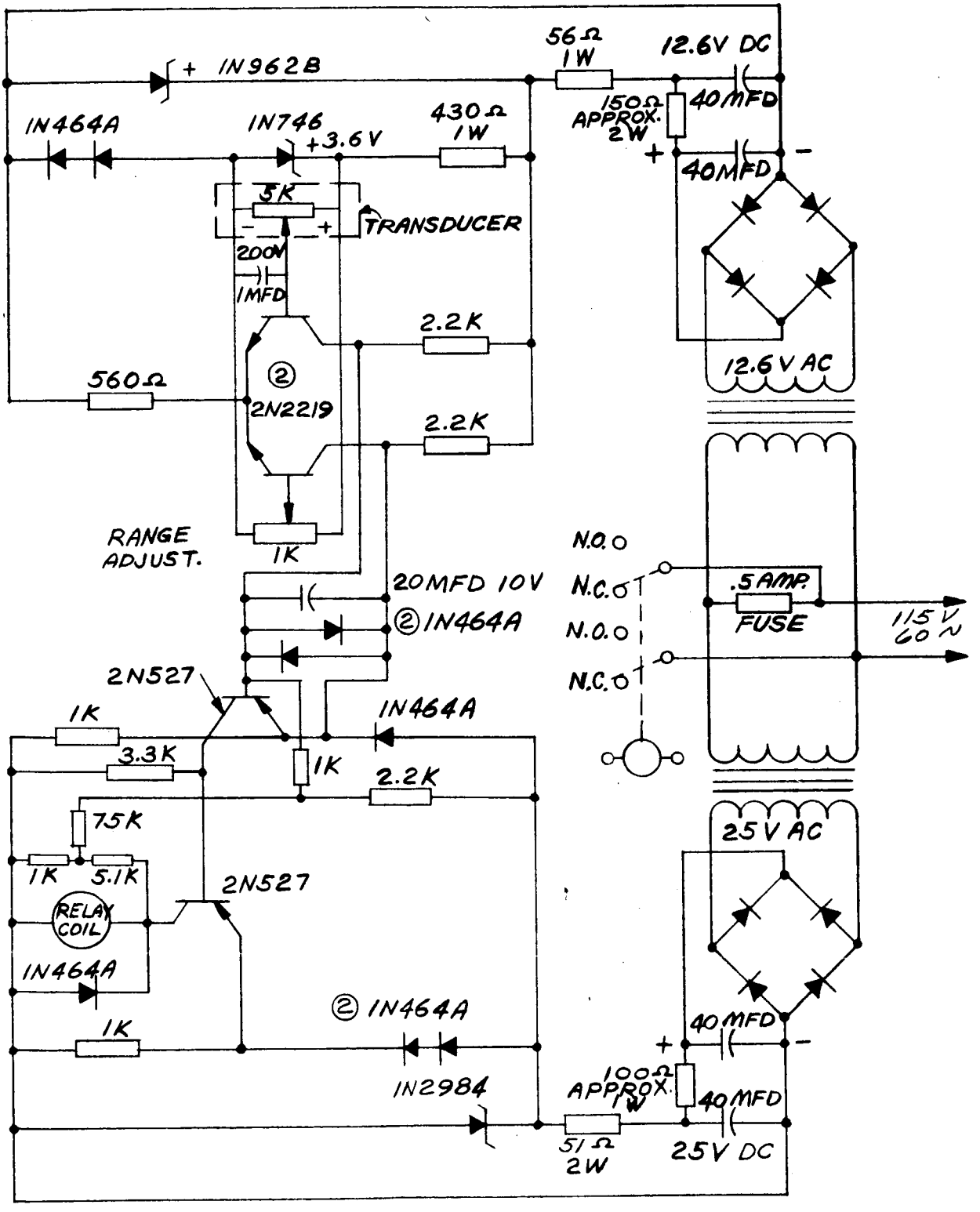

FIGURE 22

DIMENSION MODEL

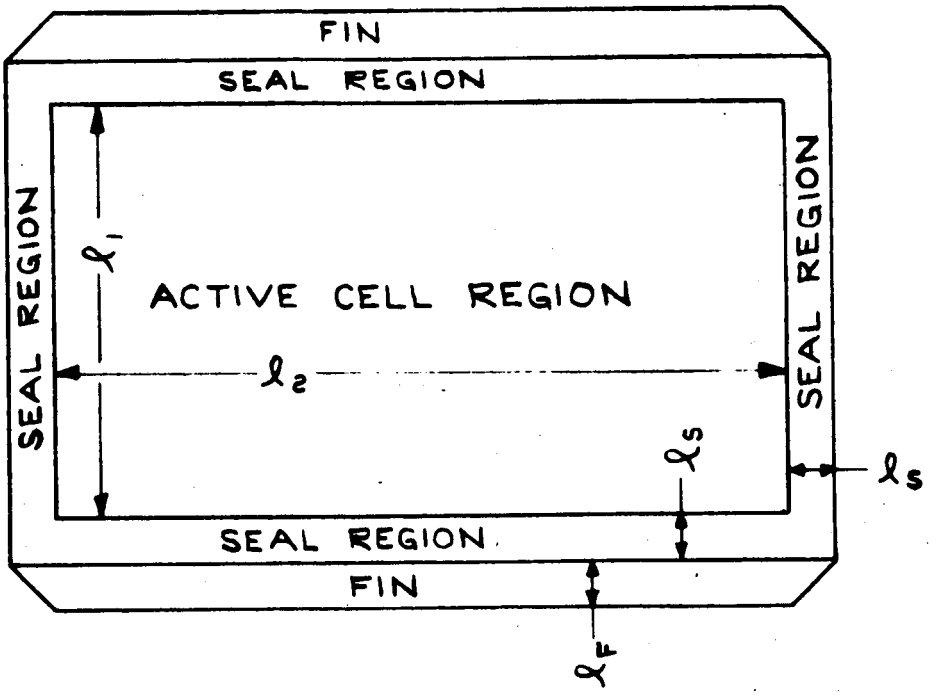

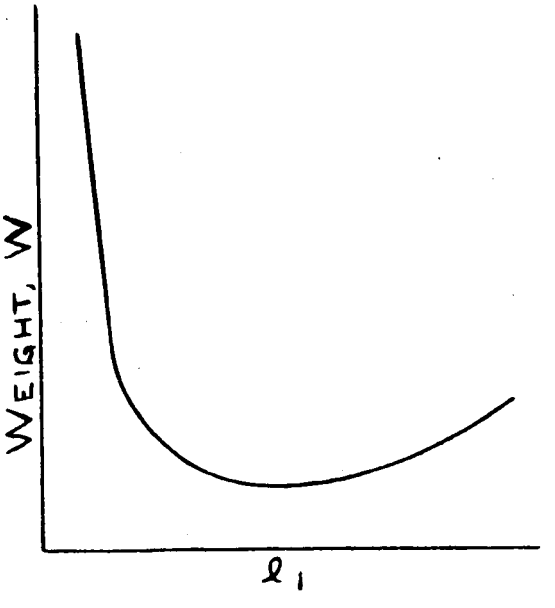

FIGURE 23

FUEL CELL MODULE
FOR
THERMAL PROFILE TESTS

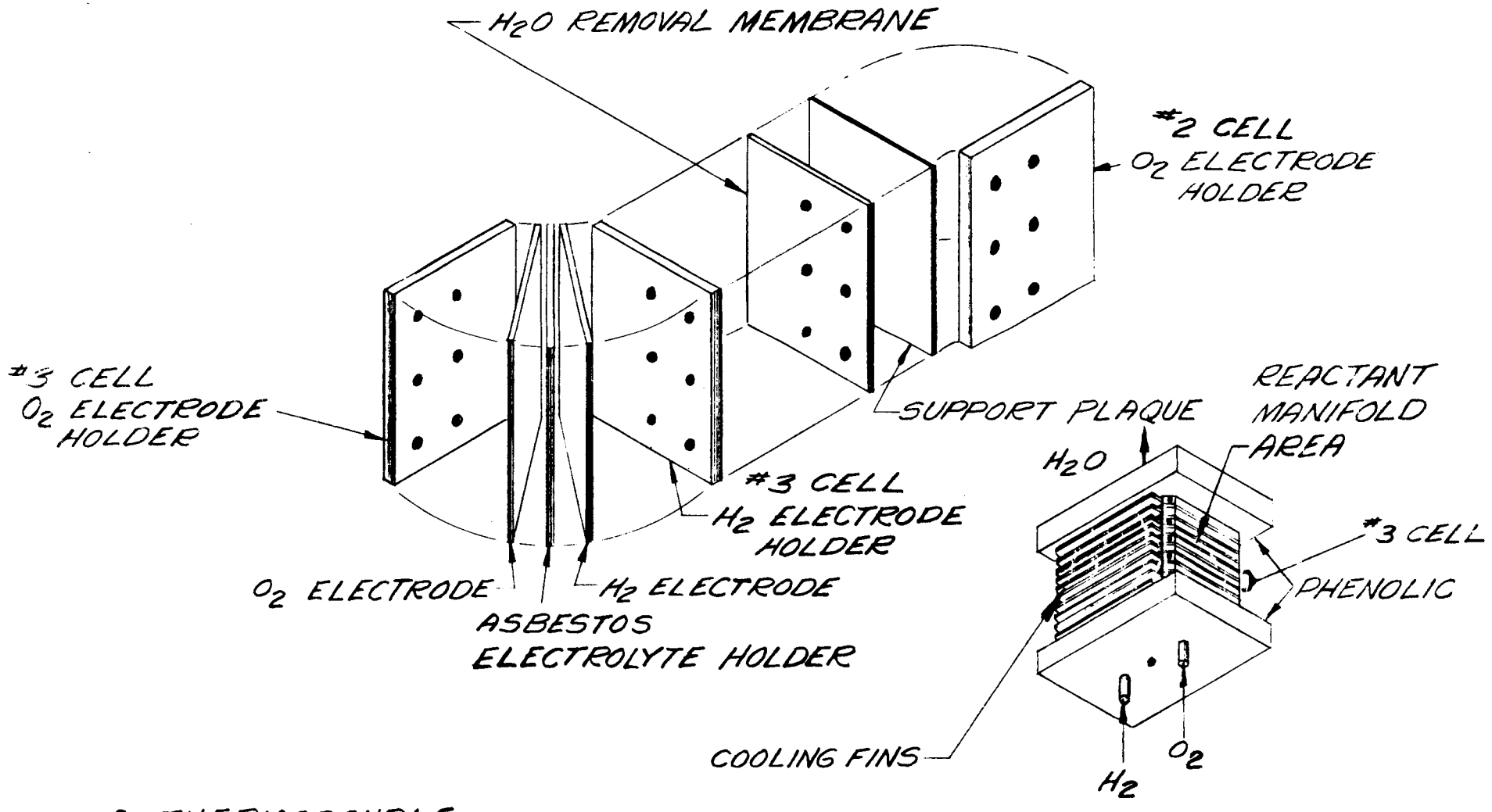

FIG. NO. 24

• - THERMOCOUPLE

PART II TASKS

8.0 1.5 KW FUEL CELL BREADBOARD SYSTEM THERMAL STUDIES

In the engineering design of a gas cooling system for the 1500 watt fuel cell breadboard system, it was necessary to make several design assumptions.

8.1 Thermal Mockup

In order to check the validity of these assumptions and to provide preliminary verification of the system design, a thermal mockup of the fuel cell system was constructed and tested prior to construction of the 1500 watt fuel cell breadboard system. This mockup, shown in Figures 25 and 26, basically consisted of a simulated fuel cell module in a canister with fans recirculating the gas coolant over the cooling fins of the simulated module and through a heat exchanger. Heat was transferred from the gas coolant to a primary liquid coolant in the heat exchanger. Necessary ducting and instrumentation was included inside the canister. Heat input to the simulated fuel cell module was varied to simulate the operation of a fuel cell module under various loads.

The instrumentation was included to acquire design data in the following areas:

(a) Fan characteristics
(b) Parasitic Power
(c) Flow distribution
(d) Pressure drops
(e) Temperature profiles and control
(f) Cooling capacity

Prior to testing the mockup, several tests were conducted to check the performance of the coolant circulating fans. These tests were conducted with air, helium and hydrogen. The results indicated that the performance was similar to, but slightly greater than, the manufacturer's prediction. Power input was slightly lower than expected. The fans were "off-the-shelf" items and not flight hardware.

A short initial test was run with the canister evacuated to 10 microns to determine the friction losses of the motor and fan. These indicated that each fan-motor combination had a loss of about 42 watts with no circulation of gas. Analysis of the above test data indicated the motor efficiency to be about 30%. A special design for this application could be made with a considerably higher efficiency. However, the power required to circulate the gas would remain essentially the same depending only on the fan efficiency.

After the performance test, the fans were installed in the thermal mockup. A short initial run was conducted with air at the same density as hydrogen at 2.4 atmospheres and 80° C in order to check out the system. Initial tests were conducted with helium at 2.4 atmospheres. Helium was used for this initial verification stage because it is easier to work with than hydrogen but has somewhat similar properties. After alterations and improvements to the system were made, final testing was conducted with hydrogen as the coolant.

After the preliminary tests with helium as the coolant gas, changes in baffling and ducting of the coolant gas were made to provide a more proportional flow in both directions along the fin and a more even flow distribution from top to bottom of the simulated fuel cell module.

The best indicator of the performance of the cooling system was the measurement of the Δ T along the simulated fuel cell plate cooling fin. This Δ T was measured in the cooling fin from the center of the inlet duct to the end of the fin.

In the first tests with helium as coolant, the average Δ T was 13.5° C. After the above alterations were completed, this average Δ T was 12° C. At this point hydrogen was substituted for helium as the coolant gas which decreased the Δ T to about 9° C. Analysis of the data indicated that the pressure drop from the return duct through the heat exchanger was higher than expected. By increasing the distance between the heat exchanger and the end plate, this pressure drop was reduced by 50 % and the Δ T on the fins decreased to about 8.5° C. Each fan was then run individually. Performance again increased as indicated by an average Δ T of 6° C on that side, and by other operating data. Since the suctions of the fans were separated by a baffle, it appeared that the improved performance was not due to a difference in suction characteristics as previously believed, but rather from a reduced system pressure drop. This is possible because the return duct and path through the heat exchanger are shared by both fans. When one fan is off, the flow, and thus the pressure drop, is lower through these areas. This illustrates the importance of further effort to reduce the pressure drops through the system. The parasitic power to operate the "off-the-shelf" fans averaged about 150 watts on helium and 120 watts with hydrogen as coolant.

The completion of the above tests terminated the thermal mockup testing. The feasibility of the hydrogen cooling system had been demonstrated and provided additional design data which was used in the design of the 28 volt fuel cell breadboard system.

9.0 1.5 KW FUEL CELL BREADBOARD SYSTEM

Following the completion of the thermal mockup tests, the design of the 28 volt, 1500 watt fuel cell breadboard system was completed, the unit was fabricated and assembled.

9.1 Reactor

The fuel cell reactor composed of 35 series connected sections, with each section consisting of two parallel connected cells, each 0.2 ft^2 (6.9" x 4.2") active area had the following material and dimensional characteristics.

Electrodes:	Nickel
Catalyst:	Platinum and Palladium
Asbestos:	0.030" electrolyte holder and water removal membrane
KOH Concentration:	Electrolyte holder 35 % Water Removal 40 %
Flat Gaskets:	Butyl rubber Water removal 0.065"
Electrical Insulation and Spacer:	Melamine Grade G-5 (wet sanded to tolerance) 0.065" thick - cell 0.045" thick - water removal

The cells are sandwiched between thermal insulation and end plates and held in compression by eight tie rods as depicted in Figure 27.

9.1.1 Heat Removal

The heat removal subsystem consists of secondary coolant blowers, heat exchanger, fin passage supply ducts, and manifolding passage provisions. Figure 28 shows the addition of the basic heat removal components to the module. The secondary coolant flow paths are completed by the placement of a canister over the assembly.

Figure 29 depicts in detail the secondary coolant flow path. The coolant exits from the fan through an inlet manifolding duct from which it enters the respective cell fin passages. After traversing the fuel cell plate fins and cooling the fuel cell module, the gas flow turns and continues down an interim passage formed by the canister walls and baffles attached to the reactor. At the lower portion of the interim passage, the accumulated gas flow enters a return passageway defined by the canister walls and baffling. It then travels the length of the reactor before entering the heat exchanger and continuing into the blower inlet.

9.1.2 Canister and Dome

The canister shell and dome, which contain and manifold the secondary coolant, complete the fuel cell unit as shown in Figure 30. Provisions are made on the dome for entry and return of the primary coolant, distilled water. A stand was constructed to make the instrumentation and water removal connections more accessible.

Prior to final assembly of the breadboard system, the canister and end bell were pressure checked at 100 psig. Leakage rates were determined with hydrogen at 75 psig and ambient temperature of 75° F. The average leakage rate was 1.6×10^{-5} pounds per hour of hydrogen. This would correspond to approximately a 3% decrease of the charged 35 psia absolute pressure in 106 hours.

9.2 Test Board and Auxiliary Controls

The 28 volt, 1.5 KW fuel cell system was constructed in breadboard fashion with most of the system monitoring and control functions panel mounted, as shown in Figure 31. A flow schematic of the complete breadboard system is shown in Figure 32, and a description of each subsystem is given below.

9.2.1 Primary Coolant Subsystem

The purpose of the primary coolant system is to remove the waste heat from the fuel cell assembly. A flow schematic of this system is shown in Figure 33. A pump is used to circulate the coolant (water) through the closed loop system. An external cooler is used to remove the heat from the primary coolant. City water (21° C, approximately constant) was used as the cooling medium for the external cooler. The flow of coolant through the heat exchanger was measured with a calibrated flowmeter. In the automatic control mode the temperature regulator controls the cell temperature by operating the solenoid valve in the coolant supply line to the heat exchanger. When the cell temperature rises above the set point, the regulator opens the solenoid valve. If the temperature falls below the set point, the regulator closes the valve. The regulator senses the cell temperature by a thermocouple embedded in the plate fin. When a thermal balance on the heat removal system is being attempted, the solenoid valve can be held in the open position and the flow of coolant manually regulated with the throttle valve located in the coolant line to the heat exchanger. Knowing the flow rate indication from the calibrated flowmeter and inlet and outlet primary coolant temperatures, a heat balance can be performed. This then serves as a check on the secondary coolant heat exchanger data and gives the magnitude of the radiation loss.

9.2.2 Water Removal Subsystem

The pressure in the water removal cavity is regulated by an electronic controller operating a solenoid valve in the line between the fuel cell module and condenser,

Figure 34. The electronic controller receives its signal from the pressure transducer in the line between the module and solenoid valve. As the pressure in the cavity rises above the set level, the controller will open the solenoid valve. The controller closes the valve as soon as the pressure falls below the set point. The vacuum pump maintains a lower pressure in the accumulator than is required in the water removal cavity. The vacuum regulator can be used as a backup in case of a failure of the automatic control system.

9.2.3 Purge Subsystem

The fuel cell is purged by solenoid valves in each of the purge lines. The excess reactant flow rate is regulated by needle valves in the respective lines. The duration of purge and frequency is controlled by a timer. The frequency can be adjusted to compensate for change in load level by changing the gears in the timer. A simple adjustment on the timer regulates the length of a purge. Either or both of the reactant solenoid purge valves can be manually operated by push button switches.

9.2.4 Reactant Control Subsystem

Each of the reactant lines contain the following controls:

(1) Pressure Regulator - The purpose of the regulator is to reduce the line supply pressure of the reactant to the pressure required by the module.

(2) Shutoff Valve - The purpose of the valve is to shut off the reactants when the module is not in operation.

(3) Flowmeter - The calibrated flowmeter is used to measure the quantity of reactant used for a specific load and during the purge cycle.

(4) Pressure Gauges and Transducers - These are used to monitor the reactant pressure entering the module.

9.2.5 Fan Power Subsystem

The electrical supply required by the circulating fans is 115 volt, single phase, 400 cycles. Wattage, voltage and amperage are monitored to each fan to determine power required, efficiency and operating characteristics.

9.2.6 Power Control Circuit

The output of the module is measured by a d.c. voltmeter and a d.c. ammeter. The electrical load for the module consists of 21 fixed resistors. The resistors are connected to the system through relays operated by toggle switches. Resistors are added or removed from the system via the relays until the desired load on the module is obtained.

9.3 Instrumentation

9.3.1 Thermal Instrumentation

Seventy-two thermocouples were utilized in conjunction with a three-position switch and twenty-four point temperature recorder to monitor the system's thermal characteristics.

Fifty-two of the thermocouples were positioned in random fashion in the reactor stack oxygen plates. There were thirty-five common oxygen plates each serving two cells and corresponding to the thirty-five sections.

Thermocouples were iron-constantan of Number 30 gauge from installation to copper junction block with three-position switch. Number 20 gauge teflon-coated wire was used from the switch to the 24-point recorder. Thermocouple junction was coated with an insulating lacquer and then teflon tape before insertion into connector pin.

The remaining twenty thermocouples were utilized to sense end plate, canister wall, and primary and secondary coolant media characteristics. Figure 35 shows the location of the secondary coolant sensor instrumentation.

9.3.2 Pressure Instrumentation

The pressure within the canister surrounding the module was measured with a static connection located at the top of the dome. This is the pressure at the discharge of the heat exchanger and the suction of the circulating fans. As this was the lowest pressure point in the system, it was used as a reference pressure for all other pressure readings.

The discharge pressure of the circulating fans was measured with a total pressure tube located within the supply duct 10 inches from the fan. This reading was the Δ P rise through the fan as the reference point was the fan suction.

The inlet pressure to the heat exchanger was measured with a pressure tube pointed toward the end plate about 1 inch from the face of the cooler. See Figure 36 for the exact location of this pressure probe.

The static pressure connection located at the end of the supply duct on the AC side gave the pressure drop in the return passage and through the heat exchanger.

The pressure of the reactant gas and water removal cavity was checked with 0 - 50 psia pressure transducers. The flow of reactants was checked with

calibrated flowmeters. The flow of coolant was measured with a calibrated flowmeter.

Pressure Measurements

(1) Reference Pressure

Fan Suction - Top of Canister. Also used as total canister pressure.

(2) Δ P - Circulating Gas Fan

Discharge pressure measured in cooling duct 8-1/2" from top plate. Total Pressure. One for each fan.

(3) Δ P - Across Heat Exchanger

Inlet measured at point one inch from cooler to top plate, 3-3/4" from common centerline of fans and 3/4" from other centerline.

(4) Δ P - Across Heat Exchanger and Return Passage

Static pressure was measured at the bottom of cooling duct on AC side.

9.3.3 Electrical Instrumentation

The output of the module was measured by a d.c. voltmeter and a d.c. ammeter. The power input to the circulating fans was monitored with a voltmeter, ammeter and wattmeter on each unit.

Individual section voltages were monitored by leads passing through specially constructed potting fixtures positioned in the bottom end plate.

9.4 Test Description

The initial series of tests on the experimental breadboard had three main objectives in that a definition of series-parallel nominal 28 volt fuel cell reactor performance was to be obtained concurrently with characteristics of a secondary gas coolant heat removal system. The third objective is to define the proper cavity pressure setting to effect static moisture removal over the design electrical load range. During the above system's definition, there was an attempt made to optimize purge requirements but only to the extent that time would allow.

Thermal characteristics of the breadboard system along with the proper cavity setting were defined at 1/3, 2/3, and full load, and 33% overload. Voltage - current density performance was monitored at discreet intervals, and values defined at increments of 1/6 of full load to 66% overload.

9.5 Test Sequence

The first test was performed utilizing gaseous helium as the secondary supply and water as the primary coolant supply. Reactor load level was approximately 20 amperes (50 ASF) with canister and reactor pressure held at 35 psia and reactor at 190° F inlet fin passage temperature. Cavity pressure was initially set at 213 mm Hg (40% KOH, and 195° F) and adjusted accordingly for best performance. Reaction purge was set to occur at intervals of 15 minutes for a 15 second duration, and the excess flow corresponded to approximately 3% of reactant stoichiometric hourly consumption.

After a cursory analysis of the data obtained from the helium test, the remaining tests in the definition series were run utilizing hydrogen as the secondary coolant and water glycol (60 percent by weight) as the primary coolant. The canister

was evacuated with reactor pressure at atmospheric and purged with hydrogen to flush out as much inerts as possible. Reactor pressure was returned to 35 psia and open circuit individual voltages noted, and the reactor heated to 190° F inlet fin passage temperature with proper cavity pressure defined from previous test. A minimum run of 24 hours at approximately 20, 40, 60, and 80 amps each followed with proper cavity pressures being defined or confirmed at each level. Thermal data was taken.

Utilizing cavity pressure and purge magnitude defined at the 60 ampere load, tests at 40 and 20 ampere loads were performed, each of 12-hour duration, noting differences from previous tests at the respective loads, with voltage-current density data recorded at arbitrary intervals.

9.6 Results of Test

The nominal 28 volt, 1.5 KW experimental unit successfully operated for 162 hours under load. Only normal fuel cell degradation associated with nickel electrode construction was noted during this period. The average section dropoff was 0.20 mv/hour at 100 ASF, and 0.40 mv/hour at 200 ASF. This corresponds to single-cell test data dropoffs recorded of 0.10 mv/hour and 0.15 mv/hour respectively. The secondary heat removal blowers although inadequate in capacity provided tolerable thermal control. The vacuum cavity controller, although requiring considerable manual manipulation for thermal compensation, did provide a desired cavity setting.

At the outset of the test, meaningful thermal data could not be obtained on the system at the 20 ampere load. The heat rejected at this load level was not sufficient to maintain the desired reactor temperature and therefore heat injected via the secondary coolant loop was required to maintain the specified test thermal conditions. This condition caused a slight modification in the test plan. Added insulation would decrease the amount of heat loss.

Helium was used as the secondary coolant during the initial 25 hours of operation. Hydrogen was substituted for the remaining tests. Water was utilized as the primary coolant during the entire operational period. The primary coolant flow was automatically (full on or off) controlled during those periods of time when cavity setting, V-A characteristics or purge requirements were being defined. Manual (constant) flow control was initiated to obtain the system thermal balance at the test load levels. The primary coolant inlet temperature was varied from 75° F to 135° F and flow rate varied as required.

Warmup of the system from room temperature to normal operating temperature required 1-1/4 hours. The warmup was achieved by heating the primary coolant and circulating it through the heat exchanger to heat the secondary gas coolant. The secondary coolant was then circulated in the normal manner, transferring the heat energy to the fuel cell module.

The purge rate, interval, and duration were held constant for the first 100 hours of operation. The purge was set at approximately 3% of reactant required at full load. During the last 60 hours of operation the purge rate was varied. The purge was reduced to a point where the total voltage began to decay. From this point it was increased including a shorter time cycle.

A complete set of instrumentation readings was recorded at one-half hour intervals during the entire operating period logged. Each set of data was assigned a sequential run number.

9.7 Load Profile

The reactor operated on a step load profile as shown in Figure 37.

Some apparent discrepancies can be noted from the profile between reactor voltage and power output, i.e., increasing voltage with increasing load or conversely. The corresponding time and reasoning is as follows:

Elapsed Period	Explanation
12.2 - 19.1 hours	Cavity setting decreased to 35% KOH from 37%
19.1 - 25	Cavity setting 37% and increased purge cycle
25 - 43	Operation after weekend shutdown
68.5 - 71	Slight degradation in performance noted
119.5 - 131.3	Purge duration 6 seconds
131.3 - 139.3	Purge duration 9.5 seconds
139.3 - 146.6	Purge duration 10 seconds, V-A curve taken, and slight alterations in water cavity setting
153.4 - 162.3	Cavity leak and purge cycle manipulations

The average of the four thermocouples "embedded" in oxygen plates was used to define an operating temperature. With this temperature and a predetermined KOH concentration the corresponding cavity controller pressure setting was defined from Figure 38. The most optimum cavity setting for operation at all load levels was found to correspond to a 37% KOH concentration. Insufficient or excess water removal was obtained above and below this level. The pH readings taken from water samples varied between 6.9 and 9.8 with the majority falling in the 7.0 to 8.0 range.

9.8 Electrical Performance

Voltage-current density characteristics were recorded at 5, 65, 101 and 140 hours of elapsed operating time. Observations were not taken at or around the

160-hour period due to the unanticipated events which terminated the test. Both total and individual section voltage values were recorded.

Figures 39 and 40 summarize data obtained. Total or average section voltage is based on the measurement taken from all 35 sections.

Throughout the 162 hours of operation, one section (two cells in parallel) out of the thirty-five had consistently performed significantly lower than the average. This was section number 24, numbering from the bottom end plate. Disassembly of the reactor stack revealed that a polyethylene sheet, inadvertently left on from the initial construction, was covering the gas side of the hydrogen electrode in the lower cell of this section. Assuming that far too little hydrogen could diffuse through the polyethylene sheet to make the lower cell effective and noting that plastic is a poor electrical conductor, it is felt, with some certainty, that the upper cell of the section was carrying the full load. For brief periods of time this cell was operating as high as 500 ASF with no apparent short term damage. On a voltage-current density basis this section (upper cell) performed as well as, and in most instances, better than the remaining thirty-four.

The inclusion of this section into the results then tended to derate the total or calculated individual average section voltages shown.

9.9 System Pressure and Thermal Characteristics

During the 162 hours logged, various levels of steady state electrical load were achieved and maintained for sufficient duration to obtain secondary gas coolant subsystem performance as well as fuel cell thermal characteristics. The system was placed in thermal equilibrium by maintaining a fixed primary coolant inlet temperature and varying the primary distilled water flow rate until

the reactor internal temperatures (averaging fuel cell sections number 16 and 21) stabilized. This set condition was then maintained for approximately 1-1/2 to 2 hours during which the steady state thermal and pressure characteristics were recorded.

Of the many sets of data taken under these conditions, a selected but representative number of test runs typical of 40, 50, 60, and 80 ampere loads are summarized in Table I. A definition of the terms used in the table is given first.

The first set of data presented in column (C) was with a 39.5 ampere load ($\sim$ 2/3 full load), helium as the secondary coolant, and primary coolant (distilled water) inlet temperature of 133° F. The next seven sets of data, (Columns D through H), with the loads noted, utilized hydrogen as the secondary media; various fixed primary coolant inlet temperatures, and the first of two sets of hydrogen blowers used in the testing period.

The bearing failure of one blower of the initial set at 101 elapsed hours resulted in replacement of both blowers, per the vendors recommendation, by Rotron single-phase units. It was the manufacturer's belief that the new units would give essentially the same performance but much longer life. The last two sets of data (O and P) are again with the hydrogen secondary media at the conditions noted, but reflect the performance of the second set of circulating blowers. A significant decrease in blower characteristics is noted in comparison to the initial set.

A thorough review of the temperature data recorded during the breadboard operation indicates, with a few exceptions, that the prescribed thermal characteristic was obtained and the results are valid. Exceptionally good data were obtained from the sensors "embedded" in the oxygen plates of reactor section number 16 and 21.

There were three general areas in which the temperature recorded was not indicative or could not be correlated. The cell plate fin measurements taken at the secondary coolant fin passage entrance (along the inlet duct) all appear to be biased to some extent. The magnitude of the observed temperatures in proximity to the inlet duct increases from the top end plate (blower exit) along the reactor length to the bottom end plate. In contrast the plate fin measurements taken at the fin passage exit increase along the length of the reactor to the center section and then begin to decay toward the bottom end plate. The latter trend is more reasonable as one would expect a relatively symmetric thermal gradient to exist about the middle of the stack length. The sheath in which the thermocouple was placed was sufficiently cooled by the secondary media in the inlet duct and as a consequence, through conduction, biased the true plate fin reading.

The primary coolant thermocouples placed in the aluminum fitting just before and aft of the heat exchanger gave some very erratic readings and could not be correlated to the data recorded from the primary coolant measurements taken in the lines external to the canister. The erroneous information obtained is believed to have resulted from a second junction formed in the return passage. The conclusion here is based on the fact that a number of the readings were at or near the secondary media temperatures recorded in the return passage. Since the thermocouple lead was not continuous from the installation through the potting fixture, but was spliced internal to the canister, a secondary junction could have been formed. A check on the installation prior to startup, at the 101 hour elapsed shutdown, and during post checkout, did give a true temperature readout.

A third area of primary concern was the secondary media thermal characteristics obtained from the instrumentation just aft of the heat exchanger or before the blower inlet. Data recorded before the heat exchanger at two locations and after each blower exit plate was consistent within instrumentation errors. But it is noted from the data presented that the temperatures recorded aft of the

heat exchanger at two points did not agree. The data observed from the thermocouple on side BD was consistently 8 degrees lower than the temperature recorded at the blower exit on that side. In contrast the thermocouple on side AC was consistently 2 to 3 degrees higher than that recorded at the blower exit on its side. There presently is no conclusion that can be drawn for this anomily unless it is a function of the secondary media flow field.

It is noted here than at average of these two temperatures was utilized in conjunction with the temperature recorded before the heat exchanger to define the weight flow rate or with the calculated density a volume flow rate for the secondary media. This naturally dictated the blower performance noted in the summary table.

From measured data and pressure values, an envelope of the estimated system ΔP was drawn up. To minimize the cell gradient to approximately 7° F, a previous calculation imposed a hydrogen flow rate of 75 cmf/fan (or approximately 0.96 inches of H_2O pressure drop for an estimated value.

10.0 CONCLUSIONS AND RECOMMENDATIONS

The following comments are made after the preliminary analysis of the tests which were run on the 1.5 KW module.

10.1 Temperature Measurements

The installation utilized for measuring fin plate temperature is a thermocouple embedded in a sheath which is inserted in a tapered hole in the cell plate fin. The sheath due to its construction will pick up some heat energy from the surrounding gas and from the fin of the cell plate. Therefore, the temperature of the thermocouple will be at some point between the fin and surrounding gas temperature.

Discrepancies exist in the temperatures observed of the coolant in and out of the heat exchanger aluminum fittings. The thermocouples installed in the coolant lines external to the canister, appeared to be reading the true temperature. They were used for the heat balanced calculations. The thermocouples installed in the coolant lines (aluminum fittings) near the heat exchanger within the canister did not appear to be reading the coolant temperature.

10.2 Radiation Losses

There is considerable variation in the amount of radiation calculated at the higher loads. This could be due to the inaccuracy of test data obtained. The radiation losses are based on the thermal heat balance of the unit. The radiation loss was the difference between the heat removed by the heat exchanger (based on data) and the theoretical heat generated within the unit plus the power input to the circulating gas fans.

10.3 Fan Performance

At the end of the first 100 hours of operation, a failure occurred in one of the circulating gas fans. Visual inspection indicated that the failure was due to malfunction of one of the bearings. This was discussed with the supplier who indicated that it was as a result of operating the unit in low density atmosphere. The vendor recommended that we use a varying flow density, high altitude motor driven fan. These were purchased and operated approximately 60 hours with no apparent mechanical difficulties. A verification test was run on one of these fans. This test as well as the test on the 1.5 KW module performance revealed that these fans did not develop as much head as the initial units. A concentrated effort should be expended to obtain the circulating blower performance necessary to minimize the active area thermal gradient.

10.4 Water Removal Cavity Control

Problems were encountered with the system utilized to control the pressure in the water removal cavity. Initially, the solenoid valve was installed improperly. Twice during the latter portions of the test the solenoid vibrated off of the valve itself leaving the cavity port open to vacuum until corrective action was taken. Even with these minor difficulties corrected, a constant watch had to be maintained on minor average cell temperature variations since they required immediate compensation to the pressure in the water removal cavity in order to maintain the desired electrolyte concentration. A more sophisticated control should be developed to automatically adjust the pressure of the water removal cavity to compensate for cell temperature variations. An additional volume or chamber between the module and solenoid valve would lengthen the time cycle and probably improve reliability.

10.5 Circulating Coolant Control

The present control functioned very well at steady load condition. Each time the load was changed, the control had to be reset to maintain a constant cell temperature. A constant internal cell temperature may have been more fully realized if the sensing thermocouple had been within the cell instead of the cell plate fin. A thermal time lag may inject some control problems for sudden load changes.

10.6 Power Circuit Control

No trouble was encountered with the present power circuit control.

10.7 Purge System

The purge system functioned as programmed. No modifications are required unless a load integrating technique is desired to operate the purge.

10.8 Reactant Supply Subsystem

There were no indications of any malfunctions of this system. There was a minor modification to the oxygen flowmeter to reduce the magnitude of the gas pressure drop.

10.9 Primary Coolant Inlet Temperature

The desired or limiting coolant inlet temperature was maintained by regulating

the flow of cooling water to the external cooler. (See Figure 32, Primary Coolant Subsystem) At times it was advantageous to use a mixture of cold water and steam to obtain high inlet temperature (above 100° F) of coolant. With the maximum flow of cold water to external cooler the coolant inlet temperature was 80 - 90° F. These tests were run with distilled water. In the near future, the module should be run with the primary coolant as a mixture of 60% methanol and 40% water, by weight, since the primary to secondary coolant heat exchanger was designed to these requirements and may not be as effective with distilled water.

11.0 STATIC MOISTURE REMOVAL SUBSYSTEM GENERAL CONCLUSIONS

The Static Moisture Removal System has been proved by feasibility and breadboard tests to be continuously operable over a range of cell loads up to 214 ma/cm^2. Tests on the breadboard system have further simplified the system by verifying water removal from only one side of the cell with a single cavity pressure setting for loads varying over a broad range is possible.

Tests conducted on single fuel cell units employing the Static Moisture Removal method have demonstrated extended operation at current densities of 300 ma/cm^2 and above.

The Static System is well suited for operation in a space environment since all fluid transport occurs in a single gas state and all liquid in the system is contained in capillary pores. Where recovery of product water is not desired, a significant thermal advantage is realized with this system. About 35% of the waste heat burden produced in the cell may be ejected directly to space vacuum as latent heat of vaporization of the product water, thus reducing the heat burden imposed upon the space vehicle rejection system.

The Static Moisture Removal Method in a non-condensing system eliminates the requirements of recirculating reactant pumps, condensers and gas-water separators. The absence of these components and their associated parasitic power requirements, valves, piping and connections makes the Static Moisture Removal System an inherently more efficient and reliable system.

A 1500 watt breadboard fuel cell system utilizing the Static Moisture Removal System has been constructed and successfully operated for 160 hours under load. Several periods of operation were demonstrated at 2,000 watts and a brief overload of 2,850 watts, which is equivalent to 172% of rated load, was demonstrated.

12.0 LIFE CHARACTERISTICS

Life characteristics on present operating fuel cells were demonstrated in excess of 2,000 hours at a constant current density of 162 ma/cm^2 with less than a 5% decrease in cell voltage.

THERMAL MOCK-UP OF FUEL CELL SYSTEM WITH GAS COOLANT

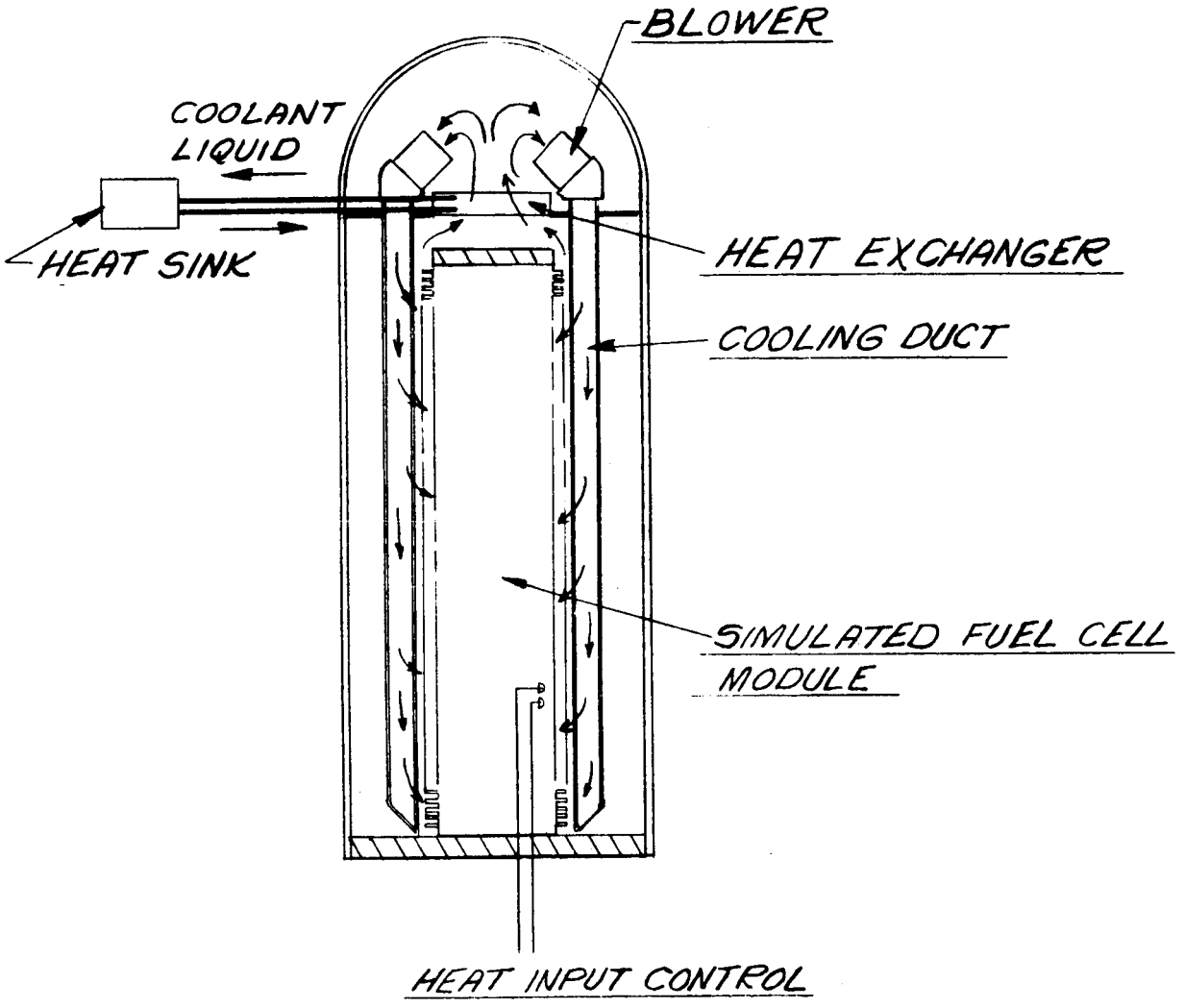

FIGURE 25

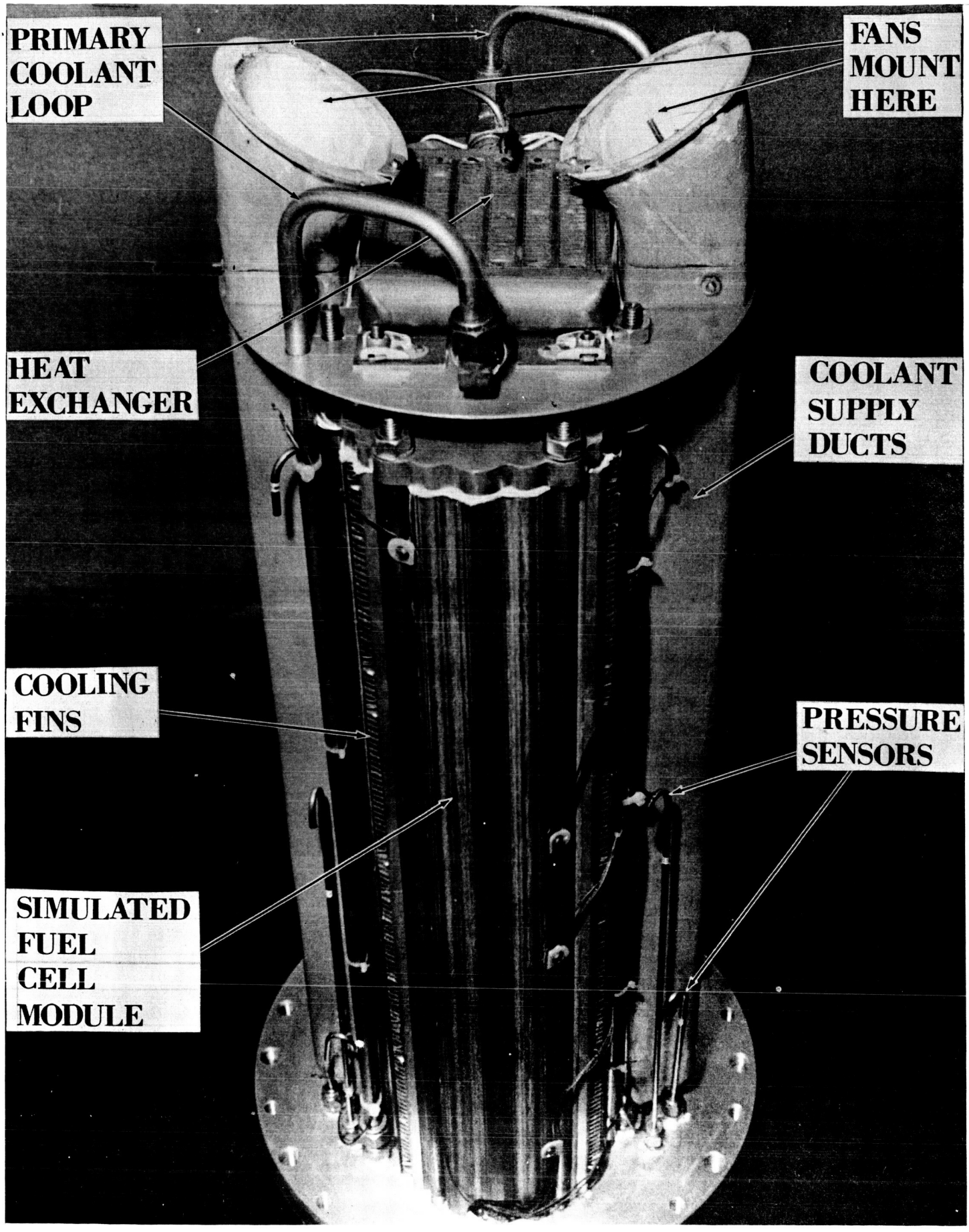

THERMAL MOCKUP

FIGURE 26

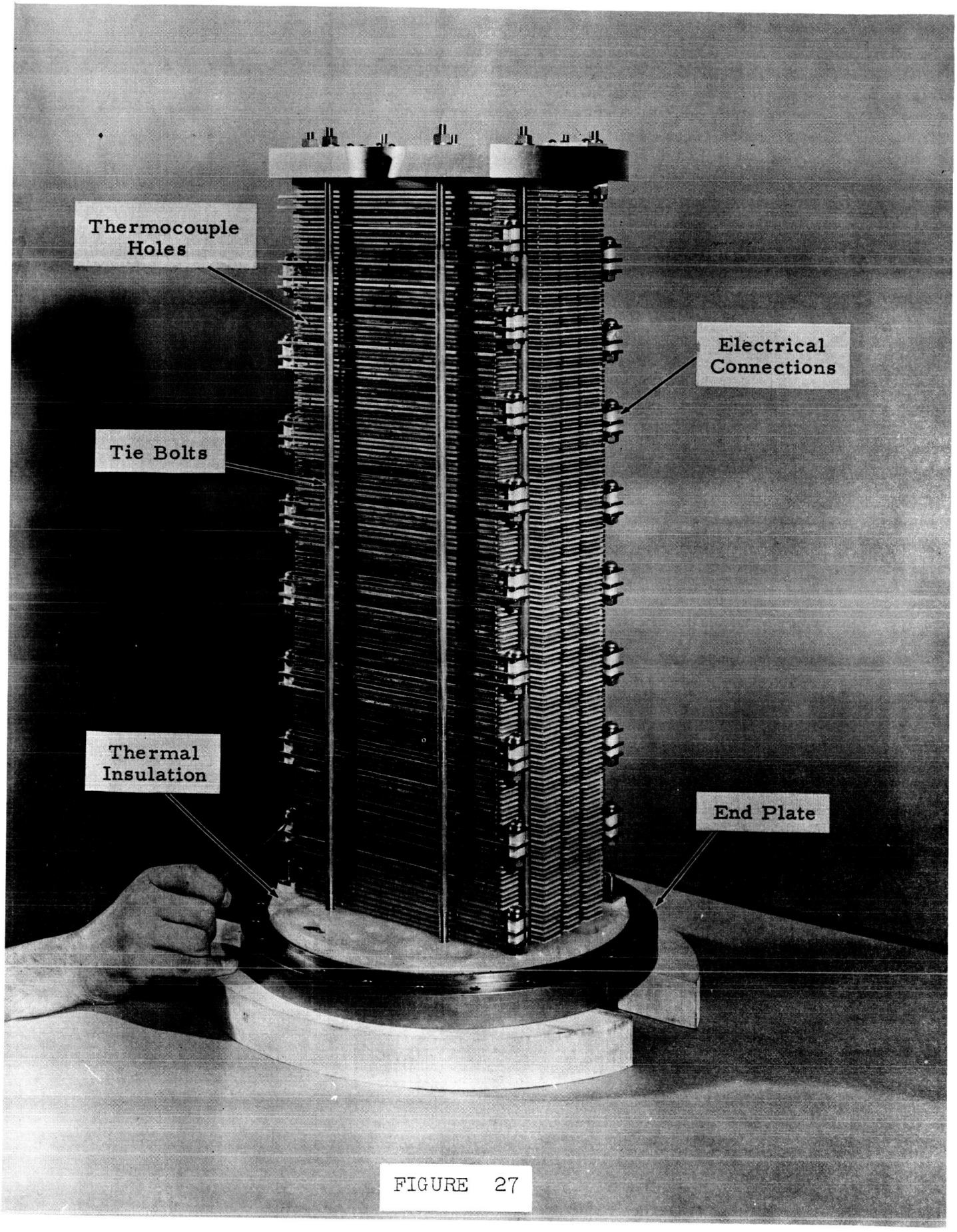
Thermocouple Holes
Electrical Connections
Tie Bolts
Thermal Insulation
End Plate

FIGURE 27

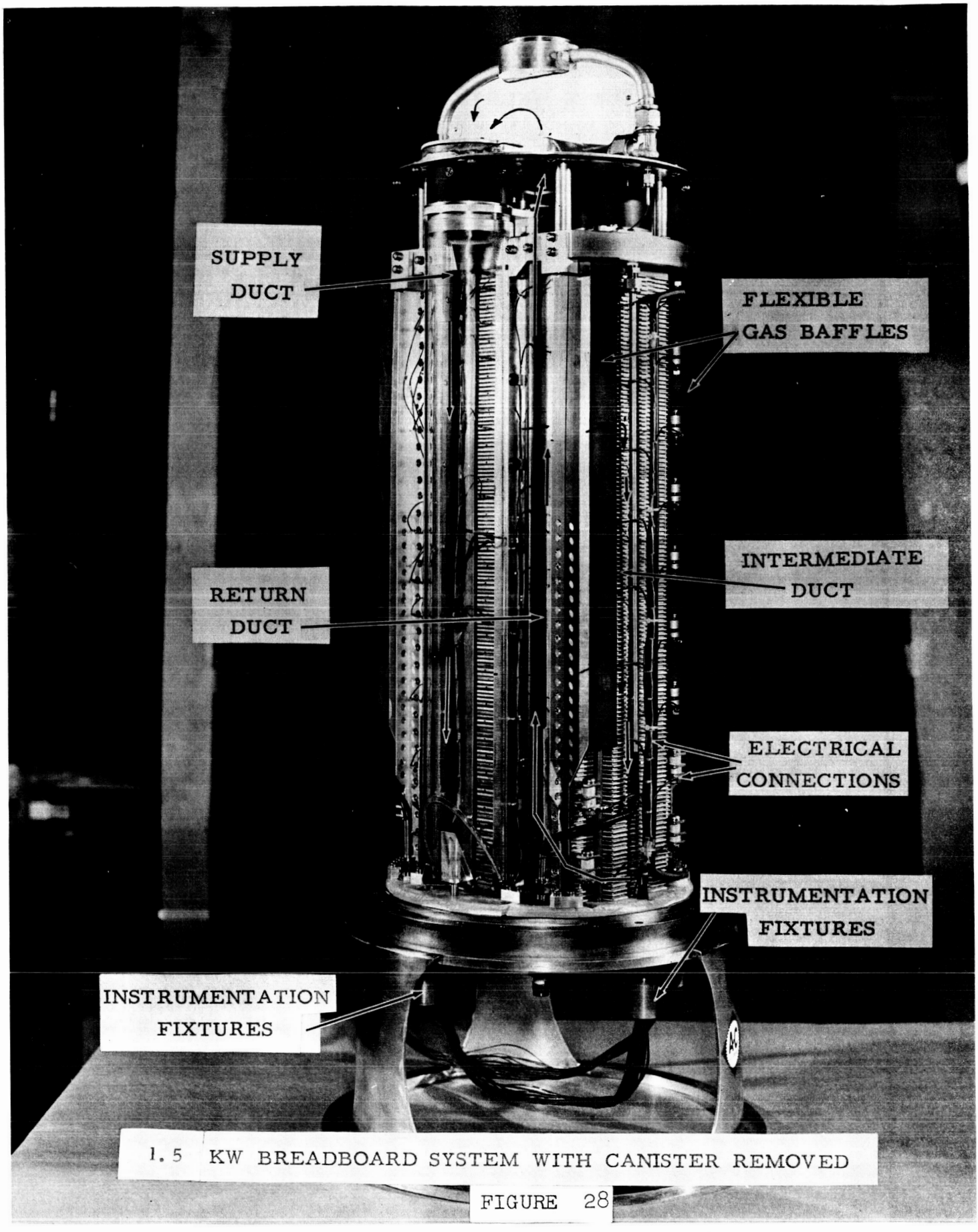

1.5 KW BREADBOARD SYSTEM WITH CANISTER REMOVED

FIGURE 28

HEAT REMOVAL SUBSYSTEM FLOW SCHEMATIC

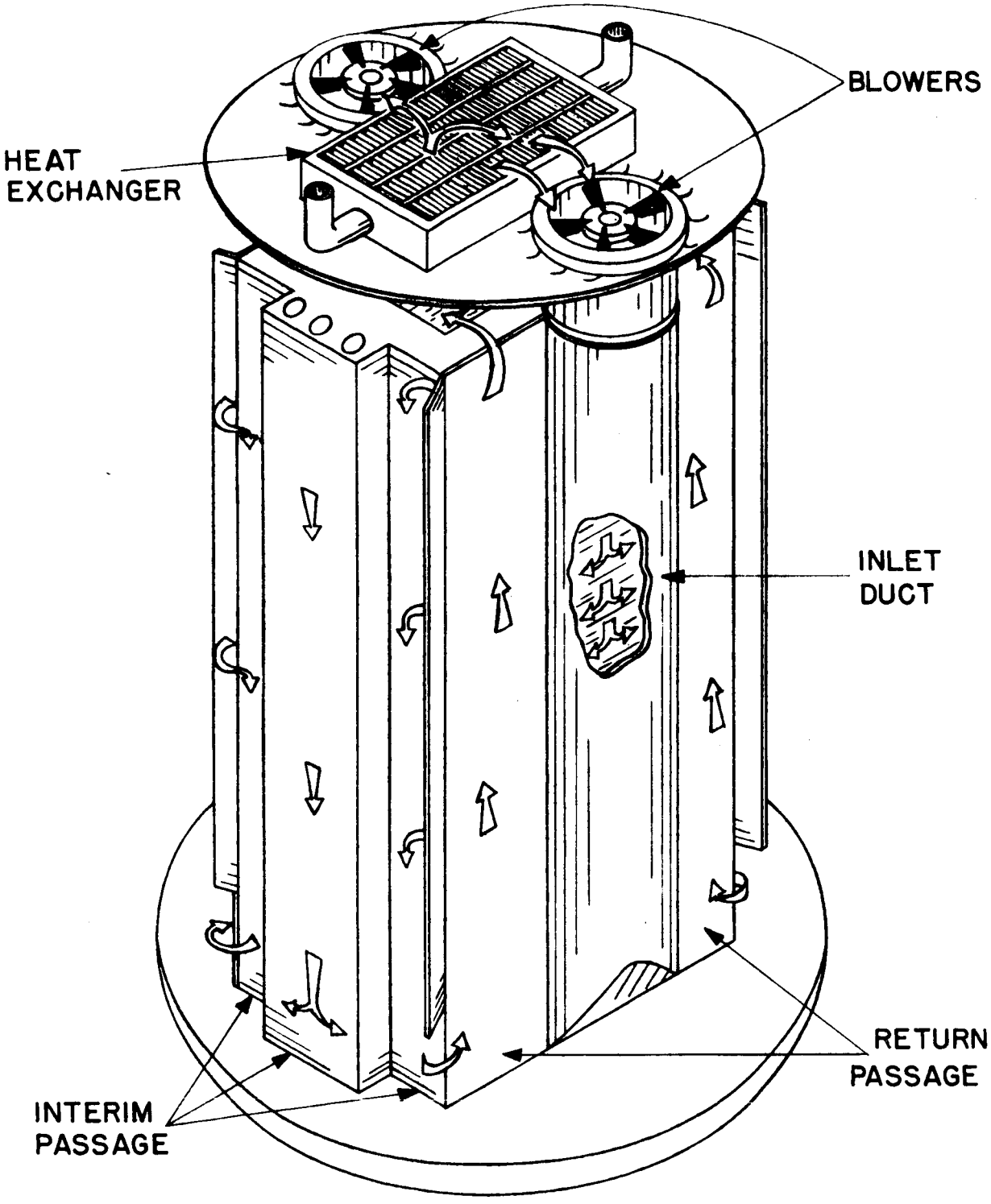

FIGURE 29

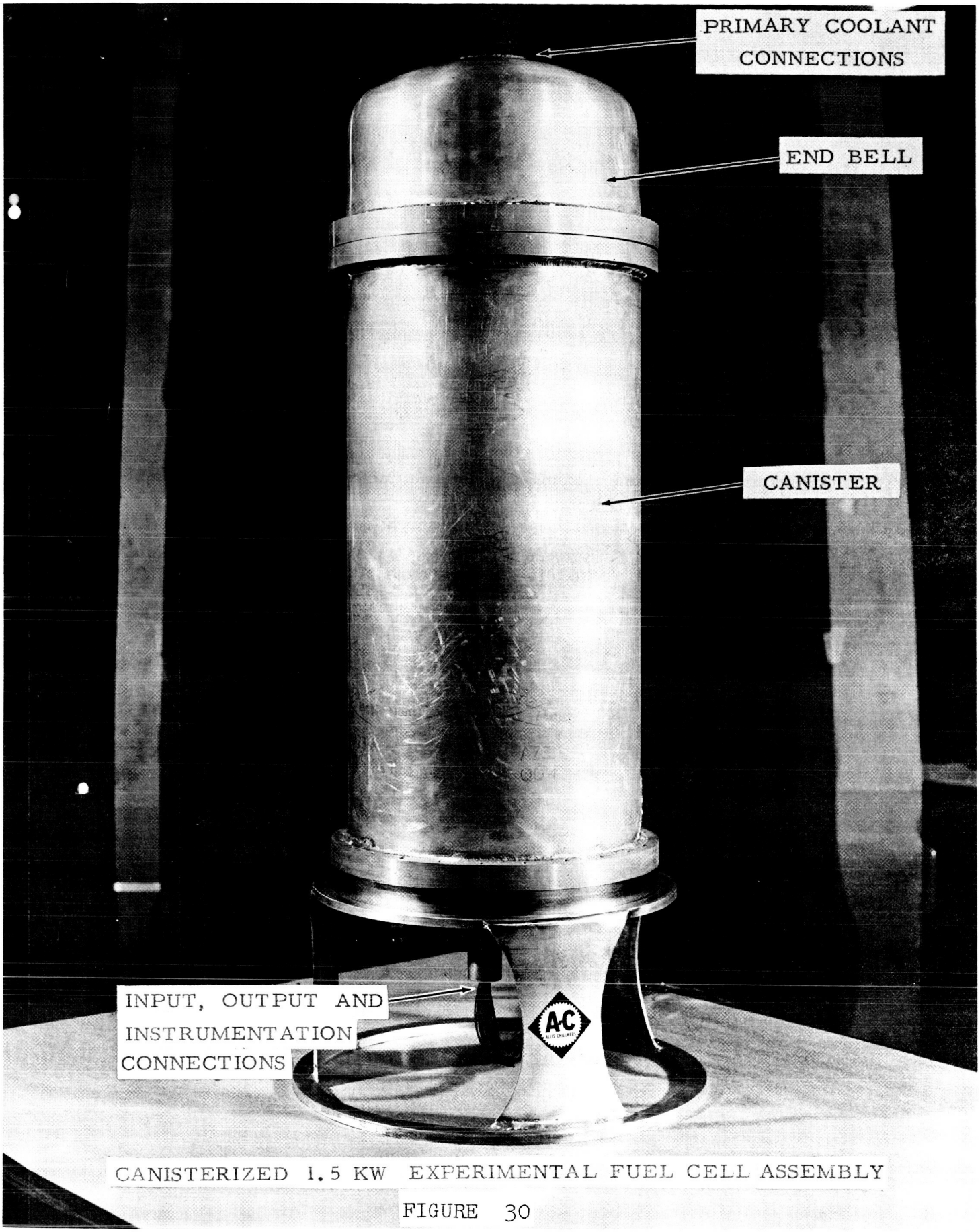

CANISTERIZED 1.5 KW EXPERIMENTAL FUEL CELL ASSEMBLY

FIGURE 30

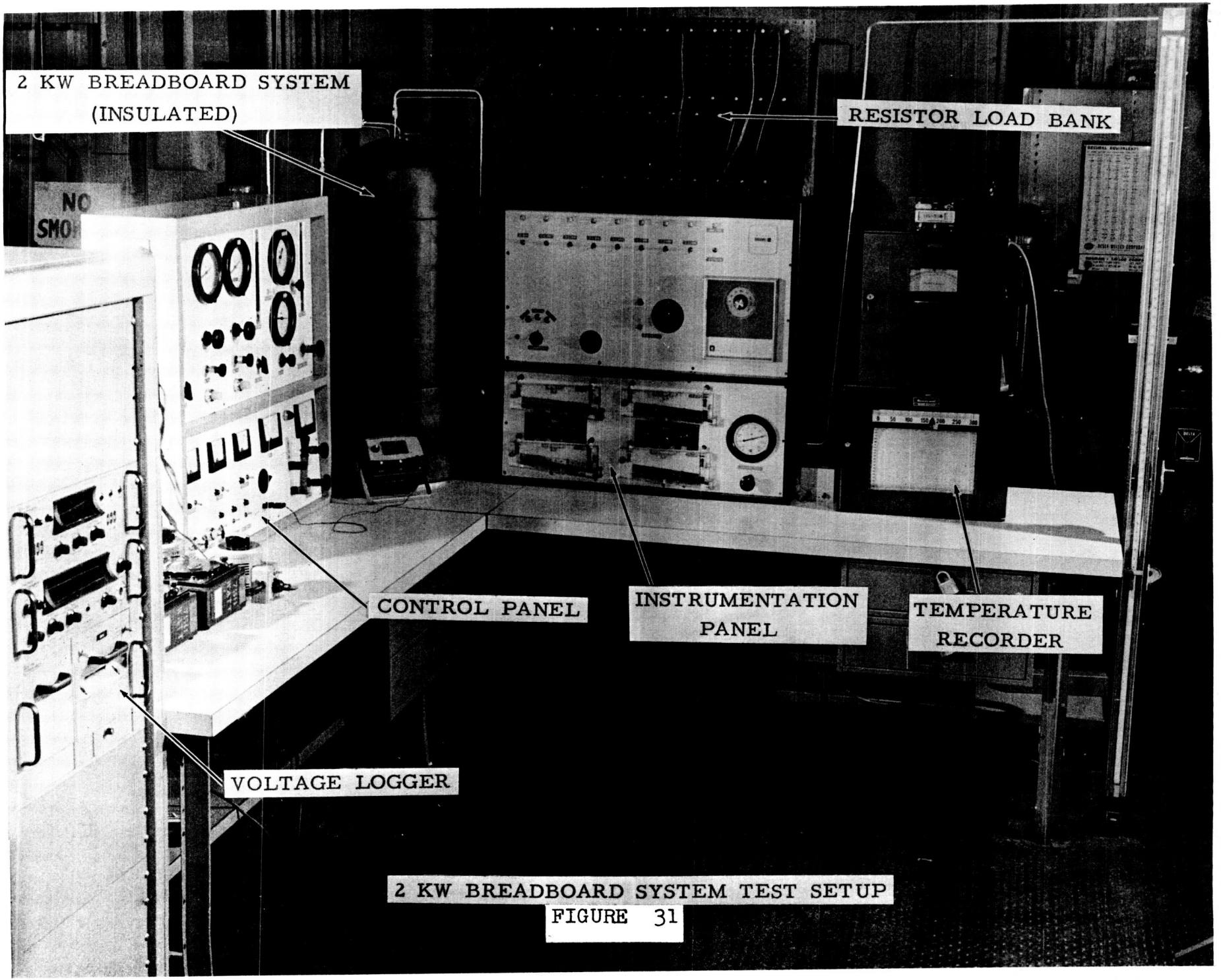

2 KW BREADBOARD SYSTEM TEST SETUP

FIGURE 31

SCHEMATIC OF TEST SET UP FOR 1.5 KW FUEL CELL

FIGURE 32

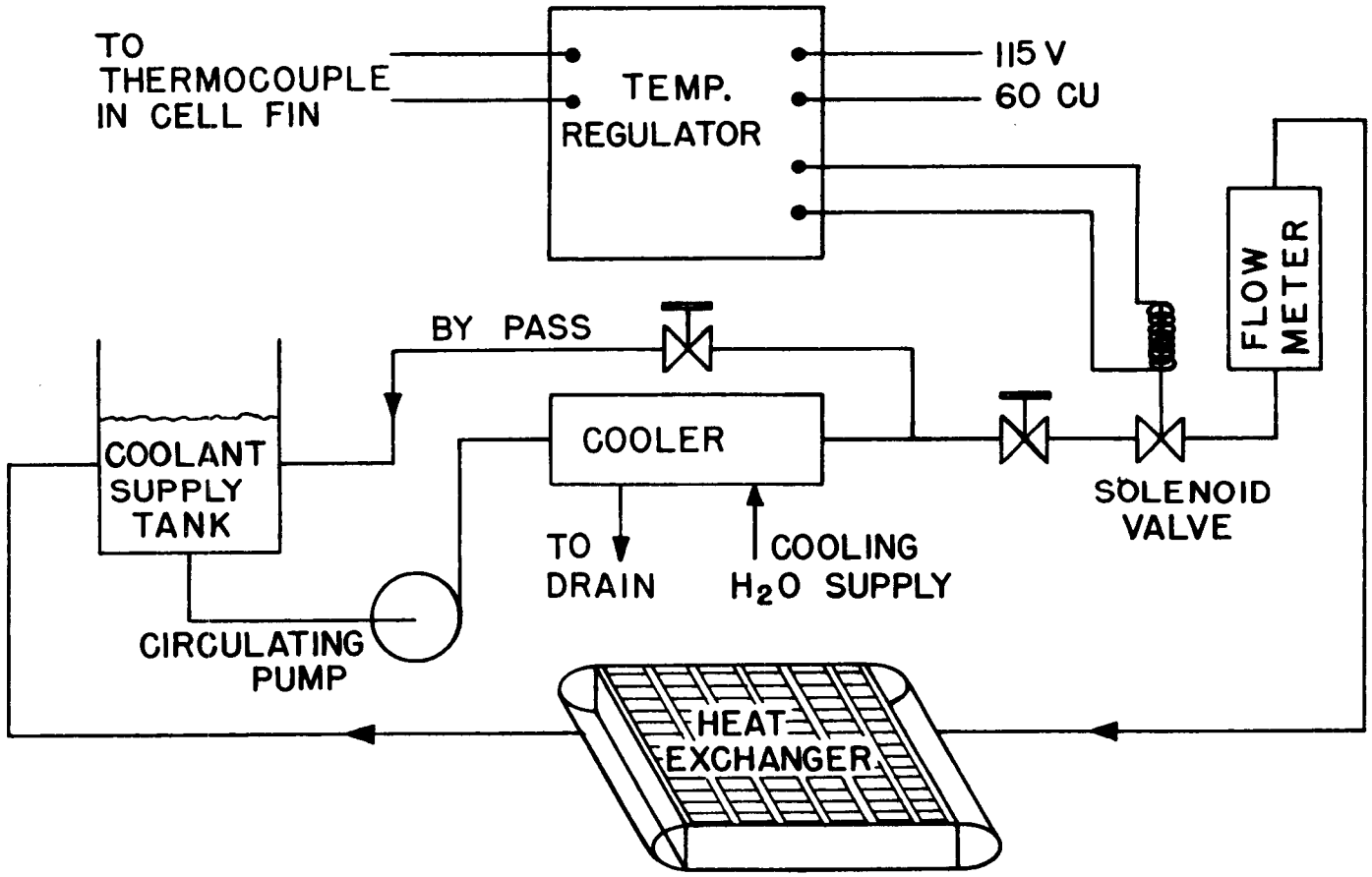

FIGURE 33

SCHEMATIC OF PRIMARY COOLANT LOOP

SCHEMATIC OF WATER REMOVAL SYSTEM

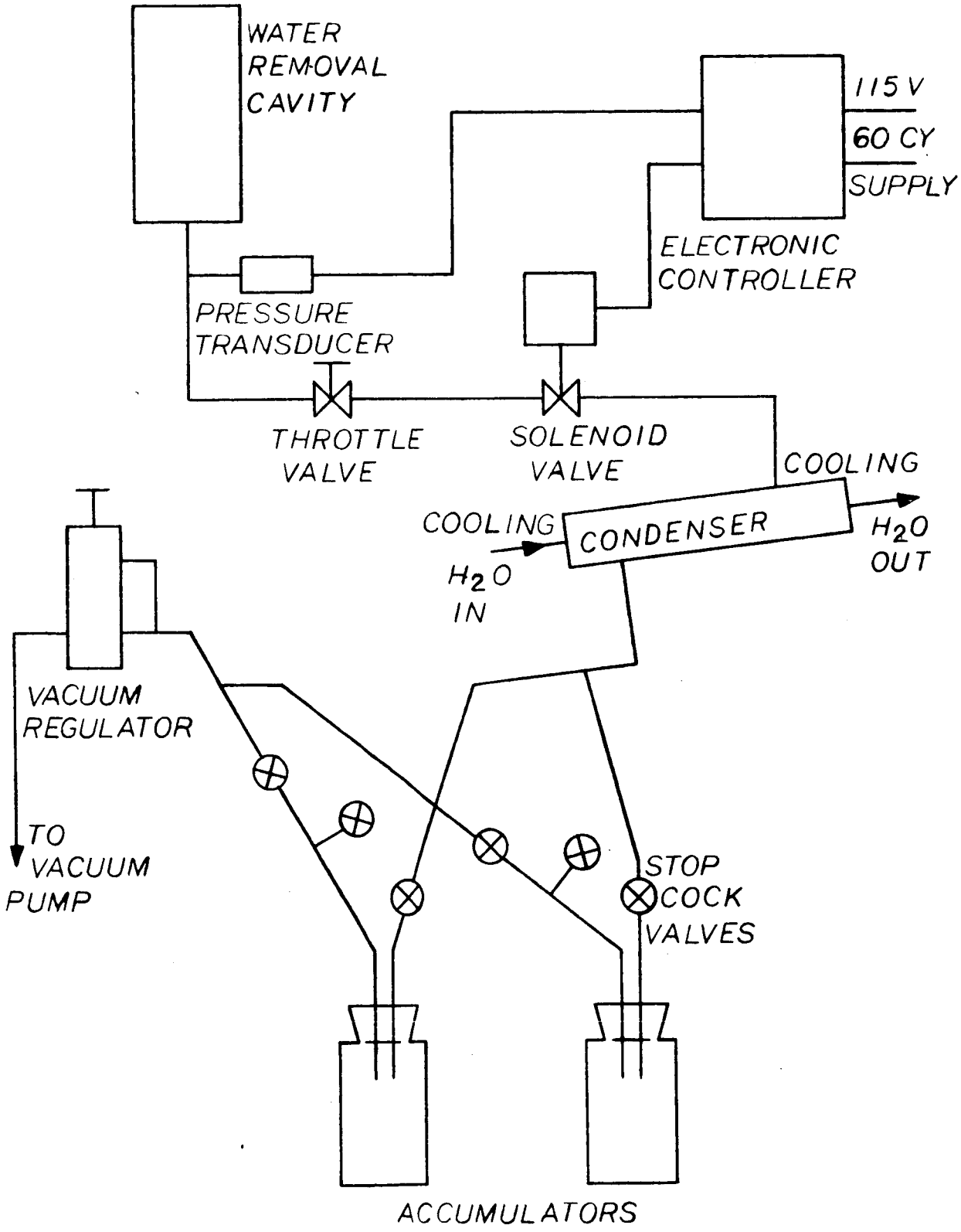

FIGURE 34

SCHEMATIC OF 1.5KW BREADBOARD THERMAL INSTRUMENTATION & RESULTS OF A TYPICAL TEST RUN (#132)

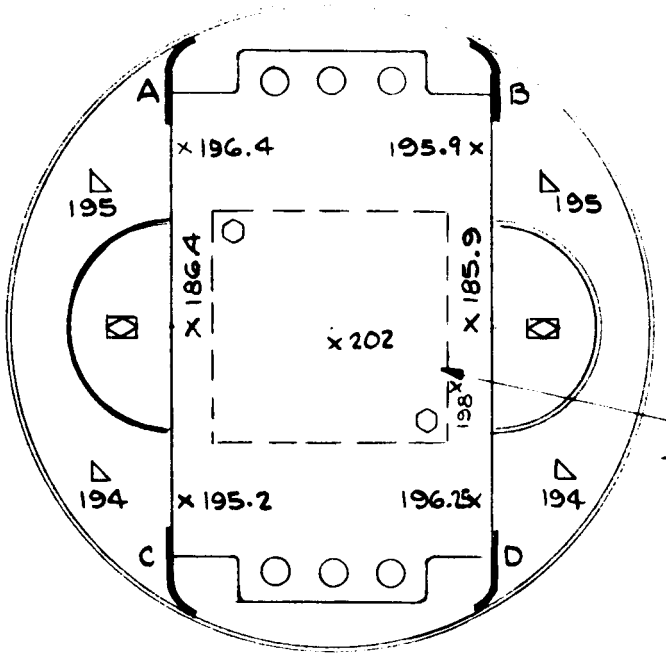

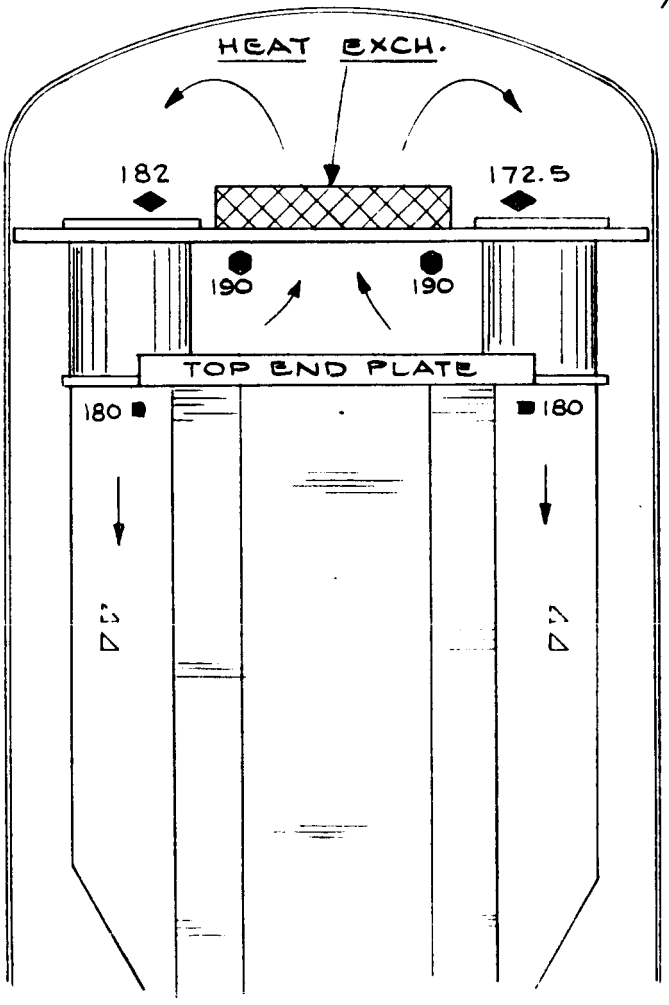

KEY:

X OXYGEN PLATE LOCATIONS

△ SECONDARY COOLANT RETURN PASSAGE

○ SECONDARY COOLANT BEFORE HEAT EXCH.

◇ □ SECONDARY COOLANT INLET DUCT.

TEMPERATURES IN °F

FIGURE 35

LOCATION OF PRESSURE INSTRUMENTATION

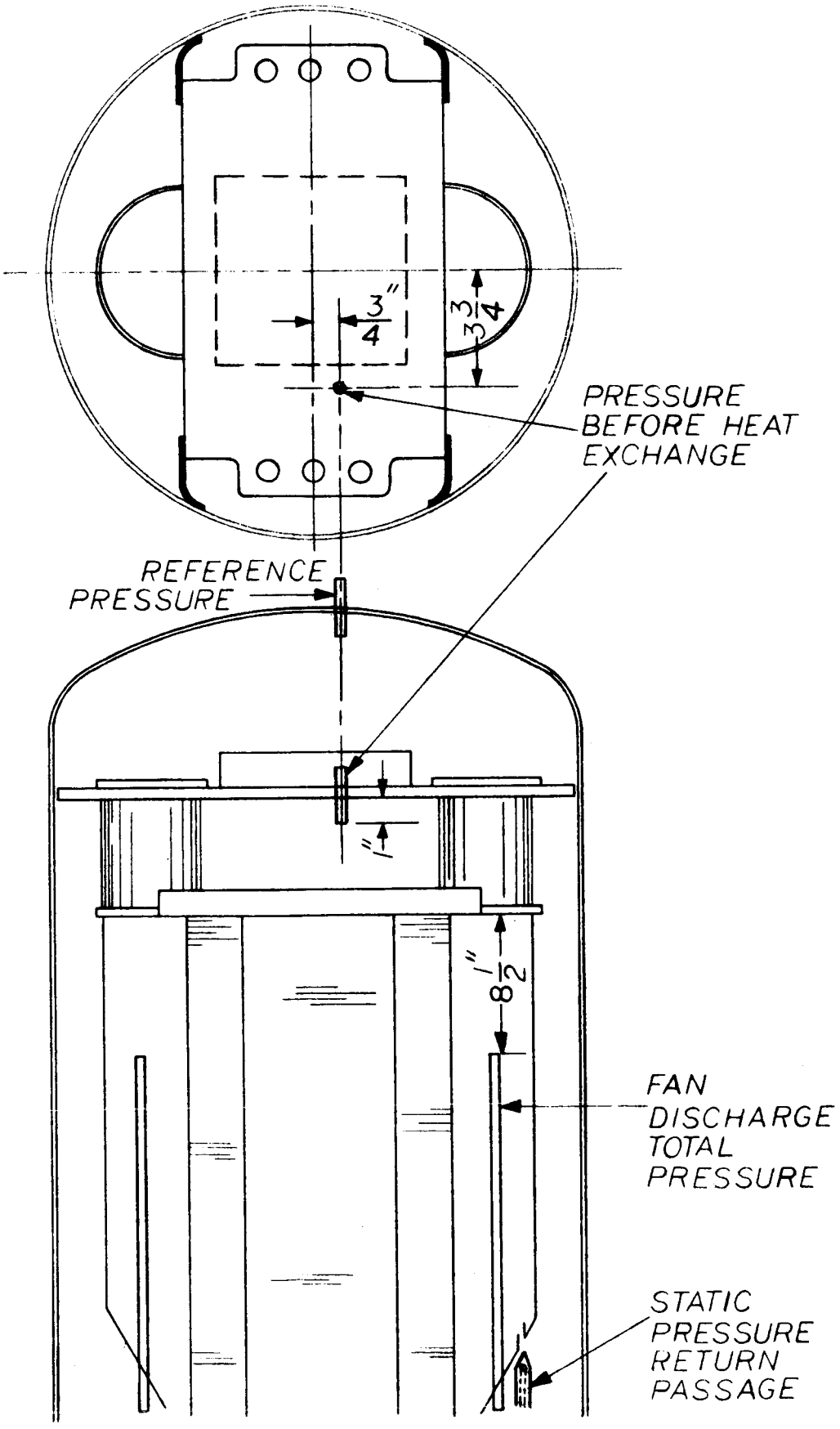

FIGURE 36

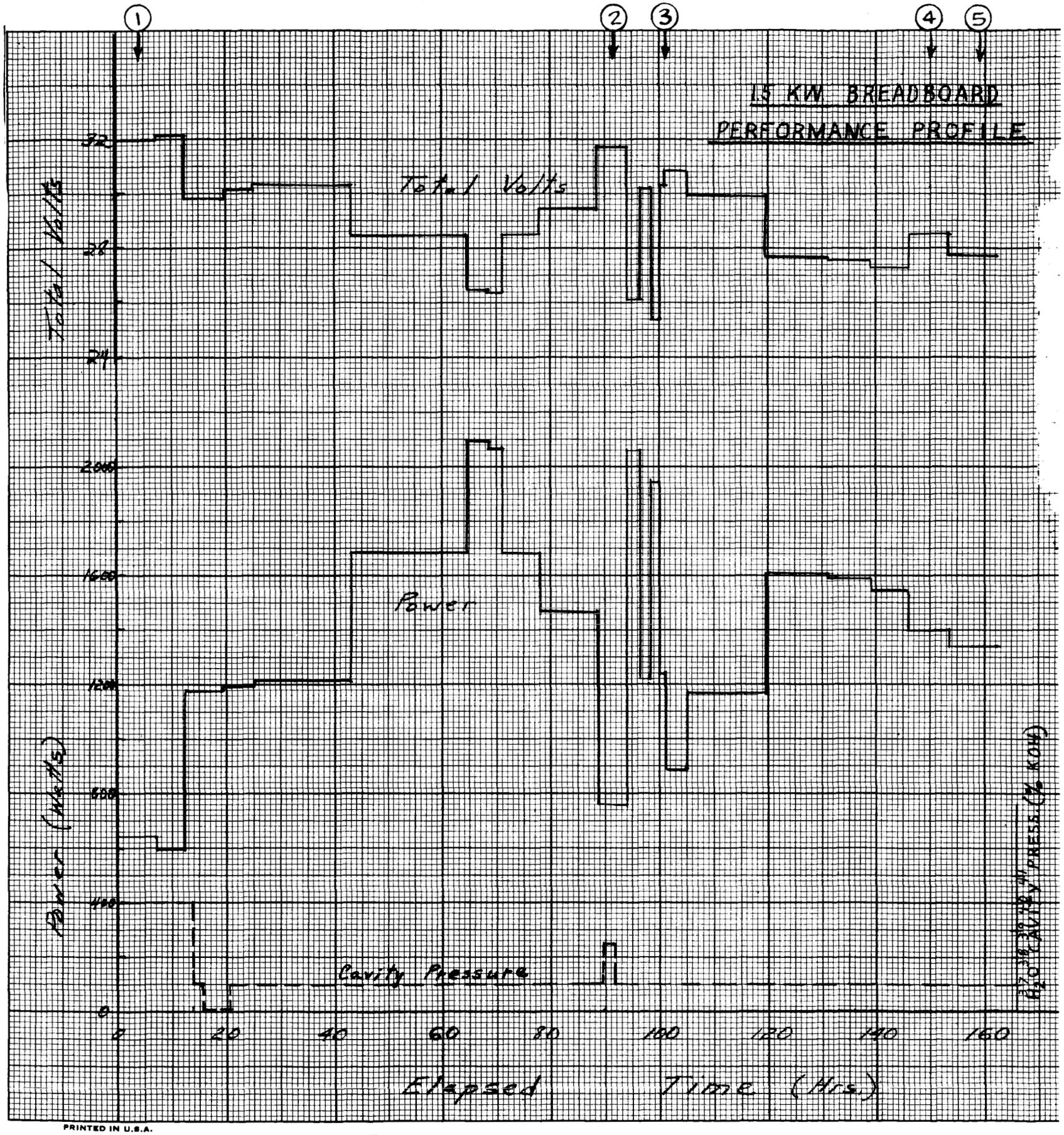

PRINTED IN U.S.A.

FIGURE 37

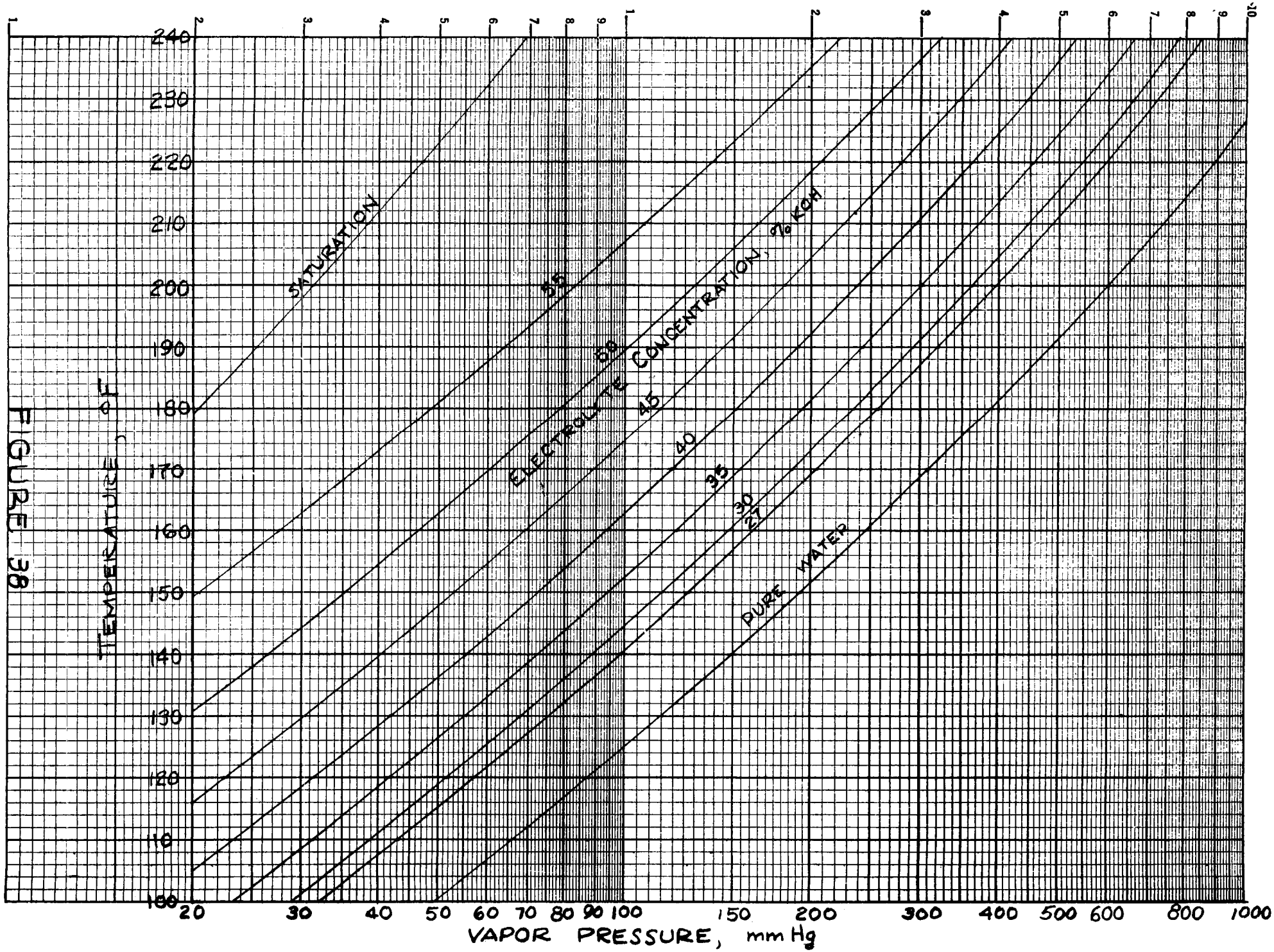
SATURATION
55
50
45
40
35
30
27
ELECTROLYTE CONCENTRATION, % KOH
PURE WATER
TEMPERATURE, °F
VAPOR PRESSURE, mm Hg
240
230
220
210
200
190
180
170
160
150
140
130
120
110
100
20
30
40
50
60
70
80
90
100
150
200
300
400
500
600
800
1000

FIGURE 38

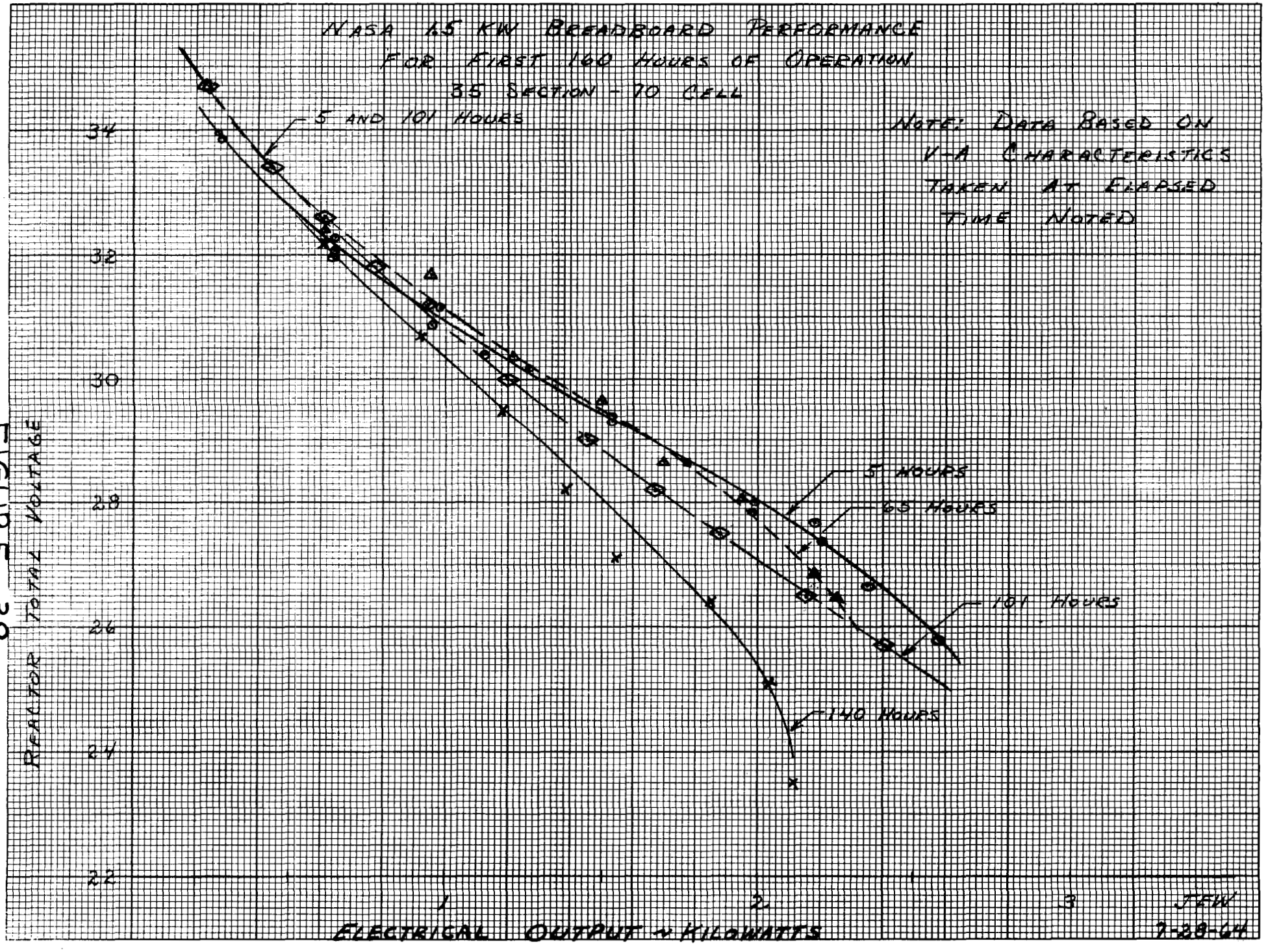
NASA 1.5 KW BREADBOARD PERFORMANCE
FOR FIRST 160 HOURS OF OPERATION
35 SECTION - 70 CELL
NOTE: DATA BASED ON V-A CHARACTERISTICS TAKEN AT ELAPSED TIME NOTED
5 AND 101 HOURS
5 HOURS
65 HOURS
101 HOURS
140 HOURS
34
32
30
28
26
24
22
1
2
3
READ FOR TOTAL VOLTAGE
ELECTRICAL OUTPUT - KILOWATTS
JFW
1-28-64

FIGURE 39

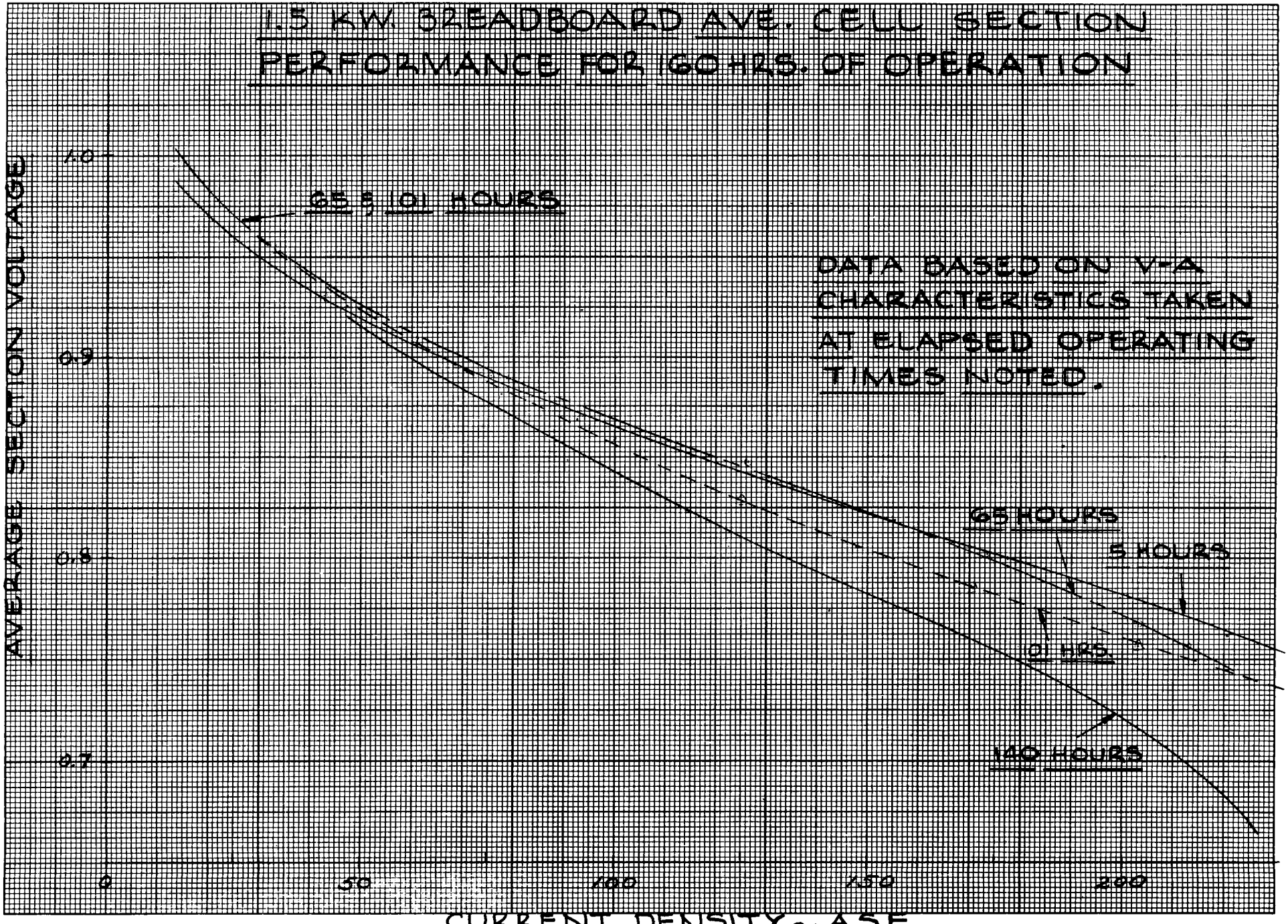
1.5 KW. BREADBOARD AVE. CELL SECTION
PERFORMANCE FOR 160 HRS. OF OPERATION
65 & 101 HOURS
DATA BASED ON V-A CHARACTERISTICS TAKEN AT ELAPSED OPERATING TIMES NOTED.
65 HOURS
5 HOURS
101 HRS.
140 HOURS
AVERAGE CELL VOLTAGE
1.0
0.9
0.8
0.7
0
50
100
150
200
CURRENT DENSITY ~ ASF

FIGURE 40

TABLE 1 TEST DATA DEFINITIONS

The TABLE 3 Test Summary lists the measured and computed system characteristics for a number of load levels. The run depicted for each is typical of three to five runs taken during the test interval at the prescribed input conditions. Listed below are definitions of the terms used in the table.

Item 1 Secondary Gas Coolant - media which transports reactor thermal burden to primary coolant loop

Item 2 Sequential Run Number - Number assigned data taken at one-half hour intervals during the duration of the test and referenced to the start

Item 3 Elapsed Operating Time - the actual time that the unit had been operating when the run data was taken

Item 4 Load Amperes - taken from log sheet

Item 5 Total Reactor Volts - taken from log sheet

Item 6 Gross Output Watts - product of volts and amperes

Item 7 Volts/cell - total volts divided by number of sections

Item 8 Current Density amperes per square foot - load in amperes divided by the effective cell area in square feet.

Item 9 Theoretical heat rejected = $(150.5 - 3.41\ V)\ I_T$ = Btu/hr

I_T = Total current - amperes

V = Total volts

TABLE 1

Item 10 Primary Coolant Inlet Temperature - distilled water temperature recorded (T/C 72) external to canister on inlet line to heat exchanger

Item 11 Δ T Primary Coolant Heat Exchanger - distilled water temperature rise across heat exchanger measured external to canister

Item 12 Primary Coolant Flow - distilled water flow rate measured with a calibrated flowmeter

Item 13 Heat Removed in Heat Exchanger - product of primary coolant flow rate and temperature rise

Item 14 Total Fan Input - power input to both circulating blowers measured with a wattmeter

Item 15 Net Convective - Radiation Loss - difference between theoretical heat generated within the unit plus the energy input to the circulating blowers and thermal burden removed by heat exchanger

Item 16 Δ T Circulating Gas - secondary gas coolant temperature difference recorded across heat exchanger

Item 17 Flow of circulating gas - lbs/hr - heat exchanger thermal burden extracted divided by specific heat and temperature drop of gas across the heat exchanger

Item 18 Canister Pressure - secondary coolant total pressure measured in the canister dome

Item 19 Flow Circulating Gas - cfm/fan - flow in lbs/hr divided by density equals total volume rate in cfm. One-half of total volume rate will be capacity of one blower.

TABLE 1

Item 20 — Δ P Circulating gas across fan in inches of water - taken from log sheet

Item 21 — Δ P across Heat Exchanger - inches of water taken from log sheet

Item 22 — Δ P across Heat exchanger and return passage - taken from log sheet

Items 23 and 24 — Taken from temperature data sheets

Item 25 — Average Δ T Fin Temperature - difference between the average plate fin temperature at the fin passage exit plane and the plate fin temperature at the passage inlet

Item 25 — Δ T Across Active Area - measured temperature difference across half width of cell active area taken at two sections

Item 27 — Δ T Plate $\mathrm{C_L}$ to Fin Exit - thermal gradient measured from center of cell active area to plate fin passage exit.

TABLE I

TEST	C	D	G	K	H	I	M	N	O	P
1. Secondary Gas Coolant	Helium	Hydrogen	Hydrogen	Hydrogen	Hydrogen	Hydrogen	Hydrogen	Hydrogen	Hydrogen	Hydrogen
2. Sequential Run Number	62	78	93	181	116	132	207	215	264	323
3. Elapsed Operating Time - Hours	23	31	38	82	50	58	96	100	124	153
4. Load - Amperes	39.5	40	40	50	59.1	59.1	78.6	76.2	57.2	49.1
5. Total Reactor Volts	30.0	30.2	30.4	29.3	28.4	28.4	26.1	25.3	27.5	28.5
6. Gross Output - Watts	1186	1209	1214	1467	1679	1677	2052	1923	1572	1400
7. Volts/Section or Cell	0.867	0.863	0.867	0.838	0.812	0.811	0.746	0.721	0.787	0.815
8. Current Density - ASF	98.8	100	100	125	148	148	197	190	143	123
9. Theoretical Heat Rejection - BTU/hour	1900	1896	1880	2525	3166	3174	4834	4905	3240	2590
10. Primary Coolant Inlet Temperature - ° F	133	77	135	84	88.5	102	95.5	113.5	101	92
11. $\triangle$ T Primary Coolant Heat Exchanger	42	103.5	52	95.3	82.7	71.9	68.3	40.2	69.7	86.3
12. Primary Coolant Flow - Pounds/hour	41.2	16	31.5	23.5	38.5	38.5	63	107	42	24
13. Heat Removed in Heat Exchanger - BTU/hour	1730	1656	1638	2240	3184	2767	4302	4301	2910	2070
14. Total Fan Input - Watts	171.5	149.8	156.2	147.8	147	146.5	146	144	71.5	71.3
15. Net Convection-Radiator Loss - BTU/hour	753	746	771	789	584	918	1035	1099	579	782
16. $\triangle$ T Circulating Gas - ° F	11.5	7.4	7.5	11.0	10.8	13.0	18.5	20.2	15.0	11.7
17. Flow Circulating Gas - Pounds/hour	121	65.5	63.8	59.8	86.4	62.2	68	62.5	56.7	52.7
18. Canister Pressure - psia	34.2	34.1	34.4	34.6	33.2	33.5	35.2	34.9	34.0	33.8
19. Flow Circulating Gas - CFM/Fan	50	55	53	49	74	53	64	50	47	44
20. $\triangle$ P Circulating Gas Fan " H_2O	0.95	0.53	0.56	0.55	0.51	0.54	0.54	0.54	0.43	0.43
21. $\triangle$ P Across Heat Exchanger " H_2O	0.21	0.08	0.08	0.08	0.07	0.08	0.08	0.08	0.05	0.06
22. $\triangle$ P Heat Exchanger and Return Passage " H_2O	0.18	0.11	0.11	0.11	0.10	0.11	0.11	0.11	0.06	0.08
23. Plate Fin Center Temperature - ° F Max/Min	193/187	193.5/188.5	196/190.5	193/187	189.5/179	189/182.5	187/176	183/172.5	188.5/179.5	192/184
24. Plate Fin Exit Temperature - ° F Max/Min	198.5/194.5	197.5/194	200/196	198.5/194.5	196/191	197.5/193	199/190	195.5/188.5	197/192	198.5/194
25. Average Plate Fin $\triangle$T - ° F	6.94	5.35	5.6	7.4	10.3	9.6	14.6	15.2	11.4	9.2
26. $\triangle$ T Across Active Area - ° F	2.5	2.5	3.75	3.5	4.25	4.25	7.0	7.5	4.5	3.75
27. $\triangle$T From Plate Centerline to Fin Exit	4.75	4.5	5.5	4.5	5.0	5.5	9.5	7.2	4.25	3.5